CHARACTERIZATION OF BIOACTIVE COMPOUNDS IN AMERICAN ELDERBERRY (*Sambucus nigra* subsp. *canadensis*) JUICES

A Dissertation

presented to

the Faculty of the Graduate School

at the University of Missouri-Columbia

In Partial Fulfillment

of the Requirements for the Degree

Doctor of Philosophy

---

by

AMANDA DWIKARINA

Dr. Chung-Ho Lin, Dissertation Supervisor

DECEMBER 2025

The undersigned, appointed by the dean of the Graduate School, have examined the dissertation entitled

CHARACTERIZATION OF BIOACTIVE COMPOUNDS IN AMERICAN ELDERBERRY (*Sambucus nigra* subsp. *canadensis*) JUICES

presented by Amanda Dwikarina,

a candidate for the degree of doctor of philosophy,

and hereby certify that, in their opinion, it is worthy of acceptance.

_____

Dr. Chung-Ho Lin

_____

Dr. Hsin-Yeh Hsieh

_____

Prof. Andrew L. Thomas

_____

Dr. C. Michael Greenlief

_____

Dr. Ronald Revord

DEDICATION

This dissertation is dedicated to my dear parents, Alex Hartana† and Ni Made Armini Wiendi, whose love, patience, and unwavering support have guided me through every step of this journey. I dedicated this dissertation especially to my father, whose memory remains a constant source of strength and inspiration, although he passed away before seeing this work completed. This work is dedicated to my sister, Andina Prameswari, my brother in-law, Hartono Ang and my little nephew Nathanael Alexander Ang, you are my personal therapists who listen and cheer me up whenever my experiments in the lab failed; to my brother Abinata Triatama, who keeps me grounded; and to my personal support system, Vito Amadio Sunoto, who always believes in me even when I doubt myself. Lastly, I dedicated this work to myself for holding onto the dream of becoming a scientist and for never giving up.

ACKNOWLEDGMENTS

I want to express my deepest gratitude to my advisor, Dr. Chung-Ho Lin, for giving me the opportunity to pursue a PhD degree and for the continuous guidance, encouragement, and support throughout my doctoral studies. I would like to thank my mentor, Dr. Hsin-Yeh Hsieh, for her invaluable guidance in shaping both my scientific thinking and professional development. I would also like to thank my committee members, Prof. Andrew Thomas, Dr. C. Michael Greenlief, and Dr. Ronald Revord, for their insightful feedback, support, and expertise. This journey would not have been possible without the generous support from the staff at the Center for Agroforestry, University of Missouri, and the assistance of UMCA Business Specialist Caroline Todd, who provided invaluable help.

I'm especially thankful to my lab members and friends for their encouragement, advice, and many shared moments in and outside the lab. I would also like to thank the Missouri Indonesian Student Association, especially Mbak Indah, Kak Deasy, Dita, Yoko, and Bang Paul, who made Columbia feel like home. I'm deeply grateful to my dear friend, Quincy Rosemarie, who completed her PhD journey before me and generously shared her invaluable experiences along the way. To Vito Amadio Sunoto, thank you for showing constant support and for accompanying me through every challenging time with patience and understanding from the start of this journey.

I owe my deepest gratitude to my family, whose love, patience, and faith have carried me through every obstacle. Finally, I thank God, for without His will, I wouldn't be able to make it.

CHARACTERIZATION OF BIOACTIVE COMPOUNDS IN AMERICAN ELDERBERRY (S*ambucus nigra* subsp. c*anadensis*) JUICES

Amanda Dwikarina

Dr. Chung-Ho Lin, Dissertation Supervisor

ABSTRACT

American elderberry (*Sambucus nigra* subsp. *canadensis*) is an emerging specialty crop in North America, valued for its rich composition of bioactive compounds, which have demonstrated nutritional and therapeutic potential. However, comprehensive chemical and functional characterization of American elderberry remain limited. This dissertation integrates advanced metabolomic analysis, bioassay screening, and molecular mechanism studies to elucidate the chemical diversity and antiviral activity of American elderberry.

An untargeted ultra-high performance liquid chromatography coupled with high-resolution mass spectrometry (UHPLC–HRMS) metabolomics analysis, combined with high-throughput bioassay screening, was employed to characterize juices from 18 propagated accessions and three established American elderberry cultivars. More than 100 putative bioactive compounds were identified, revealing genotype-dependent differences in metabolite composition. Cultivar Ozark and several wild accessions, such as accession 1911, displayed distinct chemical signatures. Among 32 tested compounds, 14 exhibited strong antioxidant activity, and six demonstrated antiviral effects against HIV-1, highlighting elderberry's potential in functional food and nutraceutical applications.

This study further investigated the antiviral properties of American elderberry against the *Influenza* A Polymerase Acidic (PA) protein using fluorescence resonance energy transfer (FRET)-based endonuclease assay. Four cultivars, Ozark, accession 1892,

1196, and 2084, showed inhibition activity greater than 65% against PA activity, surpassing the European cultivar 'Haschberg'. Several phenolic compounds, including gallic acid, myricetin, caffeic acid, and luteolin, displayed potent inhibition of PA endonuclease activity (IC_{50} < 30 μM), suggesting their role as key bioactive constituents underlying elderberry's anti-influenza potential.

A targeted ultra-high performance liquid chromatography-tandem mass spectrometry (UHPLC–MS/MS) method was developed and validated to quantify the bioactive compounds in American elderberry across 21 cultivars. The optimized UHPLC–MS/MS platform achieved excellent detection limits (< 1 ng/mL), minimized matrix effects, and provided accurate quantification of complex juice extracts. This study revealed genotype-dependent variation in metabolite composition, highlighting opportunities for targeted breeding and cultivar selection to enhance desired phytochemical traits, such as antioxidant capacity, antiviral bioactivity, and overall nutritional quality. Notably, wild-propagated accession 1199 exhibited high levels of cyanidin-based anthocyanins, suggesting its utility as a natural food color source. Phenolic acid compounds were found most abundant in accession 1196, whereas the flavonoid isorhamnetin 3-rutinoside was found highest in cultivar Ozark.

Collectively, this work establishes a robust, comprehensive, analytical, and bioactivity framework for the characterization of American elderberry. By integrating metabolomic profiling, targeted quantification, and antiviral mechanism studies, these findings advance the understanding of elderberry phytochemistry and support its development as a source of functional and bioactive compounds for nutraceutical applications.

TABLE OF CONTENTS

LIST OF TABLES

LIST OF FIGURES AND ILLUSTRATIONS

LIST OF EQUATIONS

LIST OF APPENDIX

Table

Figure

INTRODUCTION

Elderberries are perennial fruit-producing shrubs or small trees belonging to the family Viburnaceae and genus *Sambucus*[1]. *Sambucus nigra* subsp. *nigra* (European elderberry) and *Sambucus nigra* subsp. *canadensis* (American elderberry) are two taxa of elderberry that are increasingly being commercially produced. American elderberry is native to much of eastern and midwestern North America and has been used for both food and medicine by indigenous communities for millennia[2–4]. It is emerging as an important specialty crop in the midwestern USA, mostly cultivated for processing markets[5]. Both fruits and flowers have become increasingly popular for use in a variety of foods, wines, and health supplements[6,7].

Elderberry fruits and flowers contain abundant health-promoting bioactive compounds, including phenolics, flavonoids, and antioxidant phytochemicals[8]. Several studies analyzed the bioactive composition of American and European elderberries, identifying different polyphenolic compounds in the fruits, flowers, leaves, and stems[9–12]. Elderberry's major phenolic and flavonoid compounds include gallic acid, neochlorogenic acid, rutin, and quercetin[9–12]. In addition, elderberry fruits contain large amounts of anthocyanins, such as cyanidin-3-glucoside and cyanidin-3-sambubioside, which exhibit antioxidant activity [8,13].

Previous research has demonstrated the potential health benefits of elderberry, showcasing a wide range of biological functions, including antioxidant[10,11,14,15], anti-inflammatory[13,16,17], anticancer[18,19], antiviral[8,20], antibacterial[15,21], and anti-diabetic[22] attributes. Elderberry has also gained popularity as a potential remedy for treating colds

and flu. However, most research has focused on European elderberry, with only limited studies on the health-promoting activities of American elderberry. Modern bioanalytical techniques, such as high-throughput screening bioassays and metabolomic analyses, can be used to untangle and elucidate the potential health-benefitting metabolites of American elderberry at much higher levels than have been previously possible.

High-throughput screening (HTS) is a subset of the drug discovery process that incorporates the multidisciplinary fields of analytical chemistry, biology, biochemistry, and computational technologies. It plays an important role, especially when novel biochemical targets are involved[23]. The HTS allows for a standardized, rapid, and cost-effective evaluation of small molecules and novel chemical biological functions. In recent years, HTS labs have used a combination of biochemical and cell-based assays. Both are necessary for discovering and characterizing newly identified compounds in the drug discovery process[23,24]. In addition, recent advancements in computational power and database capacity for the metabolomic analyses allow exploring the bioactive molecules in American elderberry.

In this dissertation, the first chapter focuses on the metabolomic analysis and bioactive compounds exploration in American elderberry juices. This chapter also discusses high-throughput screening assays and metabolomics analyses to establish a systematic and standardized strategy for investigating the biological functions of American elderberry, including its antioxidant, antibacterial, and antiviral properties. The second chapter elaborates on the antiviral mechanisms of American elderberry compounds. This chapter aims to establish a screening method to assess the potential antiviral properties of American elderberry, targeting the viral transcription and replication mechanisms of

Influenza A viruses. Lastly, the third chapter focuses on quantifying the bioactive compounds in American elderberry juices across 21 cultivars. The findings from this research help identify the niche markets and facilitate the development of new economic opportunities for the American elderberry industry.

OBJECTIVES

The specific objectives of the work reported below were the following:

1. Identify and characterize a variety of bioactive metabolites in the juices of 21 American elderberry genotypes using untargeted metabolomics.
2. Utilize standardized high-throughput screening (HTS) protocols at the Kansas High Throughput Screening Laboratory at the University of Kansas, Lawrence, KS (https://hts.ku.edu/) to evaluate the potential health benefits of 32 selected bioactive metabolites identified in American elderberry juices.
3. Established a screening method to elucidate the possible mode of action targeting *Influenza* A viral transcription mechanism
4. Quantify the 32 select specialized metabolites in American elderberry juices using targeted metabolomics analysis.

CHAPTER 1. CHARACTERIZATION OF BIOACTIVE COMPOUNDS IN 21 CULTIVARS OF AMERICAN ELDERBERRY USING METABOLOMICS ANALYSIS

ABSTRACT

American elderberry (*Sambucus nigra* subsp. *canadensis*) is an emerging specialty crops for Missouri, recognized for its high level of bioactive compounds with significant health benefits. Here we integrated untargeted UHPLC-HRMS metabolomics with High-throughput screening (HTS) bioassays characterized American elderberry juice from 18 propagated accessions and three established cultivars. Our metabolomics study has identified >100 putative bioactive compounds in the American elderberry juices. Multivariate analysis showed significant chemical profile between genotypes. Multivariate analyses showed genotype-depended differences in metabolite composition. Cultivar Ozark and wild accessions such as 2079, 1911, and 2095, displayed distinct chemical profiles while accession 1196 accumulated high levels of key bioactive flavonoids. An array of high-throughput screening bioassays was conducted to evaluate bioactivity of the 32 selected putatively identified compounds. Our results revealed that 14 of the 32 American elderberry compounds exhibited strong antioxidant activity. Six compounds demonstrated significant antiviral activity against two strains of HIV-1 virus. These findings provide the first comprehensive study of American elderberry juices and highlight their potential use in dietary supplements and innovative applications in health and medicine.

INTRODUCTION

Elderberries are perennial fruit-producing shrubs or small trees belonging to the family Viburnaceae and genus *Sambucus* [1]. *Sambucus nigra* subsp. *nigra* (European elderberry) and *Sambucus nigra* subsp. *canadensis* (American elderberry) are two taxa of elderberry that are increasingly being commercially produced. American elderberry is native to much of eastern and midwestern North America and has been used for both food and medicine by indigenous communities for millennia. It is emerging as an important specialty crop in the midwestern USA, mostly cultivated for processing markets [5,25]. Both fruits and flowers have become increasingly popular for use in a variety of foods, wines, and health supplements [26,7].

Numerous studies have identifying a wide-range of polyphenolic compounds in fruits, leaves and stems of elderberry [27,9,8]. Their health-promoting potential is largely attributed to anthocyanin and other polyphenols, which are well-recognized free radical scavengers with strong antioxidant capacity [10]. While extensive research on European elderberry has demonstrated broad biological activities, including antioxidant [14,15], anti-inflammatory[13], anticancer[19], antiviral[8], and antibacterial attribute[15], while systematic studies of American elderberry cultivars remain limited. The recent phytochemical evaluation of American elderberry focused only on a subset of anthocyanins and polyphenols compounds in well-established American elderberry cultivars, namely Adams II, Bob Gord on, and Wyldewood [28]. Advances in analytical technologies, particularly mass spectrometry (MS)-based untargeted metabolomics and high-throughput screening bioassays, provide powerful tools to comprehensively characterize the phytochemical

properties of American elderberry and validate the health benefit claimed of identified metabolites

Advances in MS-based untargeted metabolomics, utilizing ultra-high performance liquid chromatography (UHPLC) coupled with high-resolution tandem MS, have enabled detailed exploration and characterization of natural products bioactive compounds across plant cultivars and genotypes. LC-MS/MS is among the popular analytical technique, offering high mass accuracy and fragmentation pattern data (MS/MS spectra) that allow reliable prediction of molecular compounds based on accurate *m/z* values of precursors ion [29]. Furthermore, the availability of comprehensive MS/MS spectral libraries greatly facilitates rapid and accurate metabolite annotation in untargeted analysis.

High-throughput screening (HTS) is a subset of the drug discovery process that incorporates the multidisciplinary fields of analytical chemistry, biology, biochemistry, and computational technologies. It plays an important role, especially when novel biochemical targets are involved[23]. The HTS allows for a standardized, rapid, and cost-effective evaluation of small molecules and novel chemical biological functions. In recent years, HTS labs have used a combination of biochemical and cell-based assays, both of which are essential for discovering and characterizing newly identified compounds in the drug discovery process[23]. Building on this framework, we applied HTS in combination with advanced metabolomics profiling to systematically investigate chemical profile of American elderberry and to validate the bioactivities attributed to its metabolites.

A previous study by Mudge et al. (2016)[30] analyzed polyphenol content of wild-growing American elderberry collected from eastern and midwestern United States, from which a subset of these collections was selected for propagation at the University of

Missouri's Southwest Research, Extension, and Education Center near Mt. Vernon, Missouri, USA. In this study we compared the overall metabolomic composition of the 18 selected propagated accessions and three established cultivars of *Sambucus nigra subsp. canadensis*, using advanced MS-based metabolomic analysis. In addition, HTS bioassay were utilized to evaluate and validate the potential bioactivity of putatively identified compounds. To our knowledge, this is the first study to report a complete chemical profile together with comprehensive bioactivity data across 18 diverse propagated accession of American elderberry in comparison with three well-established cultivars. By integrating metabolomics analyses with HTS assay, we developed a standardized strategy for investigating the biological functions of American elderberry, with focus on antioxidant, antibacterial, and antiviral properties. Leveraging recent advancements in instrumentation, computational power and database capacity, this study provides new insights into the bioactive potential of American elderberry, supporting breeding programs for cultivar selection, and the development of novel economic opportunities.

MATERIALS AND METHODS

Plant material

Elderberry fruits from 21 American elderberry (*Sambucus nigra* subsp. *canadensis*) accessions and cultivars (Table 0-1) were harvested from plantings at the University of Missouri's Southwest Research, Extension, and Education Center near Mt. Vernon, Missouri, U.S.A. The samples represent wild American elderberry accessions from across the midwestern and eastern USA, including collections amassed and studied in Mudge et al. (2016) [30], as well as established cultivars [31,32]. For simplicity, all elderberry accessions and cultivars described in this study are henceforth noted as "genotypes". Elderberry fruit was harvested at peak ripeness and immediately frozen. Later, the fruit was de-stemmed, thawed at ambient temperature, and the juice pressed by hand, filtered through a kitchen sieve, aliquoted into 50 mL polypropylene tubes, and re-frozen (-20 °C) until further processing.

Table 0-1 American elderberry accessions and cultivars (genotypes) evaluated in this study

Accession/Cultivar	Collector[a]	State (USA)	Accession/Cultivar Citations
ACC 1069	Meyer	Pennsylvania	30
ACC 1076	Meyer	New York	30
ACC 1191	Meyer	Arkansas	30
ACC 1196	Meyer	Alabama	30
ACC 1199	Meyer	Georgia	30
ACC 1887A	Townesmith	West Virginia	30
ACC 1889A	Townesmith	West Virginia	30
ACC 1892	Townesmith	New York	30
ACC 1896	Townesmith	Connecticut	30
ACC 1911	Townesmith	Pennsylvania	30
ACC 1913	Townesmith	Pennsylvania	30
ACC 2073	Townesmith	Mississippi	30
ACC 2079	Townesmith	South Carolina	30
ACC 2083	Townesmith	South Carolina	30
ACC 2084	Townesmith	South Carolina	30
ACC 2085	Townesmith	South Carolina	30
ACC 2089	Townesmith	North Carolina	30
ACC 2095	Townesmith	West Virginia	30
Bob Gordon (BG)	Thomas	Missouri	32
Ozark	Byers	Arkansas	6
Wyldewood (WW)	Millican	Oklahoma	31

[a]Accession/cultivar collectors are Karen M. Meyer and Andrew K. Townesmith (Missouri Botanical Garden, St. Louis, MO), Andrew L. Thomas and Patrick L. Byers (University of Missouri, Columbia, MO), and Margaret Millican (Wyldewood Cellars, Wichita, KS).

Chemical

Acetonitrile, and formic acid were purchased from Fisher Chemical (Fair lawn, NJ, USA) and were all LC/MS grade. Milli-Q water was for UHPLC-MS and was obtained from in-house Millipore water purifier (Burlington, MA, USA). Methanol for sample extraction were of HPLC-grade and purchased from Sigma-Aldrich (St. Louis, MO, USA). Chemical standards for high-throughput analysis were purchased from Sigma-Aldrich (St. Louis, MO, USA) with purity >95%, except cyanidin 3-*O*-rutinoside, peonidin 3-*O*-glucoside and isoquercetin with purity >90%; myricetin with purity >96%; kaempferol with purity >97%; caffeic acid, cryptochlorogenic acid, catechin hydrate, p-coumaric acid, cyanidin 3,5-*O*-diglucoside, cyanidin 3-*O*-glucoside, epicatechin, gallic acid, neochlorogenic acid, and isorhamnetin 3-*O*-glucoside with purity >98%; ferulic acid was of certified reference standard grade; and isorhamnetin 3-rutinoside was purchased from Fisher Chemical (Fair lawn, NJ, USA) with purity >95%.

Sample preparation

All American elderberry juice samples were thawed, then centrifuged at 8000 rpm for 20 minutes. One mL of supernatant was mixed with four mL of HPLC-grade methanol. The mixture was then sonicated for 60 minutes using a sonicator (Fisher Scientific, Pittsburgh, PA, USA). The mixture was then filtered through a 0.2 μm PTFE Acrodisc syringe filter (Waters, Milford, MA, USA) to remove solid components and transferred to an HPLC autosampler vial (Waters, Milford, MA, USA) for further analyses.

Untargeted metabolomics analyses

The untargeted metabolomics profiling was performed on a Bruker maXis impact II quadrupole-time-of-flight (Q-ToF) mass spectrometer (MS) coupled with Waters Acquity Ultrahigh Performance Liquid Chromatography (UHPLC). High-resolution mass spectrometry was performed in negative and positive electrospray ionization mode as a preliminary experiment to identify the chemical compounds in the plant extract. Separation was achieved on a Waters C18 column (2.1 x 150 mm, BEH C18 column with 1.7 µm particles) using a linear gradient of 95%:5% to 30%:70% eluent A:B (A: 0.1% formic acid in water, B: acetonitrile) over 30 min. Between 30 – 33 min, the linear gradient was increased from 70% to 95% B and maintained at 95% B for 3 min. The percentage of B was maintained at 5% from 36 – 40 min. The flow rate was 0.56 mL/min, and the column temperature was 60^{o}C. Mass spectrometry was performed in the positive and negative electrospray ionization mode with the nebulization gas pressure at 43.5 psi, dry gas of 12 L/min, dry temperature of 250^{o}C, and a capillary voltage of 4000 V. Auto MS/MS tandem mass spectral data were collected using the following parameters: MS full scan: 100 to 1500 *m/z*; the number of precursors for MS/MS: 3; threshold: 10 counts; active exclusion: 3 spectra, released after 0.15 min; collision energy: dependent on mass, 10eV at 50 Da, 20 eV at 200 Da, 30 eV at 500 Da, 40 eV at 1000 Da, and 50 eV at 1500 Da. The MS and MS/MS data were auto-calibrated using sodium formate that was introduced at the end of the gradient and after data acquisition.

Metabolomics data analysis

Bioactive compounds were identified in elderberry juice using the web-based platform XCMS Online, which is equipped with the METLIN database and is freely available at https://xcmsonline.scripps.edu. The METLIN library contains over one million molecules to facilitate metabolite identification. UHPLC-MS chromatograms were aligned using the R package XCMS. CentWave settings were used for feature detection (maximal tolerated *m/z* deviation = 10 ppm, minimum peak width = 5 s, and maximum peak width = 20 s). Obiwarp settings were used for retention time correction (profStep = 1). The chromatogram alignment setting for peak alignment was as follows: bw = 5, minfrac = 0.5, mzwid 0.015. The statistical tests are carried out systematically following feature detection and profile alignment using the Welch t-test (p-value <0.05).

Metabolite UHPLC-MS/MS mass spectral data were analyzed using MS-DIAL Software (Version 4, http://prime.psc.riken.jp/) to further aid compound identification. Data files were converted to ABF format using AnalysisBaseFile Converter (https://www.reifycs.com/AbfConverter/) before import to MS Dial software. Peak picking, alignment, deconvolution, and MS/MS database search were performed with the following parameter: MS1 tolerance 0.01 Da, MS2 tolerance 0.05 Da, identification score cut off 70%, minimum peak height 3000, mass slice width 0.1 Da, retention time tolerance 0.05 min, MS/MS databases ESI(+) and (-)-MS/MS from authentic standards.

High-throughput screening assay (HTS)

Metabolomics analysis of American elderberry juices putatively identified more than 100 bioactive compounds, of which 32 compounds were selected to further validation

of their antioxidant, anti-HIV, and antibacterial activities using high-throughput screening assays (HTS) at the Kansas High Throughput Screening Laboratory at the University of Kansas, Lawrence, KS (https://hts.ku.edu/).

1. Total antioxidant capacity

The total antioxidant activity of American elderberry compounds was evaluated using an electron transfer-based Cupric Reducing Antioxidant Capacity (CUPRAC) method [33]. Briefly, the compounds were solvated in 100% DMSO and transferred acoustically to prepare assay plates using ECHO 655 (Beckman Inc.). The compounds were tested in a 7-concentration dose response in 384 well microplates. The compounds were mixed with 50 µL of freshly prepared CUPRAC reagent (Cu(II)-neocuproine). After mixing at 650 rpm for 2 mins, the plates were sealed and incubated for up to 3 h at 25°C. The absorbance of the samples of Cu(I)-neocuproine (Nc) chelate formed from redox reaction between antioxidants and CUPRAC reagent was read at 1.5 h and 3 h at 450 nm using a microplate reader (BioTek Neo, Agilent). A Trolox standard curve was included on each assay plate, and the total antioxidant capacity of the compounds was interpolated and expressed as Trolox equivalent (mM) from the Trolox standard curve of the Trolox control.

2. Antioxidant response element (ARE) activation

American elderberry compounds were evaluated for Nuclear factor erythroid 2-related factor 2 (Nrf2) activation using ARE-Luciferase reporter-based assay in the HepG2 cell line[34]. The method for ARE activation assay is as follows: a HepG2 hepatic cell line stably expressing firefly luciferase (Luc) reporter under the control of ARE was obtained from BPS Bioscience. Briefly, the HepG2-ARE-Luc cells (10,000 cells/well) were seeded

in 384-well plates in 50 µL complete media per well using a Multidrop Combi dispenser (Thermo Fisher Scientific, Waltham, MA, USA). Compounds (7-concentration dose-response) were transferred to the plates and incubated at 37°C in a 5% CO_2 humidified incubator for 18 h. Each assay plate also contained known positive controls [tert-butylhydroquinone (TBHQ) and DL-Sulphorane] as well as DMSO (as a vehicle negative control). The reporter activity was measured by the addition of 25 µL Steady-Glo® luciferase assay reagent (Promega Inc.) for 30 min. The luminescence intensities of the 384-well plates were read on a BioTek Neo microplate reader (Agilent Inc.). The increase in luciferase activity correlates with compound-induced activation of Nrf2. The fold increase in luciferase was normalized to the positive and negative controls on each assay plate.

The ARE fold induction of the compounds was measured by dividing the luminescence absorbance of the treatment by the specific luminescence absorbance of the control sample and multiplying by 100. The control sample (in the presence of DMSO vehicle and without the compounds) was set at 100%. The compounds with ARE fold induction to 10-fold over the vehicle controls in one or more concentrations were considered to have significant ARE induction activity. The bioactive compounds' relative cytotoxicity (%) was calculated by dividing the specific luminescence absorbance of the treated sample by the specific luminescence absorbance of the control sample and multiplying by 100. The control sample (in the presence of DMSO vehicle and without the compounds) was set at 100%.

3. Evaluation of anti-HIV activity.

The anti-HIV activity of 32 putative compounds identified in American elderberry juices was evaluated at the Kansas High Throughput Screening Laboratory at the University of Kansas, Lawrence, KS (https://hts.ku.edu/). The method for anti-HIV activity assay provided by Dr. Anuradha Roy is as follows: all reagents for HIV neutralization assay were obtained through the HIV Reagent Program, Division of Acquired Immunodeficiency Syndrome (AIDS), National Institute of Allergy and Infectious Diseases (NIAID), NIH. TZM-bl reporter cells, derived from Hela cell clone expressing CD4 glycoprotein, CC-chemokine receptor type 5 (CCR5), and CXC-chemokine receptor 4 (CXCR4) as well as an HIV-trans-activator of transcription (HIV-Tat) regulated firefly luciferase & β-galactosidase reporters (Cat. no. 8129), used to optimize the HIV-1 neutralization assay according to reference [35]. Briefly, the TZM-bl cell line was grown at 37°C in humidified 5% CO_2 in Dulbecco's Modified Eagle's Medium with L-glutamine, sodium pyruvate, glucose, and 10% heat-inactivated fetal bovine serum (FBS) and 50 µg gentamicin/ml. Two HIV-1 strains, NL4-3 [ARP-114, X4 tropic] and Bal [ARP-11414, R5 tropic] viruses, were prepared by transfecting 293T/17 cells with DNA constructs containing full-length wild type (WT) sequences, as described previously[36]. The virus was titrated in TZM-bl cells to achieve an average tissue culture infectious dose (TCID) of 150,000 relative light unit (RLU) equivalents for pNL4-3 and TCID of 20,000 for pBAl WT corresponding to 8-10 times the background, respectively.

To identify compounds that interfere with viral replication, 5000 cells/well were seeded in 384 well plates containing compounds. An equal volume of virus (2X stock) was added to the cells in 8 µg/mL diethylaminoethanol (DEAE)-Dextran. After 48h at 37°C,

5% CO_2, Promega Steady Glo Luciferase detection reagent was added to detect Firefly luminescence. Percent inhibition was normalized to DMSO controls. Four known HIV inhibitors (AZT, JM2987, TAK779 and Maraviroc) were used as positive controls.

4. Antibacterial growth assay

The activity of American elderberry compounds was tested against *Staphylococcus aureus* subsp. *aureus* Rosenbach, ATCC 29213, *Pseudomonas aeruginosa,* PAO1, ATCC 15692, and *Klebsiella pneumoniae* subsp. *pneumoniae,* ATCC 27736. The bacteria from a single colony were grown overnight in Mueller Hinton cation-adjusted broth at 37°C, 250 rpm. The overnight culture was diluted 100-fold, and 40 µL of bacterial suspension was grown in the presence of American elderberry compounds (7 concentration dose-response) for 24h at 37°C. The activity of compounds was also evaluated against *Mycobacterium smegmatis,* which was grown in Middlebrook 7H9 OADC supplemented media at 37°C, 250 rpm, for 24h and 48h. Positive controls included Vancomycin and Amikacin, while DMSO was the negative control on each assay plate. The plates were read at Abs 600 nm at 24 h and 48 h. After the absorbance reads, Bact-Titer Glo was added to the plates, and an ATP-based luminescence assay was read using BioTek Synergy. Percent inhibition of growth was normalized to positive and negative controls on each assay plate.

Statistical analysis

The relative abundance of putative metabolites identified was statistically analyzed using the web-based platform MetaboAnalyst ver. 6.0 (https://www.metaboanalyst.ca/). Features were normalized by sum, log transformed and scaled by the pareto scaling method. Unsupervised multivariate analysis of principal component analysis (PCA) was

performed to determine differences in metabolic profiles between genotypes. Supervised multivariate method of partial least squares-discriminant analysis (PLS-DA) was used to identify altered metabolites between groups. Heatmap clustering analysis was performed to compare relative abundance of compounds across genotypes.

For total antioxidant capacity analysis, linear regression analysis was performed using GraphPad Prism 10 (San Diego, CA, USA) to identify the linear regression equation for each compound. The coefficient of the compound equation was compared with the coefficient of the Trolox control to determine each compound's relative total antioxidant capacity. The fold increase over Trolox was calculated by dividing the compound models' coefficient by the Trolox control coefficient. The compounds that exhibited a fold increase over Trolox greater than 5 were considered to possess significant total antioxidant capacity.

For ARE activation assay, HIV inhibitory assay and antibacterial analysis, GraphPad Prism 10 was used to generate non-linear regression analysis of data to identify the dose-response curve for each compound. The IC_{50} values (half maximal inhibitory concentration) of each compound were determined from the dose-response curve for the A549 and MRC-5 cell lines for ARE activation assaya and TZM-bl cell line for HIV inhibitory assay. The compounds that exhibited IC_{50} values < 10 µM in the A549 cell line and had no toxic effects on the control cell line MRC-5 were considered potent antiproliferative compounds. Compound with IC_{50} values >100 µM were considered to not have inhibitory effect against HIV virus strains NL4-3 and BaL Data are presented as mean ± standard deviation (n=2). One-way analysis of variance (ANOVA) was performed using GraphPad Prism 10 to determine the significance differences among mean values.

RESULTS

Untargeted metabolomic analysis

Spectral data generated from UHPLC-QTOF-MS were analysis using XCMS online platform, resulting in the putative identification of more than 10,000 peaks in American elderberry juices (data not shown). Among these, over 100 compounds with potential bioactivity were putatively identified in both positive and negative ionization modes through comparison of MS spectral data and accurate mass values with the METLIN library. For this study, the bioactivities of 72 compounds were further summarized based on previously published reports (Table 0-2 and Table A 1). These findings demonstrated the utility of XCMS platform for broad chemical profiling, due to the extensive coverage of the METLIN spectral library. However, because of limited storage capacity and incomplete integration of XCMS with METLIN-MRM library, compound annotation relied primarily on accurate mass matching. Therefore, further validation is required to increase confidence in compound identification.

We further analyzed the untargeted UHPLC-QTOF-MS/MS data using MS-DIAL platform, which resulted in MS/MS spectral matching of 110 putative compounds against the MS-DIAL metabolomics MSP library using an identification score cutoff of 70% (Table 3 and Table A 2). While XCMS-based annotation yielded a wider range of putative compounds overall, only 10 of these overlapped with MS-DIAL identification, suggesting the limited MS/MS spectral library available in MS-DIAL compared with XCMS-METLIN library. Furthermore, the peak height cutoff of 3000 set, may have reduced the number of matches, as compounds present at low concentration in the juice may have been

excluded. In total, we identified more than 100 putative compounds in American elderberry juices, including at least 31 flavonoids, 15 anthocyanins, and 23 polyphenolic compounds (Table 0-3, Table A 1, and Table A 2).

Principal component analysis (PCA), an unsupervised method used to identify patterns between multivariate samples, was performed, and the result is presented in Figure 0-1. The PCA analysis showed a separation among genotypes, reflecting differential metabolic profile between groups. Two principal components (PCs) explained 35.4% of the total variability, with the first principal component (PC1) explained 25% of the data variability and the second PC (PC2) accounted for 10.4% of data variability.

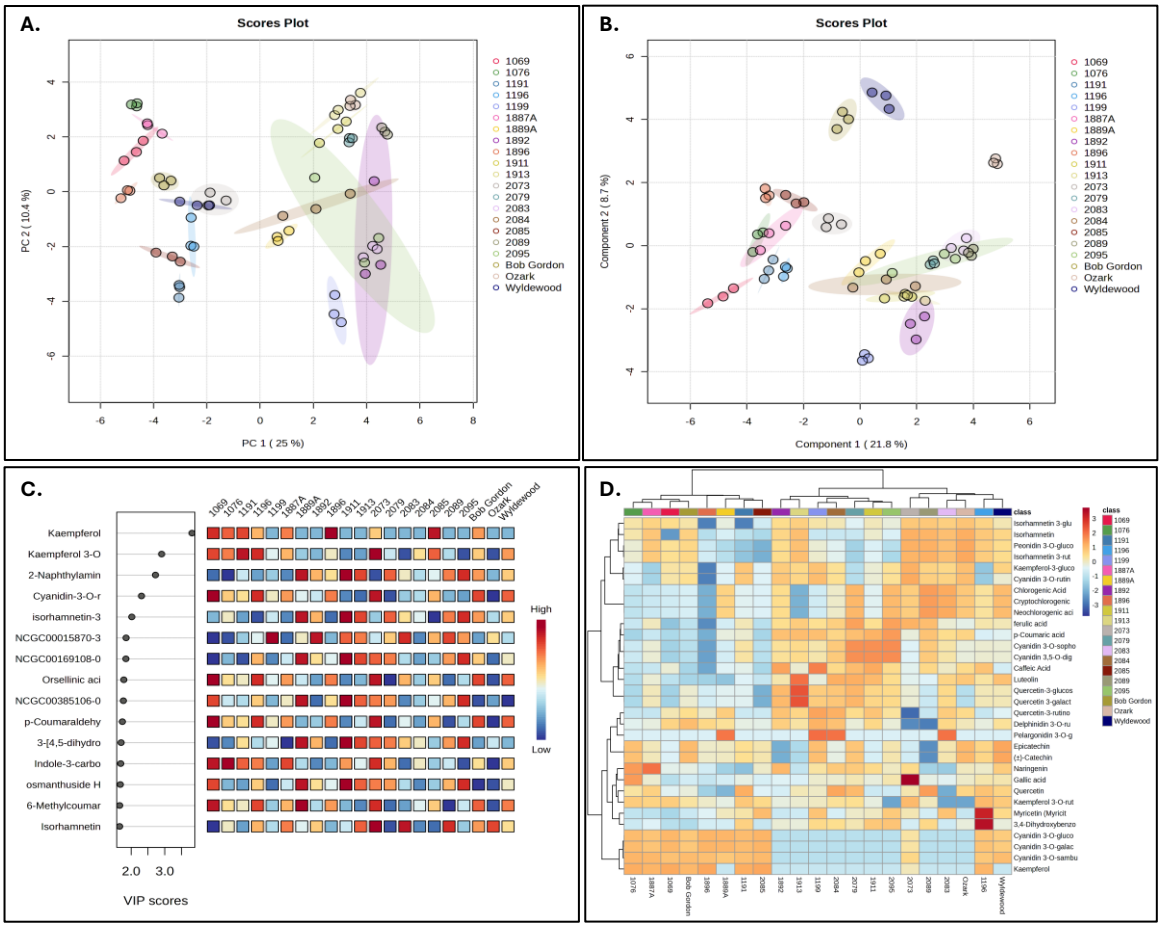

Figure 0-1. Result of untargeted metabolomic analysis. A. PCA scores plot and B. PLS-DA scores plot of putatively identified compounds in juices of 21 American elderberry genotypes revealed differences in the metabolomic profiles between genotypes. Circles with the same color represent analytical replicates (n=3). The colored ellipses indicate 95% confidence regions of each group. C. Important features identified by PLS-DA. The colored boxes on the right indicate the relative abundance of the corresponding metabolite in each American elderberry genotype under study, with dark red representing high abundance and dark blue representing low abundance. D. The heatmap shows the relative abundance of 32 selected identified compounds in the juices collected from various American elderberry genotypes. Each color represents a relative abundance of compounds in the juices. The scale ranges from dark red to dark blue, representing the range of high to no abundance of compounds. Heatmap features the top thirty-two metabolite features as identified by t-test analysis ($p < 0.05$ and intensity $\geq$10,000). The distance measure is by Euclidean correlation, and clustering is determined using the Ward algorithm.

To further resolve group-specific differences, partial least-square discriminant analysis (PLS-DA), a supervised analysis model, was performed (Figure 0-1B). PLS-DA highlighted the specific similarities and differences among groups, identifying metabolites most responsible for genotype discrimination [37]. The variable importance in projection (VIP) scores indicated the top 15 most importance variables (Figure 0-1C) that identified as metabolites responsible for the discrimination between genotypes. Overall, PLS-DA revealed significant differences in the metabolomic profiles of American elderberry genotypes, with two PCs explaining 30.5% of the total variability of the data (PC1 21.8% and PC2 8.7%). Notably, cultivars Bob Gordon and Wyldewood exhibited highly similar metabolomic profiles, whereas the cultivar Ozark displayed a distinctively different profile compared to other genotypes. Complementary partitional clustering using k-means analysis (k=3) further grouped Ozark separately from the other genotypes (Figure A 5).

Table 0-2. List of bioactivities of 32 selected compounds identified in American elderberry juices, as previously reported in literatu res.

No	Compounds	Formula	Activities	Ref
1	Gallic acid	$C_7H_6O_5$	Antioxidant, anti-inflammatory, anticancer, antimicrobial, antiviral	38
2	3,4-Dihydroxybenzoic acid	$C_7H_6O_4$	Antioxidant, anti-inflammatory	39
3	Rutin (quercetin-3-rutinoside)	$C_{27}H_{30}O_{17}$	Anticancer, antioxidant, anti-inflammatory	40–43
4	Delphinidin 3-*O*-rutinoside	$C_{27}H_{31}O_{16}$	Antioxidant, anticancer	44,45
5	Caffeic acid	$C_9H_8O_4$	Antioxidant	46
6	Cryptochlorogenic acid	$C_{16}H_{18}O_9$	Anti-inflammatory, antioxidant, antidiabetic	47,48
7	Chlorogenic acid	$C_{16}H_{18}O_9$	Antimicrobial, antidiabetic, antioxidant, anti-obesity, antihypertension	49,50
8	Neochlorogenic acid	$C_{16}H_{18}O_9$	Antioxidant, antifungal, anti-inflammatory and anticarcinogenic effects	51,52
9	Cyanidin 3-*O*-galactoside	$C_{21}H_{21}O_{11}$	Antioxidant, anti-inflammatory, anticancer	53
10	Cyanidin 3-*O*-glucoside	$C_{21}H_{21}O_{11}$	Antioxidant, anti-inflammatory	54–56
11	Kaempferol	$C_{15}H_{10}O_6$	Antimicrobial, antioxidant	57,58
12	Cyanidin 3-*O*-sambubioside	$C_{26}H_{29}O_{15}$	Anticancer, antihypertension, antioxidant, antimicrobial	59,60
13	p-Coumaric acid	$C_9H_8O_3$	Antimicrobial, antioxidant, anticancer	61–63
14	Ferulic acid	$C_{10}H_{10}O_4$	Antioxidant, anti-inflammatory, anticancer, antimicrobial	64,65
15	Pelargonidin 3-*O*-glucoside	$C_{21}H_{21}O_{10}$	Anti-inflammatory, antioxidant	66–68
16	Catechin	$C_{15}H_{14}O_6$	Antioxidant, anticancer, cardiovasculo protective potency	69,70
17	Epicatechin	$C_{15}H_{14}O_6$	Antioxidant, anti-inflammatory, neuroprotective agent	71–73
18	Luteolin	$C_{15}H_{10}O_6$	Anticancer, antiviral	74–77
19	Kaempferol 3-*O*-rutinoside	$C_{27}H_{30}O_{15}$	Antioxidant	78,79
20	Quercetin	$C_{15}H_{10}O_7$	Antioxidant, anti-inflammatory, anticancer	41,80–82

21	Cyanidin 3,5-*O*-diglucoside	$C_{27}H_{31}O_{16}$	Anticancer, antioxidant	[83,84]
22	Cyanidin 3-*O*-sophoroside	$C_{27}H_{31}O_{16}$	Antioxidant, anti-inflammatory, skin hydration effect	[85,86]
23	Quercetin 3-galactoside	$C_{21}H_{20}O_{12}$	Anticancer, anti-inflammatory, antibacterial, antiviral, antidepressant	[87]
24	Isoquercetin	$C_{21}H_{20}O_{12}$	Antioxidant, anti-inflammatory, neuroprotective	[42,88,89]
25	Kaempferol 3-glucoside	$C_{21}H_{20}O_{11}$	Anti-inflammatory, antioxidant, antidiabetic, anticancer, cardioprotective agent, cosmetic use	[90]
26	Cyanidin 3-*O*-rutinoside	$C_{27}H_{31}O_{15}$	Antioxidant, anti-inflammatory	[54,56]
27	Isorhamnetin	$C_{16}H_{12}O_7$	Anticancer, antioxidant	[91,92]
28	Isorhamnetin 3-*O*-rutinoside	$C_{28}H_{32}O_{16}$	Antiviral, antioxidant, antimicrobial, anticancer	[93–95]
29	Peonidin 3-*O*-glucoside	$C_{22}H_{22}O_{12}$	Anti-inflammatory	[96]
30	Isorhamnetin-3-*O*-glucoside	$C_{22}H_{23}ClO_{11}$	Anti-inflammatory, antioxidant, anticancer	[97,98]
31	Naringenin	$C_{15}H_{12}O_5$	Anticancer, antioxidant, anti-inflammatory, antidiabetic, neuroprotective agent	[99,100]
32	Myricetin	$C_{15}H_{10}O_8$	Anticancer, anti-inflammatory, antidiabetic, cardio-cerebrovascular protection agent, anti-neurodegenerative	[101]

Table 0-3. Identification of specialized metabolites in American Elderberry juices through untargeted metabolomics analysis.

No.	Compound	RT (min)	Formula	Adducts	Theoretical Mass	Observed Mass	Δm (ppm)	Identification*
1	Gallic acid	0.73	$C_7H_6O_5$	$[M+NH_4]^+$	170.0215	170.0212	2.1090	b
2	3,4-Dihydroxybenzoic acid	1.38	$C_7H_6O_4$	$[M-H]^-$	154.0266	154.0269	1.8600	b
3	Rutin (quercetin-3-rutinoside)	1.40	$C_{27}H_{30}O_{17}$	$[M-H]^-$	610.1534	610.1537	0.5086	a, b
4	Delphinidin 3-*O*-rutinoside	1.44	$C_{27}H_{31}O_{16}^+$	$[M]^+$	611.1612	611.1616	0.6000	b
5	Caffeic acid	2.24	$C_9H_8O_4$	$[M+H]^+$	180.0423	180.0417	1.9560	b
6	Cryptochlorogenic acid	2.34	$C_{16}H_{18}O_9$	$[M+H]^+$	354.0951	354.0948	1.2440	b
7	Chlorogenic acid	2.34	$C_{16}H_{18}O_9$	$[M+H]^+$	354.0951	354.0948	1.2440	b
8	Neochlorogenic acid	2.34	$C_{16}H_{18}O_9$	$[M+H]^+$	354.0951	354.0948	1.2440	b
9	Cyanidin 3-*O*-galactoside	2.39	$C_{21}H_{21}O_{11}^+$	$[M]^+$	449.1084	449.1078	1.3950	a, b
10	Cyanidin 3-*O*-glucoside	2.39	$C_{21}H_{21}O_{11}^+$	$[M]^+$	449.1084	449.1078	1.3950	b
11	Kaempferol	2.39	$C_{15}H_{10}O_6$	$[M+H]^+$	286.0477	286.0474	1.2554	a, b
12	Cyanidin 3-*O*-sambubioside	2.50	$C_{26}H_{29}O_{15}^+$	$[M]^+$	581.1507	581.1495	1.9020	a, b
13	p-Coumaric acid	2.67	$C_9H_8O_3$	$[M+H]^+$	164.0473	164.0468	2.9680	a, b
14	Ferulic acid	2.76	$C_{10}H_{10}O_4$	$[M+H]^+$	194.0579	194.0575	2.2420	b
15	Pelargonidin 3-*O*-glucoside	2.91	$C_{21}H_{21}O_{10}^+$	$[M]^+$	433.1135	433.1132	0.6510	a, b
16	Catechin	3.13	$C_{15}H_{14}O_6$	$[M+H]^+$	290.0790	290.0786	0.1520	b
17	Epicatechin	3.13	$C_{15}H_{14}O_6$	$[M+H]^+$	290.0790	290.0786	0.1520	a, b
18	Luteolin	4.70	$C_{15}H_{10}O_6$	$[M-H]^-$	286.0477	286.0478	0.1138	a, b
19	Kaempferol 3-*O*-rutinoside	5.11	$C_{27}H_{30}O_{15}$	$[M+H]^+$	594.1585	594.1585	0.2772	b
20	Quercetin	5.14	$C_{15}H_{10}O_7$	$[M+H]^+$	302.0427	302.0424	0.7919	b
21	Cyanidin 3,5-*O*-diglucoside	5.16	$C_{27}H_{31}O_{16}^+$	$[M]^+$	611.1612	611.1613	0.1790	b

22	Cyanidin 3-*O*-sophoroside	5.16	$C_{27}H_{31}O_{16}^+$	$[M]^+$	611.1612	611.1613	0.1790	b
23	Quercetin 3-galactoside	5.24	$C_{21}H_{20}O_{12}$	$[M-H]^-$	464.0955	464.0955	0.1265	b
24	Quercetin-3-glucoside (isoquercetin)	5.24	$C_{21}H_{20}O_{12}$	$[M-H]^-$	464.0955	464.0955	0.1265	b
25	Kaempferol 3-glucoside	6.09	$C_{21}H_{20}O_{11}$	$[M+H]^+$	448.1006	448.1006	1.5000	b
26	Cyanidin 3-*O*-rutinoside	6.10	$C_{27}H_{31}O_{15}^+$	$[M]^+$	595.1663	595.1663	0.0370	b
27	Isorhamnetin	6.46	$C_{16}H_{12}O_7$	$[M+H]^+$	316.0583	316.0580	0.8660	b
28	Isorhamnetin 3-*O*-rutinoside	6.46	$C_{28}H_{32}O_{16}$	$[M+H]^+$	624.1690	624.1691	0.0889	a, b
29	Peonidin 3-*O*-glucoside	6.49	$C_{22}H_{23}ClO_{11}^+$	$[M]^+$	498.0929	463.1242	0.2465	b
30	Isorhamnetin-3-*O*-glucoside	6.49	$C_{22}H_{22}O_{12}$	$[M+H]^+$	478.1111	478.1113	0.3520	b
31	Naringenin	6.54	$C_{15}H_{12}O_5$	$[M+H]^+$	272.0685	272.0684	0.3503	b
32	Myricetin	8.31	$C_{15}H_{10}O_8$	$[M-H]^-$	318.0376	318.0377	0.2884	b

*Procedures employed for the identification or putative identification [102,103]: a. comparison with literature MS/MS tandem mass spectral data using MS-DIAL; b, comparison with MS spectral data or accurate mass using XCMS platform with METLIN library.

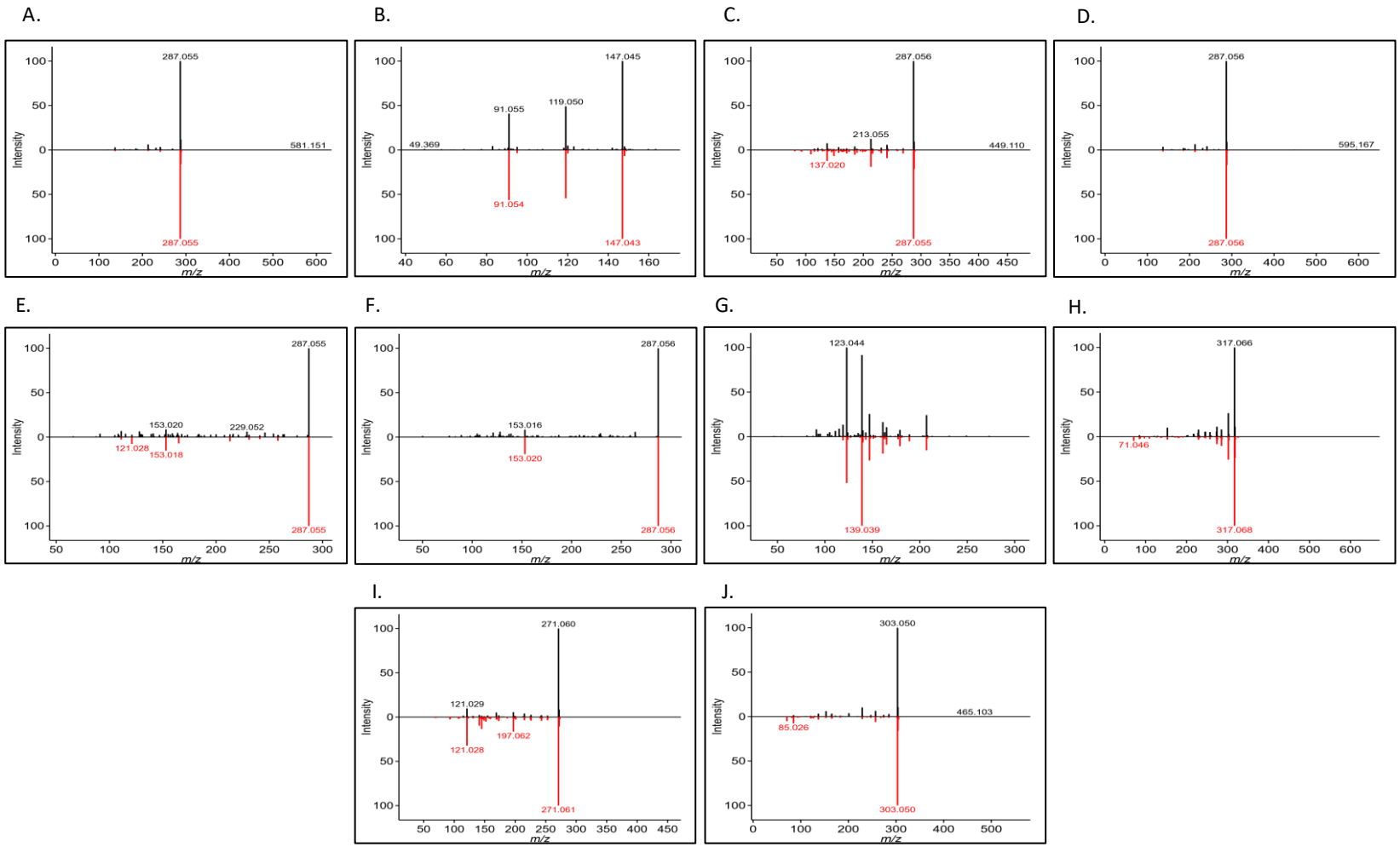

Figure 0-2. Experiment spectrum (in black) versus reference MS/MS tandem spectrum data (in red). A. Cyanidin-3-*O*-sambubioside, B. p-Coumaric acid, C. Cyanidin-3-*O*-galactoside, D. Cyanidin-3-*O*-rutinoside, E. Kaempferol, F. Luteolin, G. Epicatechin, H. Isorhamnetin-3-*O*-rutinoside, I. Pelargonidin-3-*O*-glucoside, J. Quercetin-3-*O*-rutinoside (Rutin).

From the compounds identified, 32 metabolites were selected for further analysis based on their unique relevance to American elderberry (Table 0-2). Several cyanidins, including cyanidin 3-*O*-sophoroside, cyanidin 3-*O*-sambubioside, cyanidin-3-*O*-rutinoside, and cyanidin 3-*O*-galactoside, were putatively identified in elderberry juice. Multiple quercetin derivatives were also detected, such as quercetin, quercetin-3-glucoside (isoquercetin), quercetin-3-rutinoside (rutin), and quercetin-3-galactoside (hyperoside). In addition to cyanidins and quercetins, other polyphenols, including isorhamnetin, kaempferol, luteolin, and myricetin, were also putatively identified. Ten metabolites, catechin, p-coumaric acid, cyanidin-3-*O*-galactoside, cyanidin-3-*O*-rutinoside, cyanidine-3-*O*-sambubioside, epicatechin, isorhamnetin-3-*O*-rutinoside, kaempferol, luteolin, pelargonidin-3-*O*-glucoside, and quercetin-3-*O*-rutinoside (rutin), were further supported by MS/MS spectral matching with reference data (Figure 0-2), hence increasing confidence in their identification. To complement the metabolic analysis, a comprehensive literature review was conducted to summarize the reported biological functions of these compounds (Table 0-2).

Hierarchical clustering of metabolomic profiles from 21 American elderberry genotypes revealed a significant variation in the relative abundance of compounds (Figure A 1). A heatmap of 32 selected metabolites is shown in Figure 0-1D. Cyanidin 3,5-*O*-diglucoside and cyanidin 3-*O*-sophoroside accumulated at higher levels in genotypes 2079, 1911, and 2095, which also exhibit the greatest overall anthocyanins and polyphenol content. In contrast, 3,4-dihydroxybenzoic acid and myricetin were detected at highest relative abundance in genotype 1196, while gallic acid was detected with the highest relative abundance in genotype 2073. The commercial cultivars Ozark and Wyldewood,

displayed moderate accumulation of both anthocyanin and flavonoid, while Bob Gordon showed the lowest levels of metabolites, particularly polyphenols, relative to other genotypes. Notably, cyanidin 3-*O*-glucoside (isoquercetin), cyanidin 3-*O*-galactoside (hyperoside), cyanidin 3-*O*-sambubioside, and kaempferol were accumulated in a subset of genotypes (Bob Gordon, 1076, 1887A, 1069, 1896, 1191, 2085, and 1196), suggesting genotype-specific patterns of metabolite accumulation. Furthermore, quercetin 3-glucoside (isoquercetin) and quercetin-3-rutinoside (rutin) were especially abundant in genotype 1913, highlighting this genotype as a promising candidate for cultivar selection as a potential source of antioxidant or anticancer compounds.

Antioxidant compounds in American elderberry

To validate the bioactive potential of compounds identified in American elderberry, a series of high-throughput screening assay was performed. Putatively identified compounds in American elderberry juice were screened for antioxidant activity at the University of Kansas High Throughput Screening laboratory, Lawrence KS (https://hts.ku.edu/). The total antioxidant capacity (TAC) of American elderberry compounds was performed using CUPRAC methods [33] with Trolox as control. The total antioxidant capacity was expressed as Trolox equivalent, and compounds that showed TAC values greater than 5 Trolox units at any one concentration tested were considered significant. From 32 compounds tested, 14 compounds showed TAC five-fold greater than Trolox, which are quercetin 3-galactoside, cyanidin 3-*O*-sambubioside, quercetin, cyanidin 3-*O*-galactoside, isorhamnetin, myricetin, delphinidin 3-*O*-rutinoside, cyanidin 3-*O*-sophoroside, cyanidin 3-*O*-rutinoside, cyanidin 3-*O*-glucoside, isoquercetin (quercetin 3-

glucoside), cyanidin 3,5-*O*-diglucoside, neochlorogenic acid, and gallic acid (Figure 0-3A).

Of the 32 compounds putatively identified in American elderberry juices, 12 showed TACs ranging from two to 4.9 times greater than Trolox. These compounds are rutin, peonidin 3-*O*-glucoside, caffeic acid, epicatechin, 3,4-dihydroxybenxoic acid, luteolin, kaempferol, catechin, 4-caffeoylquinic acid (cryptochlorogenic acid), chlorogenic acid, isorhamnetin 3-*O*-rutinoside, and pelargonidin 3-*O*-glucoside. Ferulic, acid, naringenin, isorhamnetin 3-*O*-glucoside, p-coumaric acid, kaempferol 3-glucoside, and kaempferol 3-*O*-rutinoside showed TACs in the same range as Trolox.

Putatively identified compounds in American elderberry juices were also evaluated for their ability to activate the Nrf2 transcription factor-ARE signaling pathway in the HepG2 cell line. Four American elderberry compounds (kaempferol, luteolin, quercetin, and isorhamnetin 3-*O*-glucoside), activated ARE activity. At a concentration of 10 μM, kaempferol exhibits the highest level of ARE activation, followed by luteolin, isorhamnetin 3-*O*-glucoside, and quercetin, respectively (Figure 0-3B). All four compounds were found to be non-cytotoxic to the cells (

Figure A 7). Despite their ability to activate the ARE pathway, they may not be potent inducers of the Nrf2-ARE pathway compared to Trolox.

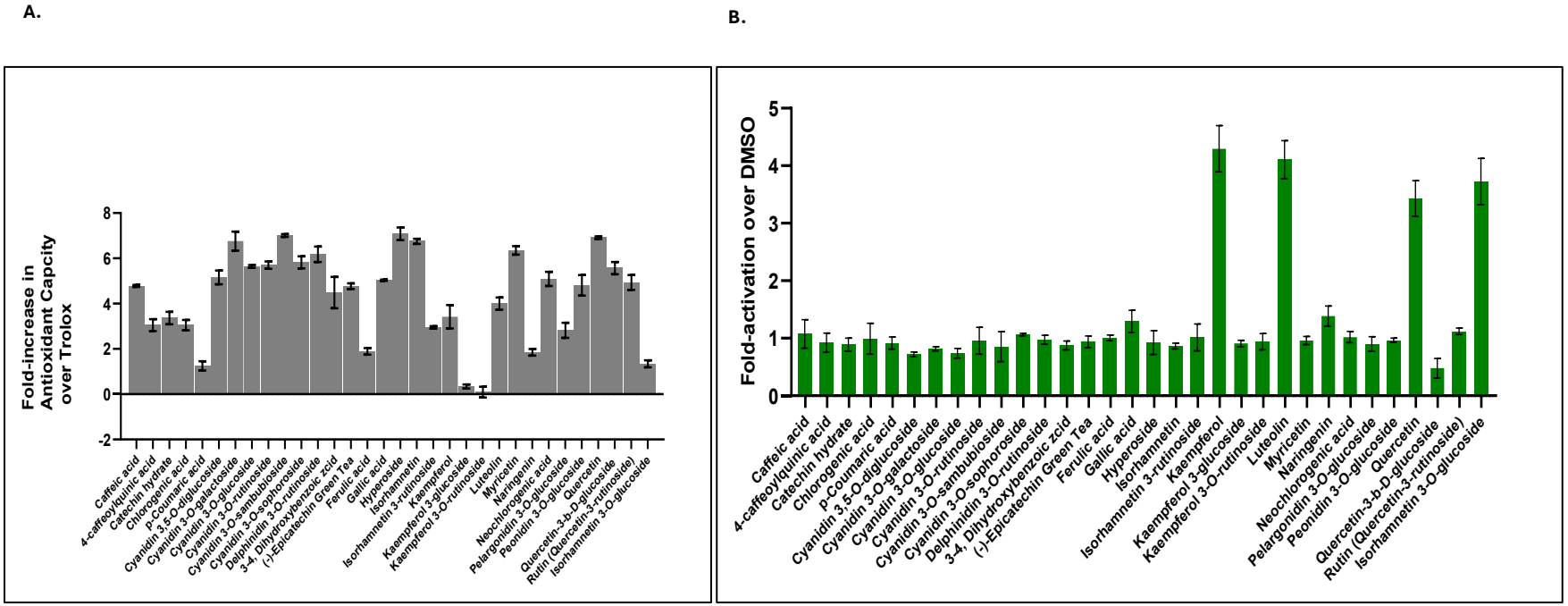

Figure 0-3. Antioxidant activity result. A. Total antioxidant capacity of compounds in American elderberry juices. Data was expressed as Trolox equivalent (n=2). B. Evaluation of American elderberry compound (at a concentration of 10 µM) on activating antioxidant response element (ARE) in HepG2-Nrf2 reporter cell line (n=2).

Antiviral compounds in American elderberry

Thirty-two putatively identified compounds of American elderberry juices were evaluated for their ability to inhibit HIV. Two HIV strains were used: CXCR4-dependent NL4-3 virus and CCR5-dependent BaL virus. Six of the 32 compounds tested (gallic acid, isorhamnetin, kaempferol, luteolin, myricetin, and quercetin) showed significant inhibition of HIV viruses at any one concentration (Figure 0-4). Luteolin showed the strongest inhibition on both strains, with more than 90 percent. The second strongest inhibitor is isorhamnetin, followed by myricetin. both showed more than 50 percent inhibition of HIV viruses at a concentration of 11.1 μM. This suggested that both luteolin and myricetin can inhibit infection of HIV strains that utilize both CXCR4 and CCR5 co-receptors for their entry.

Quercetin and Kaempferol inhibited the HIV strain NL4-3 virus by more than 65 percent but didn't significantly inhibit the HIV strain BaL virus. This suggests that quercetin and kaempferol can inhibit HIV infections that use CXCR4 as their co-receptor during viral entry. Gallic acid showed moderate inhibition of both HIV strains, with about 50 percent at a concentration of 11.1 μM. This suggested that a higher dose of gallic acid was required to inhibit the HIV strains significantly. The half maximal inhibitory concentration (IC_{50}) of all compounds tested against HIV strains NL4-3 and BaL are presented in Table A 3.

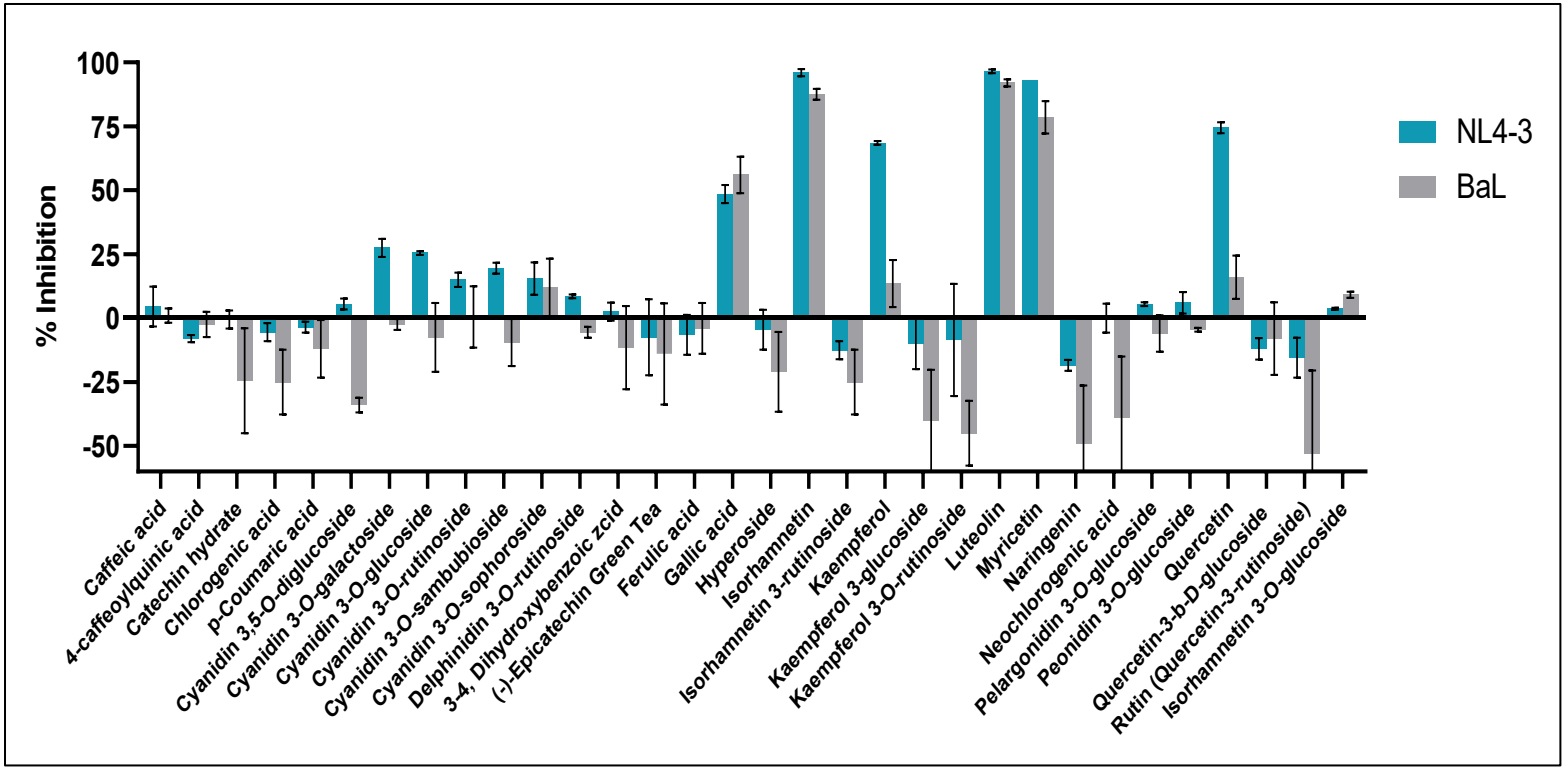

Figure 0-4. Inhibitory activity of American elderberry compounds against HIV strains NL4-3 (in blue) and BaL (in grey) at concentration 11.1µM (n=2).

Based on the anti-HIV assay of American elderberry putative compounds, isorhamnetin, luteolin, kaempferol, quercetin, myricetin, and gallic acid showed dose-dependent antiviral activity against CXCR4-dependent NL4-3 virus and CCR5-dependent BaL virus (Figure A 8). Isorhamnetin has the lowest IC_{50}, with IC_{50} of 0.64 μM ± 0.01 against NL4-3 and 1.77 ± 0.02 μM against BaL-3. Luteolin has IC_{50}s slightly higher of 1.32 μM ± 0.05 and 2.22 ± 0.69 μM against the NL4-3 and BaL viruses, respectively (Table A 3). Kaempferol has IC_{50}s of 2.45 ± 0.28 μM and 8.73 ± 0.70 μM against NL4-3 and BaL viruses, respectively. Isorhamnetin, luteolin, and kaempferol were toxic to cells, with cytotoxicity concentrations of 3.042 ± 0.27 μM, 4.28 ± 0.45 μM, and 11.00 ± 0.62 μM, respectively. Quercetin showed dose-dependent antiviral activity with IC_{50} of 2.49 ± 0.24 μM against NL4-3 virus and 3.84 ± 0.56 μM against BaL virus. Quercetin was toxic to cells at a concentration of 26.41 ± 3.91 μM. Myricetin has IC_{50} of 3.11 ± 0.12 μM and 2.97 ± 1.39 μM against NL4-3 and BaL viruses, respectively. In contrast, gallic acid has IC_{50} of 6.24 ± 0.12 μM and 6.08 ± 0.04 μM against NL4-3 and BaL viruses, respectively. Gallic acid showed cytotoxicity of 80.42 ± 0.57 μM. Only myricetin showed cytotoxicity higher than 100 μM.

Antibacterial compounds in American elderberry

Thirty-two putatively identified American elderberry compounds were evaluated for antibacterial activity against gram-positive and gram-negative bacteria. The gram-positive bacteria strain used for testing was *Staphylococcus aureus* (Figure 0-5). From 32 American elderberry putative compounds evaluated for antibacterial activity against *S. aureus*, three compounds inhibit the growth of *S. aureus* by more than 50 percent at a

concentration of 11.1 μM. These compounds are cyanidin 3-*O*-glucoside, cyanidin 3-*O*-rutinoside, and delphinidin 3-*O*-rutinoside. In higher doses (100 μM), five compounds showed antibacterial activity against *S. aureus*. Those compounds are cyanidin 3-*O*-sambubioside, cyanidin 3-*O*-sophoroside, pelargonidin 3-*O*-glucoside, peonidin 3-*O*-glucoside, and quercetin. Epicatechin showed more than 50 percent inhibition against *S. aureus* at a concentration of 300 μM.

The half maximal inhibitory concentration (IC_{50}) of eight American elderberry putative compounds with significant antibacterial activity against *S. aureus* are presented in Table A 4. Eight American elderberry compounds were found to have antibacterial activity against gram-positive bacteria *S. aureus*, with cyanidin 3-*O*-rutinoside having the most potent antibacterial activity (IC_{50} = 8.44 ± 0.01 μM), followed by cyanidin 3-*O*-glucoside (IC_{50} = 10.27 ± 0.52 μM). Although eight compounds showed antibacterial activity against *S. aureus*, it is still less potent than Vancomycin, an antibiotic used as the positive control.

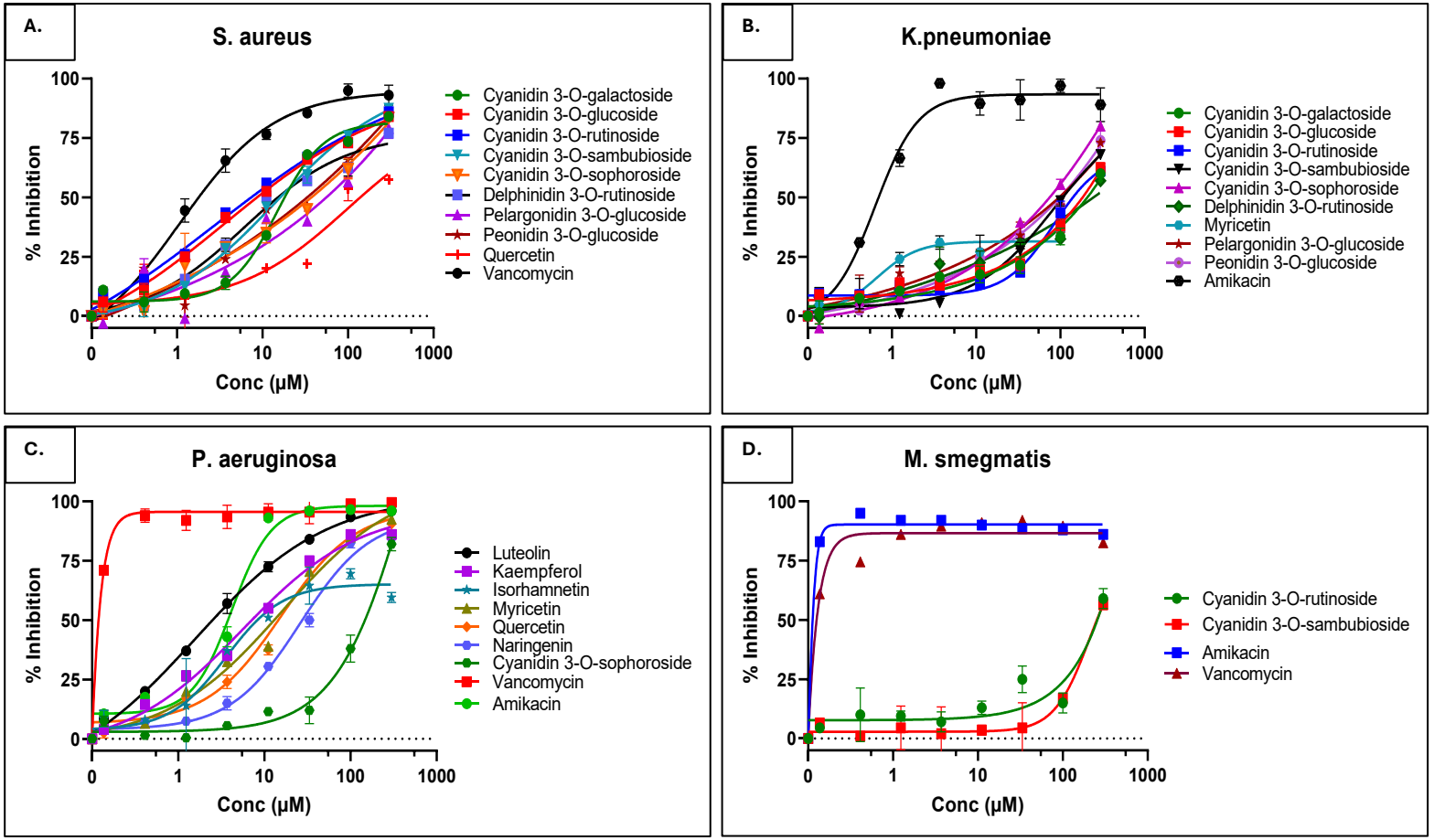

Figure 0-5. Antibacterial activity of American elderberry putative compounds against A. gram-positive bacteria *Staphylococcus aureus*, B. gram-negative bacteria *Klabsiella penumoniae*. C. gram-negative bacteria *Pseudomonas aeruginosa,* D. gram-positive and negative bacteria *M. smegmatis.* The graph showed the activity of two control compounds (Amikacin and Vancomycin) compared with two representatives of American elderberry putative compounds.

Thirty-two American elderberry putative compounds were evaluated for their antibacterial activity against gram-negative bacteria *Klebsiella pneumoniae* (Figure 0-5B) and *Pseudomonas aeruginosa* (Figure 0-5C). The majority of American elderberry putative compounds did not significantly inhibit the growth of *K. penumoniae*. Nine compounds, including cyanidin 3-*O*-sophoroside, pelargonidin 3-*O*-glucoside, and peonidin 3-*O*-glucoside, inhibit the growth of *K. penumoniae* of more than 50 percent at a concentration of 300 μM. It is less potent than the positive control antibiotic, Amikacin. The majority of American elderberry putative compounds did not significantly inhibit the growth of *Pseudomonas aeruginosa*.

Three American elderberry putative compounds, luteolin, kaempferol, and isorhamnetin, showed slightly more than 50 percent inhibition of *Pseudomonas aeruginosa* at a concentration of 11.1 μM. Five compounds showed more than 50 percent inhibition at a higher concentration (100 μM). However, they are still less potent than the positive control antibiotic Vancomycin (IC_{50} = 2.16 ± 0.42 μM). Furthermore, to extend our analysis of the antibacterial activity of American elderberry putative compounds, 32 compounds were assayed against *Mycobacterium smegmatis*, bacteria with gram-positive and gram-negative characteristics. The majority of American elderberry putative compounds did not significantly inhibit the growth of *M. smegmatis* (Figure 0-5D). Only two compounds, cyanidin 3-*O*-rutinoside and cyanidin 3-*O*-sambubioside, showed more than 50 percent inhibition at a high concentration of 300 μM.

DISCUSSION

Traditional bioassay-guided fractionation strategies for characterizing bioactive molecules in natural product are known to be time-consuming, labor intensive, and expensive. Untargeted metabolomics, using UHPLC coupled with high-resolution mass spectrometry (HRMS) in combination with HTS bioassays, has emerged as an powerful alternative to improve the early identification and characterization of metabolites while maximizing the extraction of relevant chemical information [104]. Recent advancement in metabolomics tools, including software, algorithm, computational capacity and spectral databases library, have further promoted the use of this approached for comprehensive compound characterization comparison among multiple groups. In this study, the XCMS and MS-DIAL platforms were utilized to identify putative bioactive compounds in different American elderberry genotypes.

XCMS online, first developed and introduced in 2006 by the Scripps Research Institute, incorporates a metabolomics workflow that includes raw data processing, retention time correction, and metabolite annotations [105]. The current METLIN library integrated within XCMS contains over 1 million molecules with 960,000 MS/MS spectra from pure standards [106], making it one of the most comprehensive platforms for initial metabolites identification. However, despite its extensive library capacity, peak annotations remain challenging, as identification often requires manual assignment of peaks based on the top putative candidates. In addition, limited storage capacity poses difficulties for processing larger datasets. The XCMS-MRM and METLIN-MRM platform (beta version, introduced in 2018) are still not fully integrated, further complicating

identification workflows. Considering both its advantages and limitations, we utilized XCMS online to putatively identify compounds by comparing MS spectral data and accurate mass values with references in the METLIN library. Using this approach, 72 bioactive compounds in American elderberry with reported potential bioactivities were identified in American elderberry (Table 3 and Table A 1).

MS-DIAL, another widely used metabolomics platform, provided a more automated workflow [107]. It annotates metabolites using existing MS and MS/MS spectral libraries, which currently contain approximately 320,000 molecules in positive ion mode and over 50,000 molecules in negative ion mode. Although this spectral library is considerably smaller than the XCMS-METLIN database, MS-DIAL offers automated peak annotation based on retention time, *m/z,* and MS/MS spectral matching, thus providing an additional layer of validation with higher confidence in compounds identification.

In this study, 10 compounds identified in XCMS were confirmed by the MS/MS spectral matching in MS-DIAL (Figure 2), and additional 100 compounds were identified directly through MS-DIAL including acylated anthocyanins. American elderberry has previously been reported to contain acylated anthocyanins, which are more stable and considered non-toxic form of anthocyanins compared to predominantly non-acylated forms found in European elderberry [27]. In this study, we identified at least two acylated anthocyanins in American elderberry juices, namely cyanidin-3-O-sambubioside-5-O-glucoside and cyanidin-3-O-(6"-O-(E-p-coumaroyl)-2"-O-(β-xylopyranosyl)-β-glucopyranoside)-5-O-β-glucopyranoside (Table A 2).

Beyond the 10 overlapping metabolites, compounds identified by XCMS could not be validated in MS-DIAL, likely due to the more limited spectral coverage of the MS-

DIAL library compared to XCMS-METLIN. Other contributing factors may include the complexity of samples matrix which can cause ion suppression, and the low abundance of certain metabolites in the samples. Despite these challenges, more than 100 putative compounds were identified and compared across 21 American genotypes.

Multivariate analyses, including PCA and PLS-DA, were employed to evaluate metabolomic diversity among 21 American elderberry genotypes based on the 127 compounds identified. The PCA analysis revealed both differences and similarity among genotypes, indicating that variation in metabolite composition can distinguish groups based on their metabolic profiles. PLS-DA and k-means clustering further separated the cultivars into three distinct clusters The cultivar Bob Gordon and Wyldewood were clustered together, along with genotypes 1069, 1076, 1887A, 1896, and 2085, suggesting that they share relatively similar metabolomic profiles. In contrast, the cultivar Ozark showed a distinct chemical profile compared with the other genotypes, a finding consistent with previously reported in a previous study [6]. The clustering of other wild genotypes with relatively high anthocyanins content, such as genotypes 2079, 1911, and 2095, suggests that these accessions may serve as valuable sources of antioxidant compounds for future cultivar selection. However, further studies are needed to evaluate the consistency and stability of the metabolites in these genotypes after propagation. Such evaluations will be critical to determine whether these genotypes maintain their unique metabolite signatures under different field conditions and across multiple growing seasons.

To further validate the potential health benefits of American elderberry, we employed standardized HTS protocols. From the 127 putative metabolites identified, 32 were selected for further analysis based on their unique relevance to American elderberry.

This systematic and comprehensive approach enabled the capture of a broad spectrum of metabolites, facilitating the characterization of their antioxidant, antiviral, and antibacterial activities.

Our results demonstrated that several of the selected compounds exhibit strong antioxidant activities (Figure 0-3). Antioxidants are compounds that behave as electron scavengers to neutralize the effects of an excess of oxidants, which occurs due to an imbalance of oxidants over antioxidants that may emerge due to oxidative stress conditions [33]. An electron transfer (ET)- based assay, the CUPRAC assay, was used to measure the total antioxidant capacity (TAC) of the compounds, by quantify their ability to reduce a chromogenic oxidant (probe), which undergo color changes when reduced [33]. Fourteen compounds [quercetin 3-galactoside, cyanidin 3-*O*-sambubioside, quercetin, cyanidin 3-*O*-galactoside, isorhamnetin, myricetin, delphinidin 3-*O*-rutinoside, cyanidin 3-*O*-sophoroside, cyanidin 3-*O*-rutinoside, cyanidin 3-*O*-glucoside, isoquercetin (quercetin-3-D-glucoside), cyanidin 3,5-*O*-diglucoside, neochlorogenic acid, and gallic acid] showed higher TAC values than Trolox, the positive control standard.

To complement these findings, we evaluated whether the 32 compounds could activate the Nrf2-ARE transcriptional pathway in HepG2 cells, a key regulatory pathway of gene expression of antioxidant and detoxification enzymes mediated by the ARE element [108]. Of all the compounds tested, kaempferol, luteolin, isorhamnetin 3-*O*-glucoside, and quercetin activated the Nrf2-ARE transcription pathway though none exceeded the 10-fold activation threshold to be considered as a potent inducer (Figure 3B). Nevertheless, these results indicate that certain flavonoids may modulate Nrf2-ARE signaling.

The antiviral potential of the compounds was also evaluated against two HIV-1 virus strains: the CXCR4-dependent NL4-3 virus and the CCR5-dependent BaL virus. Both CXCR4 and CCR5 serve as critical co-receptors for viral entry into host cells, making them key targets in antiretroviral therapy[109]. Six compounds (isorhamnetin, luteolin, kaempferol, quercetin, myricetin, and gallic acid) exhibit significant antiviral activity against both strains (Figure 4). These findings highlight the potential of American elderberry metabolites as inhibitors of early HIV infection and replication.

In addition, antibacterial activity was assessed against a range of gram-positive and gram-negative bacteria. Eight anthocyanin (cyanidin 3-*O*-galactoside, cyanidin 3-*O*-glucoside, cyanidin 3-*O*-rutinoside, cyanidin 3-*O*-sambubioside, cyanidin 3-*O*-sophoroside, delphinidin 3-*O*-rutinoside, pelargonidin 3-*O*-glucoside, and peonidin 3-*O*-glucoside) inhibited the growth of *Staphylococcus aureus.* Among these, cyanidin 3-*O*-rutinoside showed the strongest activity ($IC_{50} = 8.44 \pm 0.01$ μM), followed by cyanidin 3-*O*-glucoside ($IC_{50} = 10.27 \pm 0.52$ μM). Nevertheless, their potency was lower than that of vancomycin, the antibiotic control. In contrast, most compounds exhibited little or no inhibitory effect against *Klebsiella pneumoniae* and *Pseudomonas aeruginosa*. Similarly, assays against *Mycobacterium smegmatis*, a bacterium with both gram-positive and gram-negative characteristics, showed no inhibitory effect. While some anthocyanins demonstrated antibacterial potential, their efficacy remains modest relative to conventional antibiotics. Further research, including longitudinal studies with repeated doses, is needed to optimize their antibacterial application.

In general, HTS assays identified isorhamnetin, luteolin, and quercetin as particularly promising bioactive compounds in American elderberry juices. Previous

studies have documented a wide range of pharmacological activities for these flavonoids. Isorhamnetin has been reported to exhibit antioxidant, anti-inflammatory, and anticancer activities [91,92], findings consistent to our results of its antioxidant potential. Luteolin, a flavonoid with anticancer potential [75,74], has gained popularity as an antiviral agent against respiratory viruses [77,76]. Notably, this study is the first to demonstrate the ability of luteolin to inhibit HIV-1 replication likely through interaction with viral co-receptor. Quercetin is widely recognized for its diverse bioactivities, including strong antioxidant activities, and in our HTS assays, it exhibited activity across all tests performed. Interestingly, cultivar 1196 showed an accumulation of these three compounds, suggesting its potential as a breeding candidate for enhancing health promoting phytochemicals.

Building of these findings and given the growing popularity of American elderberry as a functional food and dietary supplements ingredient, our results provide important scientific evidence supporting its health-promoting potential. By characterizing the bioactivity of key metabolites, this study enhances the value of American elderberry as functional food and supports its application in nutraceutical. As consumer demand for natural health-promoting products continues to rise, further systematic studies will be essential to translate these findings into practical application, including cultivar selection in plant breeding program tailored to meet the needs of the food and nutraceutical industries.

Despite these promising results, several limitations must be acknowledged. The HTS assays employed in this study were conducted under in vitro conditions, which may not fully reflect the bioavailability, and pharmacokinetics of these compounds in vivo. In addition, the concertation tested may not be achievable through dietary intake alone. To

address these challenges, future research should include animal study to confirm the therapeutic potential of these metabolites and guide their incorporation into functional food and nutraceutical applications.

CONCLUSIONS

This study provides the first comprehensive integration of untargeted metabolomics with HTS bioassays to characterize the phytochemical diversity and bioactive potential of 21 American elderberry genotypes. Using UHPLC-HRMS/MS-based metabolomics, we putatively identified more than 100 metabolites including anthocyanins, flavonoids, and other phenolic compounds. Multivariate analyses showed genotype-depended differences in metabolite composition. Cultivar Ozark and wild accessions such as 2079, 1911, and 2095, displayed distinct chemical profiles while accession 1196 accumulated high levels of bioactive flavonoids. HTS assays highlighted isorhamnetin, luteolin, and quercetin as promising key bioactive compounds. These findings establish a foundation for linking metabolomic diversity to functional bioactivity in American elderberry. Future work should focus on in vivo validation, stability testing in food systems, and integration with genomic tools to guide cultivar selection for food and nutraceutical applications.

CHAPTER 2. EXPLORATION OF AMERICAN ELDERBERRY BIOACTIVE COMPOUNDS FOR INHIBITION OF THE INFLUENZA VIRUS POLYMERASE ACIDIC ENDONUCLEASE

ABSTRACT

Elderberries have been commonly used to relieve symptoms of influenza and the common cold. In this study, the antiviral activity of juices of American elderberry (*Sambucus nigra* subsp. *canadensis*) cultivars were evaluated against the recombinant N-terminal domain of *Influenza* A Polymerase Acidic protein using a Fluorescence Resonance Energy Transfer (FRET)-based endonuclease assay. The American elderberry cultivar Ozark showed the strongest inhibitory activity among 21 cultivars, followed by the wild accession 1196. The juice from four American elderberry cultivars Ozark, accession 1892, 1196, and 2084 demonstrated stronger inhibitory effect against nPA protein (>65% inhibition) compared to the European elderberry cultivar Haschberg, which showed 62% inhibition, suggesting a higher abundance of bioactive compounds in these cultivars, capable of interfering with *Influenza* PA activity. Among the elderberry compounds tested, gallic acid (IC_{50} 11.56 ± 1.80 μM), myricetin (IC_{50} 16.02 ± 0.06 μM), caffeic acid (IC_{50} 22.75 ± 0.9 μM), and luteolin (IC_{50} 27.92 ± 0.72 μM), showed the strongest inhibition of nPA endonuclease activity. These findings support the application of American elderberry in nutraceutical product formulations designed to help manage flu symptoms. To the best of our knowledge, this is the first study elucidating the anti-influenza mode of action of American elderberry against influenza molecular targets.

INTRODUCTION

Influenza is a respiratory pathogen that causes the seasonal flu. Influenza could lead to significant morbidity and mortality worldwide. Although vaccines and antivirals are available, both are hindered by limitations, including restricted treatment windows and the emergence of resistance mutations. These challenges underscore the urgent need for alternative or complementary antiviral strategies that utilize viral targets.

There is a strong societal trend towards the use of natural health products to manage respiratory infections. Elderberry-based supplements, particularly syrups and juices, are widely marketed to alleviate cold and Influenza-like symptoms, reflecting consumer preferences for natural remedies. Previous studies on European elderberry (*Sambucus nigra* subsp. *nigra*) demonstrated the benefit of elderberry consumption on health. A clinical study showed that consumption of elderberry syrup containing elderberry extract reduced the duration and severity of Influenza-like symptoms in adults. [110,111]. Previously, the studies with *in vitro* cell culture reported that elderberry extract not only suppresses *Influenza* replication but also modulates host immune responses, such as enhanced inflammatory cytokine production in host cells [112–114].

The anti-*Influenza* activity of elderberries has become the subject of study, with a primary focus on European elderberries [115–118]. Several antiviral mechanisms of elderberry have been proposed. A previous study utilizing plaque reduction assays demonstrated that the juice of European elderberry showed antiviral effects against *Influenza* by directly interacting with viral surface glycoproteins, hemagglutinin and neuraminidase, hence blocking viral entry [114]. Pre-treatment of viruses with elderberry juice before being exposed

to the cells reduced the *Influenza* infection, while extended exposure of elderberry juice to the cells after *Influenza* infection significantly enhanced antiviral activity, suggesting that elderberry interferes with multiple stages of the viral life cycle. However, the molecular targets underlying antiviral activity on viral replication remain poorly characterized. Moreover, the antiviral properties of American elderberry (*Sambucus nigra* subsp. *canadensis*) have not been well described in comparison to its European relatives.

Based on previous studies, elderberry has been suggested to alleviate the symptoms of influenza, raising the possibility that its bioactive compounds may act by targeting early stages of infection and interfering with the viral transcription mechanism within host cells. During *Influenza* infection, viral mRNA requires both a 5'cap structure and a poly(A) tail to be recognized and transcribed by the host transcriptional machinery. The process to acquire them is mediated by the *Influenza* RNA-dependent RNA polymerase (RdRp) complex. The viral RdRp complex consists of three subunits, Polymerase Basic 1 (PB1), Polymerase Basic 2 (PB2), and Polymerase Acidic (PA) protein. The PA protein is an essential component of the viral RdRp complex, due to the endonuclease active site in its N-terminal domain that is necessary for "cap-snatching" from the hosts' pre-mRNAs to initiate viral transcription [119]. In this mechanism, PB2 would bind to the 5' cap of the host pre-mRNA molecules for PA endonuclease to cleave it off from the host pre-mRNA, and then PB1 has polymerase activity to add it on the viral RNA and generate a capped primer required for initiating transcription in the host cells. The PB1 is also responsible for the addition of a poly(A)tail. The clinical success of baloxavir marboxil, a selective inhibitor of the PA endonuclease, validated this complex as a target for antivirals. Baloxavir binds to the active site of the PA protein, preventing it from cleaving the host RNA [120]. By

blocking the cap-snatching process, baloxavir inhibits virus's ability to replicate and produce new viral particles.

Flavonoids, a diverse group of plant-derived specialized metabolites that have well-documented antiviral activity, are abundant in elderberries. It represents a promising source of diverse small molecules with the potential to inhibit PA endonuclease activity. This study evaluated the antiviral potential of the elderberry juices and bioactive compounds identified in American elderberry against the PA protein of *Influenza* A using a FRET-based endonuclease assay to explore critical bioactive compounds underlying the antiviral effects of elderberry.

MATERIALS AND METHODS

Materials

The cDNA template encoding Influenza A/California/07/2009 (H1N1) PA ORF was purchased from Integrated DNA Technologies (Coralville, IA, USA). StrataClone PCR cloning kit was purchased from Agilent Technologies (La Jolla, CA, USA). The *Escherichia coli* expression host BL21(DE3)RIL competent cells were obtained from Agilent Technologies (La Jolla, CA, USA). Terrific broth expression media, Ni-NTA His-spin columns, and HEPES buffer were purchased from Thermo Fisher Scientific (Waltham, MA, USA). Purification buffers (binding buffer, wash buffer, and elution buffer) were purchased from Zymo (Irvine, CA, USA). Chemical standards of bioactive compounds in American elderberry were purchased from Sigma-Aldrich (St. Louis, MO, USA) but isorhamnetin 3-rutinoside was purchased from Fisher Chemical (Fair lawn, NJ, USA) with purity >95% (Table 0-1).

Table 0-1. List of 32 bioactive compounds identified in American elderberry juices that are used in this study

No.	Compound Name	Sources	Purity
1	Caffeic acid	Sigma-Aldrich	>98%
2	Cryptochlorogenic acid	Sigma-Aldrich	>98%
3	Catechin hydrate	Sigma-Aldrich	>98%
4	Chlorogenic acid	Sigma-Aldrich	>95%
5	p-Coumaric acid	Sigma-Aldrich	>98%
6	Cyanidin 3,5-O-diglucoside	Sigma-Aldrich	>98%
7	Cyanidin 3-O-galactoside	Sigma-Aldrich	>95%
8	Cyanidin 3-O-glucoside	Sigma-Aldrich	>98%
9	Cyanidin 3-O-rutinoside	Sigma-Aldrich	>90%
10	Cyanidin 3-O-sambubioside	Sigma-Aldrich	>95%
11	Cyanidin 3-O-sophoroside	Sigma-Aldrich	>95%
12	Delphinidin 3-O-rutinoside	Sigma-Aldrich	>95%
13	3-4, Dihydroxybenzoic acid	Sigma-Aldrich	>95%
14	Epicatechin	Sigma-Aldrich	>98%
15	Ferulic acid	Sigma-Aldrich	certified reference standard
16	Gallic acid	Sigma-Aldrich	>98%
17	Hyperoside (quercetin 3-galactoside)	Sigma-Aldrich	>95%
18	Isorhamnetin	Sigma-Aldrich	>95%
19	Isorhamnetin 3-rutinoside	Fisher Chemical	>95%
20	Kaempferol	Sigma-Aldrich	>97%
21	Kaempferol-3-glucoside	Sigma-Aldrich	>95%
22	Kaempferol 3-O-rutinoside	Sigma-Aldrich	>95%
23	Luteolin	Sigma-Aldrich	>95%
24	Myricetin	Sigma-Aldrich	>96%
25	Naringenin	Sigma-Aldrich	>95%
26	Neochlorogenic acid	Sigma-Aldrich	>98%
27	Pelargonidin 3-O-glucoside	Sigma-Aldrich	>95%
28	Peonidin 3-O-glucoside	Sigma-Aldrich	>90%
29	Quercetin	Sigma-Aldrich	>95%
30	Isoquercitrin (quercetin-3-glucoside)	Sigma-Aldrich	>90%
31	Rutin (Quercetin-3-rutinoside)	Sigma-Aldrich	>95%
32	Isorhamnetin 3-O-glucoside	Sigma-Aldrich	>98%

Plant material

The American elderberry juices subjected to this study were previously described above. In brief, American elderberry (*Sambucus nigra* subsp. *canadensis*) fruits from 18 propagated accessions and three established cultivars (Table 0-1) were harvested from plantings at the University of Missouri's Southwest Research, Extension, and Education Center near Mt. Vernon, Missouri, USA. The fruits were harvested at peak ripeness and immediately frozen. The fruit was then de-stemmed, thawed at room temperature, and the juice was pressed by hand. It was filtered through a kitchen sieve, aliquoted into 50 mL polypropylene tubes, and re-frozen at -20 °C until further analysis.

The fruits of the European elderberry (*Sambucus nigra* subsp. *nigra*) were of cultivar Haschberg. The seedlings were originally purchased from a local nursery in Portland, Oregon (https://onegreenworld.com/) and cultivated under greenhouse conditions at the University of Missouri, Columbia, MO, USA. The fruits were harvested at full ripeness during the summer of 2024 and immediately frozen. Prior to processing, fruits were de-stemmed, thawed at room temperature, and placed in 15 ml tubes for juice extraction. Berries were gently pressed with a clean spatula to extract juice, which was then centrifuged at 4700 rpm for 10 minutes at 10 °C to separate the pomace. The supernatant was then transferred to a 2 mL Eppendorf tube and stored at -20°C until further analysis.

Gene cloning

PCR amplification of the gene encoding the N-terminal domain of Influenza A/California/07/2009 (H1N1) PA ORF, corresponding to amino acids residues 1-257, was performed with annealing temperature of 53.6 ^{0}C and 55.5 ^{0}C, and extension time for 1

min at 72 ^{0}C. Forward primer sequences containing *XbaI* restriction site (in bold) that were used for PCR in this study were: 5' **TCT AGA** ATG GAA GAC TTT GTG CCGA CAA TG 3'. Reverse primer sequences containing *XhoI* restriction site (in bold) that were used for PCR in this study were: 5' **CTC GAG** AAT TTT GGC GTT CAC TTC TTT TG 3'.

The *npa* gene fragments were then cloned into PCR cloning vector *p*SCA (Agilent Technologies, La Jolla, CA, USA). *E. coli* SoloPack cells were then transformed with *npa* cloned *p*SCA using heat shock method by incubation at 37^{0}C for 5 min and then revivable incubation at 37^{0}C for 1 hour after adding 250 µl of LBroth, for cloning amplification. Gene fragments of *npa* were dropped out of the cloned *p*SCA by the dual digestion of *XbaI* and *XhoI* restriction enzymes (New England Biolabs, Ipswich, MA) and subcloned to a T7 expression vector, *p*ET303 vector plasmid (Invitrogen) in frame with a nucleotide region encoding for a C-terminal 6X-HisTag. The ligation reaction was prepared by mixing the digested vector and the *npa* fragments with T4 DNA ligase (NEB England Biolabs, Ipswich, MA) following the manufacturer's protocol. The ligation reactions were incubated at 16^{0}C overnight. The ligation products were then transferred into *E. coli* competent cells strain DH5α and were inoculated into LB agar media containing 100 µg/mL ampicillin. DNA extraction was performed to purified recombinant plasmids using Wizard *PLUS SV* minipreps DNA purification kit (Promega, Madison, WI, USA). The purified recombinant plasmids were digested by *XbaI* and *XhoI* restriction enzymes and run on the 1% agarose gel containing ethidium bromide. The insertion of the *nPA* gene fragments into *pET303* was confirmed by size, then the clones were sent for sequence verification at MU DNA core facility. The *p*ET303 carrying the nPA ORF was transferred into the T7 expression host *BL21(DE3)RIL* strain for protein expression.

Protein expression and purification

The nPA protein was expressed and purified following as described previously [121] with modification. Overnight cultures were grown in 5 mL of LB broth containing 100 µg/mL ampicillin and 10 µg/mL chloramphenicol and incubated with 200 rpm agitation at 37°C overnight. This starter culture was then used to inoculate 1 L of expression media (Terrific Broth media with 0.2% dextrose, 0.1 mM $MnCl_2$, and 0.1 mM $MgSO_4$) containing 100 µg/ml ampicillin and 10 µg/ml chloramphenicol. The culture was incubated at 37°C with shaking at 180 rpm until an optical density at 600 nm of 0.8 was reached. Expression of nPA protein was then induced by adding IPTG to a final concentration of 1 mM. The induced culture was incubated at 22^0C with agitation at 180 rpm for 16-18 hours. The culture for protein expression was harvested by centrifuged at 5,000 rpm at 4°C for 15 min. The cell pellets were collected and then stored at -80°C for at least 2 hours.

The cell pellets were re-suspended in the cell lysis buffer (50 mM Na_2PO_4, 300 mM NaCl, 10 mM imidazole, 1 mM $MgCl_2$, 2 mM dithiothreitol (DTT), 0.03% Triton-X, pH 7.7) with the addition of Complete EDTA-free protease inhibitor cocktail (Roche, Mannheim, Germany). The cell suspensions were sonicated for 4 cycles of 30 seconds on ice with a 1-minute rest interval. The cell lysate was then centrifuged at 5,000 rpm, at 4 °C for 15 min. The supernatant was transferred into 50 mL centrifuge tubes and incubated with DNase I (Roche, Mannheim, Germany) at a final concentration of 100 µg/mL on ice with low agitation for 1 hour. Cell lysates were then centrifuged at 5,000 rpm and 4°C for 15 minutes. The supernatant was collected as a crude extract.

The recombinant protein was purified by the His-tag at its C-terminus using affinity chromatography. Two of 3-mL His-spin columns (ThermoFisher) were equilibrated with 2-fold of resin bed volume of His-Binding buffer (50 mM Na_2PO_4, 300 mM NaCl, 10 mM imidazole, 1 mM MgCl, pH 7.7, Zymo) for 5 times. Six mL of crude extracts was loaded into each of the His-spin columns and incubated for 30 min at 4^0C with low agitation. The columns were then centrifuged at 700 *X* g for 2 min at 10 °C. The loading steps were repeated until all crude extracts were loaded into the columns. The columns were then washed three times with Wash buffer (50 mM Na_2PO_4, 300 mM NaCl, 50 mM imidazole, 1 mM MgCl, pH 7.7, Zymo) to remove unwanted protein. The recombinant protein was then eluted with Elution buffer (50 mM Na_2PO_4, 300 mM NaCl, 250 mM imidazole, 1 mM MgCl, pH 7.7, Zymo). The elution fractions were pooled and dialyzed against 50 mM HEPES buffer, pH 7.4. Protein concentrations were quantified by the Bradford assay, using BSA as a standard. Western blot analysis was performed to determine the purity of the target protein. The pools containing recombinant nPA protein were analyzed by 4-20% SDS-PAGE and then transferred to PVDF membrane. The membrane was blotted with *Influenza* A PA Polyclonal antibody (1:20,000) as the primary antibody. The HRP-conjugated anti-rabbit IgG was used to attached against the primary antibody. The blot was developed with HRP substrates, and the image was taken by iBright CL750 Imaging System instrument (Invitrogen).

In vitro endonuclease activity assay

A fluorescence resonance energy transfer (FRET)-based endonuclease assay (Figure 0-1) was employed and validated to assess the functionality of the recombinant nPA protein as

described in previously published method [122] with modification. A FRET-based endonuclease assay was set up in Black Costar 96-well microplates. Dual-labeled single-strand DNA oligonucleotide with FAM (fluorophore) and a nonfluorescent quencher conjugated to its 5' and 3' terminals, respectively (5' – 6FAM GGTTCCATGCTATATCTGGGACC MGBNFQ – 3'), synthesized by Thermo Fisher Scientific, was used as substrate (the 23mer ssDNA substrate described in the Figure 0-1).

In a 100 µL reaction, nPA protein of the concentrations (25, 12.5, 6.25, 3.125, and 1.56 µg/mL) of a serial 1:2 dilution was added to the reaction buffer containing 50 mM HEPES buffer (pH 7.8), 150 mM NaCl, and 1 mM $MnCl_2$, along with 200 nM substrate. Wells containing all assay components except the protein were used as background control. The fluorescence signals would be released due to the endonuclease cleavage and measured in BioTek Synergy Neo2 microplate reader at 39 s intervals, over 60 min at 37°C (λ_{ex} = 485 nm, λ_{em} = 535 nm). The gain was set to 50, and the fluorescence emission read for each concentration was background corrected. The slope of relative fluorescence unit (RFU) was plotted against the protein concentration to determine the optimum concentration of nPA protein applied in the endonuclease inhibitory assay.

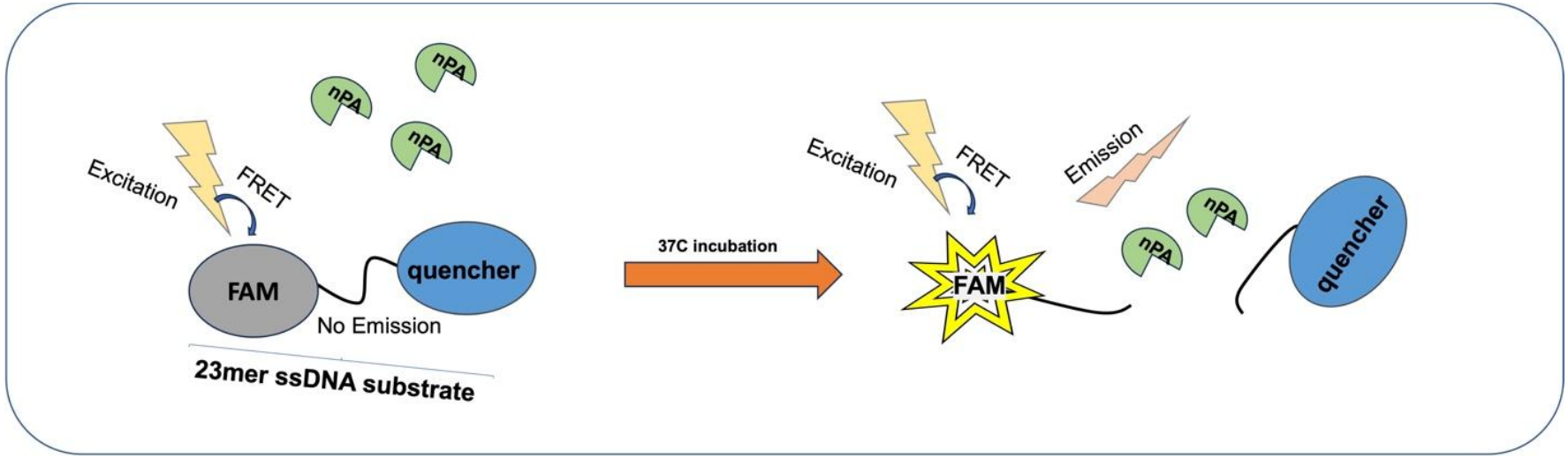

Figure 0-1. Fluorescence resonance energy transfer (FRET)-based endonuclease assay scheme. nPA = N-terminal domain of *Influenza* Polymerase Acidic protein. 23mer ssDNA substrate = single-strand DNA oligonucleotide. FAM = fluorophore.

The FRET-based endonuclease assay was performed to evaluate the antiviral property of the juices of 21 American elderberry cultivars and 1 European elderberry (EEB) cultivar. For sample preparation, 1.5 mL of juice from each elderberry cultivar was centrifuged for 5 min at 10,000 rpm and 10 °C to remove any leftover pomace and precipitate from the juice. The supernatant was transferred to a clean 1.5 mL Eppendorf tube for testing. Ten microliters of the samples were added to the well, followed by the reaction buffer (50 mM HEPES buffer pH 7.8, 150 mM NaCl, and 1 mM $MnCl_2$) and 200 nM substrate in 96-well black microplates. Then, 25 ng/µl of nPA protein was added to each well. Wells containing all assay components except the protein were used as background control. The plate was then placed in the plate reader and run the course of the assay at 37°C for 60 minutes.

Selected 32 bioactive compounds of American elderberry were screened for antiviral activity. Bioactive compounds were dissolved in pure DMSO and serially diluted to 20, 10, and 5 µM. An endonuclease inhibitory assay was carried out using the same method described above. Gallic acid, a known inhibitor of influenza endonuclease activity from a natural product [123], was used as a positive control in this assay. Wells containing all assay components except the protein were used as background control. Wells containing all assay components except the compounds were used as a negative control. Percent of inhibition of each compound was determined by normalizing the slope of fluorescence emission reads to that of the positive and negative controls.

Statistical analysis

The results of the analysis were expressed as means ± SEM (n=2). One-way analysis of variance (ANOVA) with Tukey's multiple comparison test was performed using the R programming language version 4.5.1 to determine significant differences among mean values. Statistical significance was defined at p-value of < 0.001.

RESULTS

The *npa gene* (Figure 0-2) has been successfully cloned into the T7 expression vector pET303 as confirmed by sequence analysis at the MU DNA core facility. The *npa gene* cloned pET303 was subsequently transferred into the expression host *E. coli* BL21(DE3) RIL strain (Figure 0-3A). The recombinant *n*PA protein was expressed in a 2-L culture and then isolated by the His-tag using 6xHis-tag affinity chromatography. Western blot analysis of the purified protein revealed a major band of protein species at ~30 kDa that is the estimate molecular weight of *n*PA protein, confirming the successful expression and purification (Figure 0-3B, red arrow).

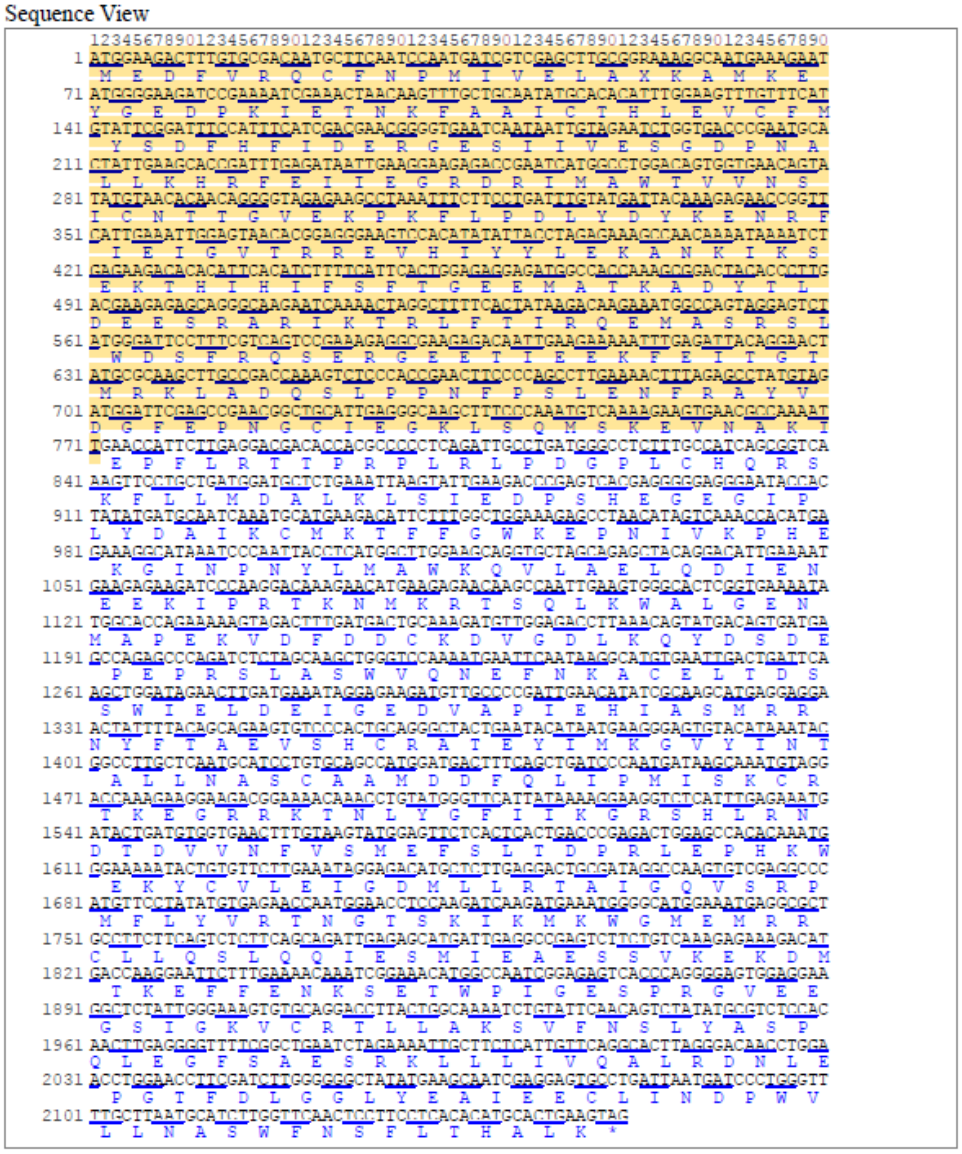

Figure 0-2. *Influenza* A (A/California/07/2009(H1N1)) segment 3 polymerase PA (PA) gene, complete cds (Source: NCBI; NC_026437.1). N-terminal domain of *PA gene* (1-771 bp) is highlighted in yellow.

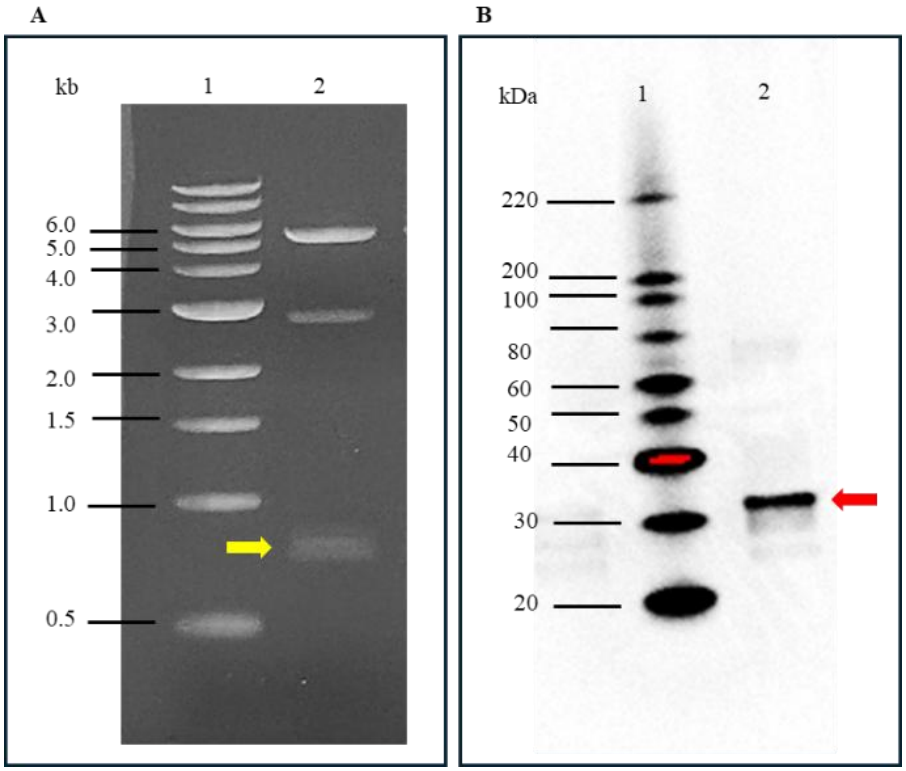

Figure 0-3. A. Analysis of nPA clones (yellow arrow) after XbaI and XhoI restriction enzyme digestion on 1% agarose gel electrophoresis. Lane 1, 1kb DNA ladders; lane 2, npa cloned pET303 isolated from BL21(DE3) RIL. B. Isolated recombinant nPA (red arrow) separated by 4-20% SDS-PAGE, transferred to PVDF membrane and developed against Influenza A PA Polyclonal antibody 1:20,000) as the primary antibody. The HRP-conjugated anti-rabbit IgG was used to attach to the primary antibody. The blot was developed with HRP substrates, and the image was taken by iBright CL750 Imaging System instrument (Invitrogen). Lane 1. protein ladder; lane 2. recombinant nPA protein (Size = 30.58 kDa).

An endonuclease assay method to determine the enzymatic activity of the recombinant nPA protein was established and validated using a FRET-based approach. The fluorescence intensity was recorded in a time course to monitor the cleavage activity of the nPA protein using the single-stranded DNA (ssDNA) substrate. The endonuclease activity of Recombinant nPA protein at varying concentrations was represented by fluorescence intensity RFU in Figure 4A. Enzyme activity was determined from the slope of fluorescence intensity over time using linear regression analysis. The resulting slopes were plotted against nPA protein concentration, demonstrating a positive correlation between enzyme concentration and endonuclease activity (Figure 4B). Protein concentration of 25 µg/ml was chosen for the inhibitory assay. To validate this endonuclease assay method for evaluating the inhibitory potential of natural product-derived compounds, gallic acid was used as a model inhibitor. Gallic acid was tested at varying concentrations of 20, 10, 5, and 0 µM, and the results demonstrated a dose-dependent inhibition of nPA endonuclease activity (Figure 4C), reflected by a decrease in the slope of enzymatic activity (Figure 4D).

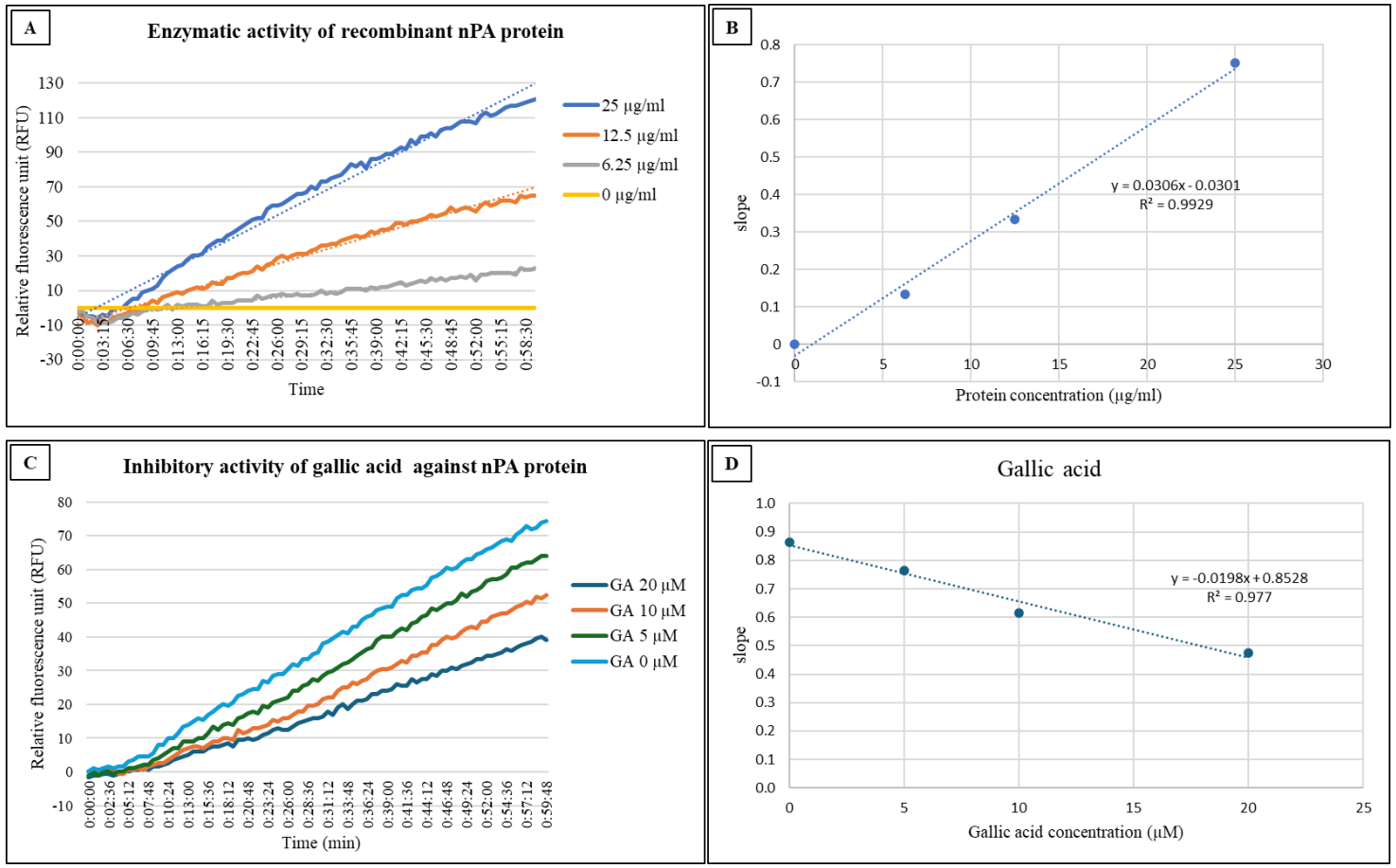

Figure 0-4. Detection of nPA endonuclease activity determined by FRET-based assay. The fluorescence intensity of each reaction was recorded at the indicated time points. (A) Endonuclease activity as a function of nPA protein concentration. The various concentration (25, 12.5, 6.25, and 0 µg/ml) of nPA protein was incubated with 200 nM ssDNA substrate and the fluorescence intensity was measured. (B) A concentration-dependent increase in fluorescence intensity over time, represented as the slope of the linear regression of nPA enzymatic activity. (C). Endonuclease activity as a function of Gallic acid inhibitor concentration. (D) Inhibitory effect of gallic acid at varying concentrations (20, 10, 5, and 0 µM) against nPA endonuclease activity (n=2) presented as the slope of nPA enzymatic activity.

The antiviral activity of elderberry juices from 3 established cultivars and 18 wild accessions of American elderberry cultivars was evaluated using the validated endonuclease inhibitory assay against the recombinant nPA protein produced in this project. All of cultivar juices were tested as undiluted juices due to the complexity of the juice matrix. Results indicated that juices of American elderberry cultivars exhibited varying level of inhibition of nPA endonuclease activity, with juices from cultivar Ozark showing the strongest inhibitory effect, followed by accession 1196 and 2083 with percent inhibition of 97.86% ± 9.42, 81.48% ± 7.68, and 75.73% ± 0.93, respectively. Among the American elderberry cultivars, Bob Gordon, and wild accessions 2084, 2079, 1889A, and 2095, demonstrated moderate inhibition levels of approximately 60%, with percent inhibition of 63.61% ± 4.55, 66.41% ± 8.86, 62.67% ± 4.98, 62.09% ± 0.45, 61.66% ± 1.59, and 60.88% ± 5.86, respectively. Wild accession 1191, 1199, and 1887A showed low inhibition levels below 25%, with inhibition levels of 19.42% ± 10.47, 15.83% ± 11.30, and 11.11% ±11.89, respectively. Interestingly, wild accession 2089 did not show the inhibitory effect.

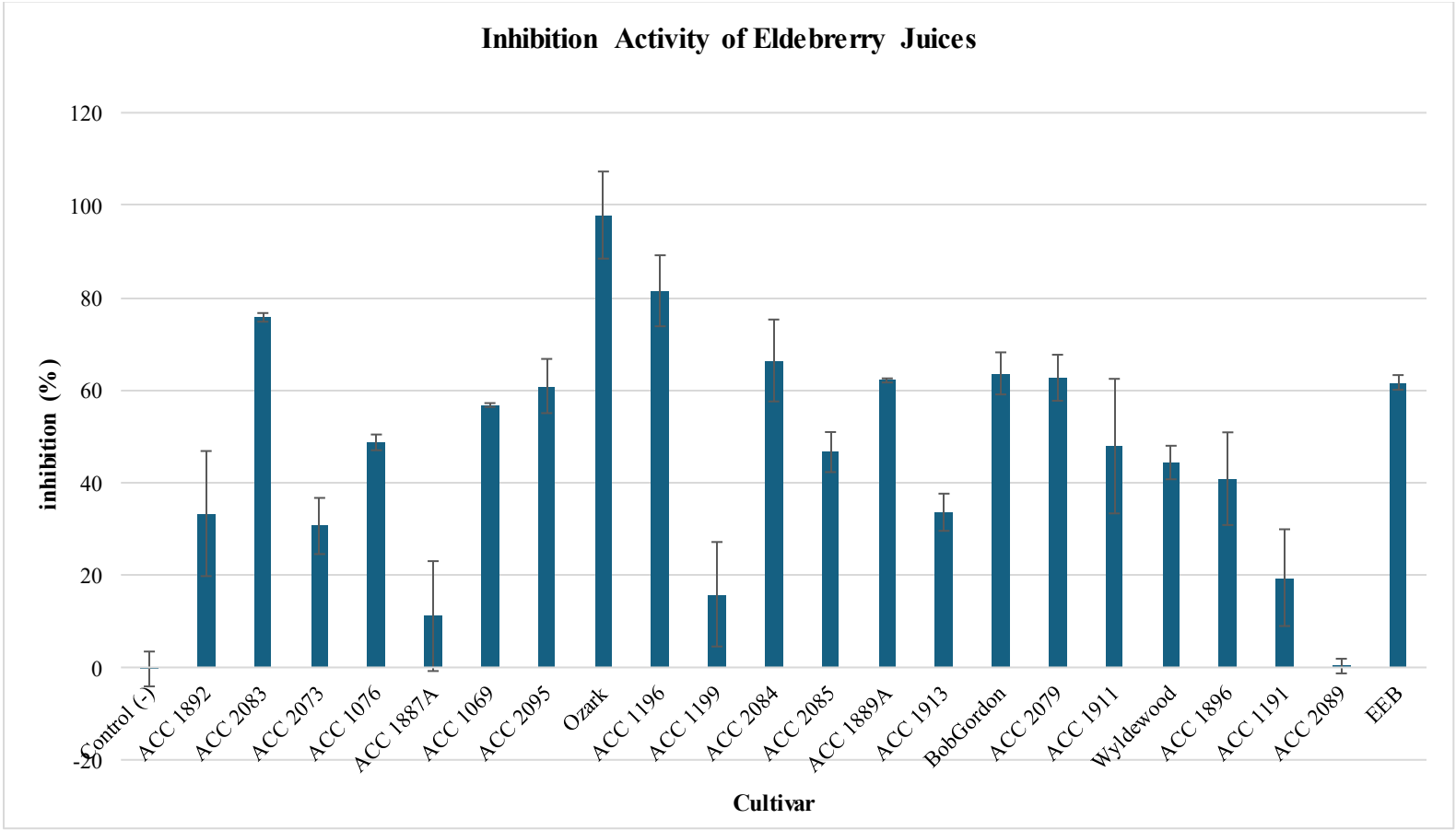

Figure 0-5. Inhibitory effects of elderberry juices from various cultivars on influenza nPA protein. The percentage of inhibitory effect as a function of the species of elderberry cultivars, determined by endonuclease inhibitory assay in duplicate. Data presented as mean ± SEM (n=2). EEB = European elderberry cultivar Haschberg.

In order to compare the antiviral activity of American elderberry with European elderberry, the juice of the European elderberry cultivar Haschberg (EEB) was also tested and exhibited the level of 61.65% ± 1.59 inhibitory effect. The results showed that four of American elderberry juices outperformed European elderberry juice in inhibitory potential to nPA endonuclease in this assay.

To further evaluate the possible bioactive compounds responsible for the antiviral activity of American elderberry juices, 32 bioactive compounds (Table 0-1) previously identified in American elderberry juices were tested using the endonuclease inhibitory assay. These compounds, which included anthocyanins, flavonoids, and other polyphenolic compounds, were selected based on their relevance to American elderberry's unique phytochemical profile and were previously evaluated for their bioactive potential [124]. Testing these compounds provided a more direct assessment of elderberry's ability to inhibit the *n*PA endonuclease activity of *influenza* A virus, hence providing the connection between metabolomic findings and functional antiviral validation.

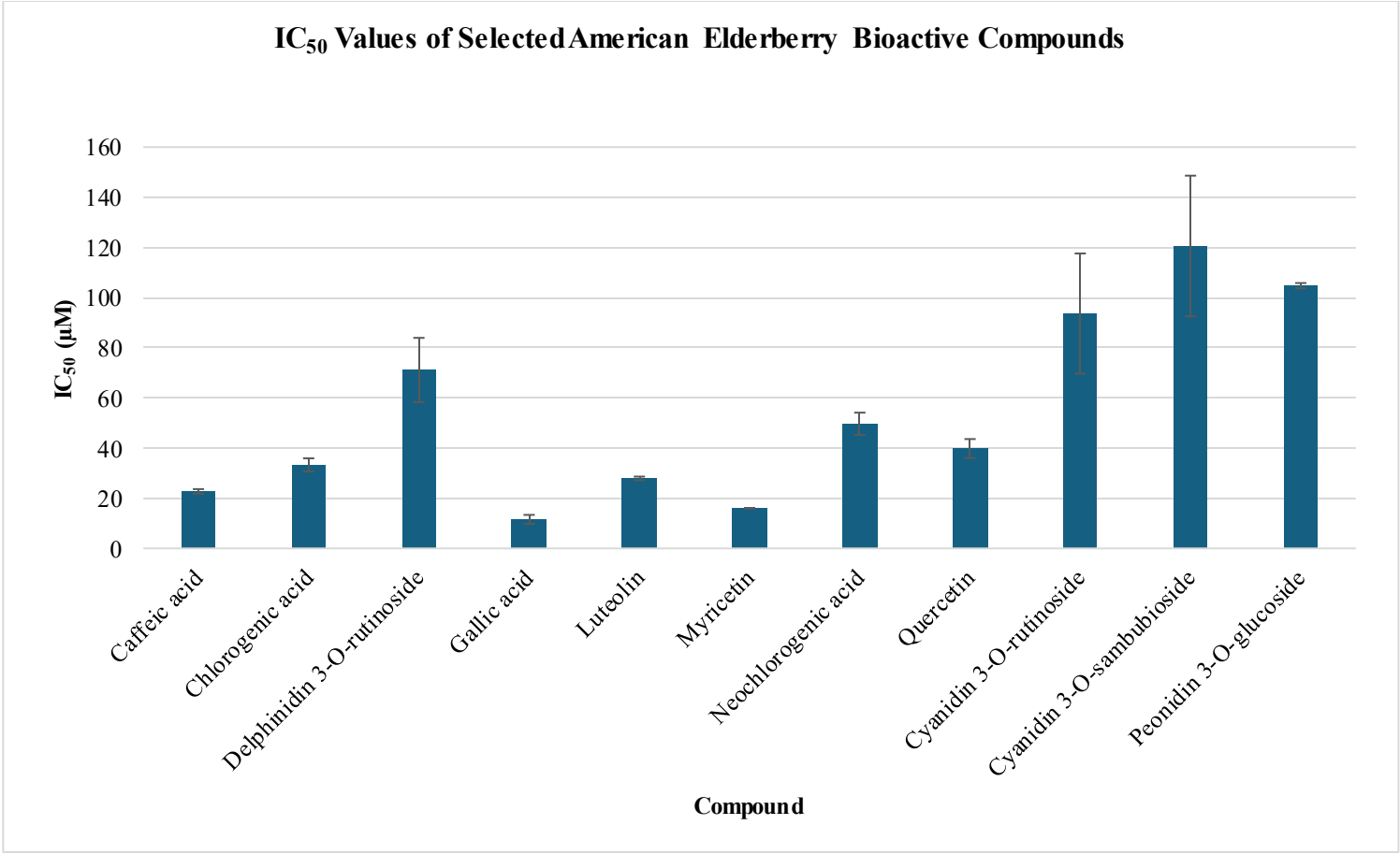

Figure 0-6. The half maximal inhibitory concentration (IC_{50}) values of American elderberry compounds against *Influenza* A *n*PA protein. Data presented as mean value ± SEM (n=2)

Table 0-2. The half maximal inhibitory concentration (IC_{50}) values of bioactive compounds against *Influenza* nPA protein

No.	Compound Name	IC_{50} (µM)	
		AVG	SEM
1	Caffeic acid	22.75	0.90
2	Cryptochlorogenic acid	NI	NI
3	Catechin hydrate	NI	NI
4	Chlorogenic acid	33.28	2.63
5	p-Coumaric acid	NI	NI
6	Cyanidin 3,5-O-diglucoside	NI	NI
7	Cyanidin 3-O-galactoside	NI	NI
8	Cyanidin 3-O-glucoside	NI	NI
9	Cyanidin 3-O-rutinoside	93.64	23.94
10	Cyanidin 3-O-sambubioside	120.60	28.02
11	Cyanidin 3-O-sophoroside	NI	NI
12	Delphinidin 3-O-rutinoside	71.11	12.83
13	3-4, Dihydroxybenzoic acid	NI	NI
14	Epicatechin	NI	NI
15	Ferulic acid	NI	NI
16	Gallic acid	11.56	1.81
17	Hyperoside (quercetin 3-galactoside)	NI	NI
18	Isorhamnetin	NI	NI
19	Isorhamnetin 3-rutinoside	NI	NI
20	Kaempferol	NI	NI
21	Kaempferol-3-glucoside	NI	NI
22	Kaempferol 3-O-rutinoside	NI	NI
23	Luteolin	27.92	0.72
24	Myricetin	16.01	0.06
25	Naringenin	NI	NI
26	Neochlorogenic acid	49.67	4.45
27	Pelargonidin 3-O-glucoside	NI	NI
28	Peonidin 3-O-glucoside	104.75	1.04
29	Quercetin	39.80	3.79
30	Quercetin-3-glucoside (isoquercitrin)	NI	NI
31	Rutin (Quercetin-3-rutinoside)	NI	NI
32	Isorhamnetin 3-O-glucoside	NI	NI

* NI = No inhibition

** Data presented as mean value ± SEM (n=2)

Among the 32 compounds tested, eight compounds showed a dose-dependent inhibition against nPA protein. Each compound was evaluated at three different concentrations (20, 10, and 5 μM), and the half maximal inhibitory concentration (IC_{50}) values were calculated based on the linear regression of the slope of their inhibitory activity. This analysis enabled a quantitative comparison of the inhibitory potency of each compound tested (Figure 6). Two compounds exhibiting the strongest inhibitory activity were classified as phenolic acid (gallic acid) and flavonoids (myricetin). Gallic acid showed the strongest inhibition, with an IC_{50} value of 11.56 ± 1.80 μM, followed by myricetin with an IC_{50} value of 16.02 ± 0.06 μM. Caffeic acid, a phenolic acid, and luteolin, a flavonoid, showed moderate inhibition with IC_{50} values of 22.75 ± 0.9 μM and 27.92 ± 0.72 μM. Other phenolic acids, such as chlorogenic acid and neochlorogenic acid, also displayed inhibitory effects, although with lower potency (IC_{50} values of 33.28 ± 2.664 and 49.68 ± 4.45, respectively). In contrast, most anthocyanins, such as cyanidin-3-*O*-sambubioside and cyanidin-3-*O*-rutinoside, showed IC_{50} values higher than 50 mM, suggesting that flavonoids and phenolic acids may be the primary contributors to the antiviral potential of elderberry (Table 0-2).

DISCUSSION

In this study, we utilized a FRET-based endonuclease assay to evaluate the inhibitory activity of elderberry juices against the *Influenza* A PA protein. This assay has previously been used to screen novel bioactive compounds and shown to be reliable for determining the inhibitory activity of compounds[122,121]. Our results demonstrated that American elderberry juices inhibited *n*PA endonuclease activity, with apparent differences across cultivars that likely reflect the variation in phytochemical composition. Notably, American elderberry juices of cultivars Ozark, accession 1892, 1196, 2084 outperformed European elderberry (*S. nigra* subsp. *nigra,* cultivar Haschberg). These findings suggest that American elderberry could have a more diverse and potentially superior chemical profile compared to its European counterpart, making it a better source of raw material for the production and development of antiviral supplement products. However, the different of growth conditions between the European elderberry and the American elderberry cultivars analyzed in this study should also be taken into consideration, as environmental factors can significantly influence the biosynthesis and accumulation of metabolites in the juices[12].

Previous studies utilizing European elderberry extract as a source of antiviral agents have identified the major anthocyanin, cyanidin 3-glucoside, as a key compound responsible for antiviral activity by inhibiting the viral hemagglutinin glycoprotein, thereby preventing viral attachment to host cells [114]. However, our findings suggested that different classes of metabolites, including flavonoids and phenolic acids, from American elderberry contribute to the antiviral activity against *Influenza* A virus through different mechanisms of action.

In addition to the inhibitory effects observed in the juices, several compounds were found to inhibit *Influenza* PA endonuclease activity, including flavonol compounds, gallic acid, myricetin, and luteolin. The inhibitory activity of gallic acid against influenza PA endonuclease has previously been reported in studies investigating the bioactive compounds of green tea[123]. Interestingly, three isomers, chlorogenic acid, cryptochlorogenic acid, and neochlorogenic acid, demonstrated various levels of inhibition against *n*PA endonuclease activity. This finding suggested potential structural specificity in the interaction between the inhibitor and the active site of the PA N-terminal domain. However, further structural binding analysis is needed to elucidate the precise molecular mechanism underlying this selectivity. In contrast, several anthocyanin compounds that are unique to American elderberries didn't inhibit the *n*PA endonuclease activity (Table 0-2).

Aside from that individual elderberry compounds exhibit inhibitory effects, potential synergistic interactions among multiple metabolites may lead to enhanced antiviral potency. Further studies are needed to elucidate how a combination of multiple metabolites could be optimal to the overall antiviral activity of elderberry. Nevertheless, these findings not only support the inhibitory effects observed at the juice level but also identify chemical scaffolds that can be used in the nutraceutical industry. This study provides the scientific evidence that American elderberry juices and their metabolite constituents interfere with the function of the *Influenza* nPA protein.

CONCLUSION

Elderberry exhibits potent antiviral properties against *Influenza,* acting through inhibition of viral replication mechanisms. This study demonstrated, for the first time, the inhibitory effect of elderberry juice against the nPA protein. The juice of several American elderberry cultivars outperformed the inhibitory potential of European elderberry juice, with the American elderberry cultivar Ozark showing the most potent inhibitory effect. Elderberry compounds gallic acid, myricetin, caffeic acid, and luteolin showed the most potent inhibitory effect against *n*PA endonuclease activity *in vitro.* In contrast, anthocyanin compounds didn't inhibit the *n*PA endonuclease activity. This finding supports the use of American elderberry as a superior raw material for application in nutraceutical formulations that aim at developing a natural product supplement to help manage Influenza symptoms.

CHAPTER 3. QUANTIFICATION OF BIOACTIVE COMPOUNDS IN THE JUICES OF 21 AMERICAN ELDERBERRY CULTIVARS

ABSTRACT

American elderberry (*Sambucus nigra* subsp. *canadensis*) is recognized as a rich source of bioactive compounds with nutritional and therapeutic potential. However, comprehensive quantification of its metabolites remains analytically challenging due to the structural complexity of phenolics and matrix interferences in juice extracts. In this study, a targeted ultra-high performance liquid chromatography-tandem mass spectrometry (UHPLC–MS/MS) workflow was developed and validated to quantify 22 bioactive metabolites, including anthocyanins, flavonoids, and phenolic acids, in juices from 21 American elderberry cultivars. An optimized UHPLC–MS/MS system demonstrated higher sensitivity, selectivity, and throughput than conventional high-performance liquid chromatography-tandem mass spectrometry (HPLC–MS/MS), achieving limits of detection and quantification below 0.1 ng/mL for most analytes. Matrix effects were effectively mitigated through sample dilution, enabling accurate and reproducible quantification across complex juice matrices. Quantification of metabolites showed that accession 1199 exhibited high levels of cyanidin-based anthocyanins, suggesting its utility as a natural food color source. Overall, high-throughput UHPLC–MS/MS method provides a robust analytical framework for metabolomic profiling for cultivar selection and the development of elderberry-derived functional products.

INTRODUCTION

American elderberry (*Sambucus nigra* subsp. *canadensis*) has gained popularity in recent decades as a rich natural source of bioactive phytochemicals with nutritional and therapeutic potential. The chemical composition of elderberries varies substantially among cultivars and plant tissues, suggesting the influence of both genetic and environmental factors on specialized metabolite biosynthesis[7,12,125]. Classes of compounds, including flavonoids, anthocyanins, and polyphenolic acids, were known to contribute to the characteristic dark purple color of elderberry [7,12,27]. Studies on European elderberry have demonstrated broad bioactivity of compounds, including antioxidant[14,15], anti-inflammatory[112], anticancer[19], and antiviral[8]. The chemical diversity within these classes results from various glycosylation, acylation, and methylation patterns that alter solubility, stability, and bioavailability[8]. This structural complexity presents analytical challenges in terms of extraction, separation, and accurate quantification of metabolites.

Comprehensive chemical identification and quantification of plant-derived metabolites is known to be challenging when applied to complex matrices[126]. Traditional analytical practices, such as gas chromatography-mass spectrometry (GC-MS), liquid chromatography with UV detection (LC-UV), and single-quadrupole liquid chromatography-mass spectrometry (LC-MS), are limited by low throughput, limited specificity, and labor-intensive sample preparation. Gas chromatography-mass spectrometry is known to be effective in analyzing volatile and low-polarity compounds[126,127]. The method development process in GC–MS is generally straightforward and easily transferable between instruments due to standardized ionization

techniques and reproducible chromatographic conditions. However, for GC-MS, evaporation and derivatization steps during the sample preparation stage significantly increased the time required for sample preparation[126]. On the other hand, LC-UV methods, though cost-effective and widely applied for quality control, lack the selectivity to distinguish co-eluting isomeric compounds with overlapping UV absorption spectra. The LC-UV is still one of the analytical chemistry techniques that many people use, which can capture a broader range of non-volatile compounds[128–130].

The development of LC-MS methods has addressed many of the limitations associated with traditional analytical techniques. The LC-MS offers greater selectivity and was optimized for the detection of a broad range of compounds[126]. Recent advances in LC separation technology, coupled with tandem mass spectrometry (MS/MS), have significantly increased analytical sensitivity and selectivity[128,126]. Advancements in column technology, such as hydrophilic-lipophilic balanced (HLB), hydrophilic interaction liquid chromatography (HILIC), and high-efficiency C18+ stationary phases, have further improved the resolution and peak capacity of compounds[131].

Matrix interferences remain a common challenge in LC–MS/MS analysis of complex biological and plant-derived samples. These matrix effects (MEs) can alter ionization efficiency and compromise quantification accuracy[132,133]. Incorporating a sample clean-up step, such as solid-phase extraction (SPE), during sample preparation can reduce MEs; however, recovery rates and potential compound losses must be carefully evaluated to ensure accurate quantification[134]. Such dependencies highlight the need for optimized compound-specific extraction and quantification strategies in metabolomic workflows.

Despite these advancements, comparative analysis of American elderberry juices using an optimized high-throughput LC-MS/MS workflow remains limited. Previous studies have focused on a selected group of chemicals, such as cyanidin[7,12,125]. A robust, validated targeted metabolomics approach is therefore needed to quantify a broad range of bioactive compounds across diverse cultivars and to identify genotype-specific metabolic signatures that may inform breeding, product development, and the standardization of elderberry-based nutraceuticals.

This study aimed to develop and validate a streamlined LC-MS/MS workflow for quantifying major bioactive anthocyanins, flavonoids, and phenolic acids in American elderberry juices. Using both high-performance liquid chromatography-tandem mass spectrometry (HPLC-MS/MS) and ultra-high-performance liquid chromatography-tandem mass spectrometry (UHPLC-MS/MS), this study compared analytical performance, evaluated matrix effect, and quantified metabolites in 21 cultivars of American elderberry.

MATERIALS AND METHODS

Chemical

Acetonitrile, and formic acid were purchased from Fisher Chemical (Fair lawn, NJ, USA) and were all LC/MS grade. Methanol for sample extraction were of HPLC-grade and purchased from Sigma-Aldrich (St. Louis, MO, USA). Chemical standards for standard calibration curve were purchased from Sigma-Aldrich (St. Louis, MO, USA) with purity >95%, except caffeic acid, catechin, p-coumaric acid, cyanidin 3,5-*O*-diglucoside, cyanidin 3-*O*-glucoside, epicatechin, gallic acid, neochlorogenic acid, and isorhamnetin 3-*O*-glucoside with purity >98%; kaempferol with purity >97%; myricetin with purity >96%; cyanidin 3-*O*-rutinoside, peonidin 3-*O*-glucoside and isoquercetin with purity >90%; ferulic acid was of certified reference standard grade; and isorhamnetin 3-rutinoside was purchased from Fisher Chemical (Fair lawn, NJ, USA) with purity >95%. The list of compounds was described in Table 0-1.

Plant materials

The elderberry juice samples analyzed in this study have been described above (Table 0-1). American elderberry (*Sambucus nigra* subsp. *canadensis*) fruits from 18 propagated accessions and three established cultivars were harvested from plantings at the University of Missouri's Southwest Research, Extension, and Education Center near Mt. Vernon, Missouri, USA. The fruits were harvested at peak ripeness, and the juice was pressed by hand. The juices were then filtered through a kitchen sieve, aliquoted into 50 mL polypropylene tubes, and were kept frozen at -20 °C until further analysis.

Sample preparation

One mL of raw juice was mixed with three mL of methanol in a glass vial. The mixture was then sonicated for 60 minutes using a sonicator (Fisher Scientific, Pittsburgh, PA, USA). The extract then centrifuged for 30 min at 5000 rpm with temperature set at 10 °C. One mL of juice extract (supernatant) was transferred to a 1.5 mL Eppendorf tubes. The extract was then filter using 25 mm 0.2µm PTFE filter (Acrodisc syringe filter). 100 µL of the juice extract was diluted with methanol to final dilution factor of 800. 1.5 mL of diluted juice extract was then transferred to the LC-MS /MS vial prior to injection to HPLC-MS/MS. 750 µL of the diluted juices extract was further diluted with methanol (1:2, v/v) then transferred to LCMS vial prior to injection to UHPLC-MS/MS.

HPLC-MS/MS Methods

The targeted metabolomic analysis of compound chlorogenic acid and neochlorogenic acid were performed on Waters Alliance 2695 Separation Module High Performance Liquid Chromatography system coupled with a Waters Acquity TQ triple quadrupole mass spectrometer (HPLC-MS/MS) consisting of a quaternary pump, autosampler and a column oven. The analytical column for HPLC was a Phenomenex (Torrance, CA, USA) Kinetex C18 100 Å (100 length x 4.6 mm internal diameter, 2.6 µm particle size) reversed-phase column. Sample injection volume was 30 µl. Column temperature was maintained at 40^{o}C ± 5^{o}C. A linear two-part mobile-phase gradient was used. Mobile phase A consisted of 100% acetonitrile, and mobile phase B consisted of 0.1% formic acid in water. The gradient conditions are: 0 - 0.3 min, 2% A; 0.3 - 7.27 min, 2-80% A (linear gradient); 7.27 – 7.37 min, 80-98% A (linear gradient); 7.37 – 9 min, 98%

A, 9 – 10 min, 98-2% A (linear gradient), and the gradient was maintained at 2% A until 15 min. The flow rate was set at 0.5 mL/min.

To identify the chemical compound in the American elderberry sample, the MS/MS system was operated using electrospray ionization (ESI) in negative ionization mode with capillary voltage of 1.5 kV. The ionization source was programmed at 150°C and the desolvation flow rate was programmed at 750 L h^{-1}. The MS/MS system was operated in multi-reaction monitoring (MRM) mode with parameters as described in Table 0-1. Optimized multiple reaction monitoring (MRM) conditions for the analysis of neochlorogenic acid and chlorogenic acid in HPLC-MS/MS. The Retention time of neochlorogenic acid was around 5.71 min, while the retention time of chlorogenic acid was around 6.07 min.

The MS/MS system was optimized using collision optimization in the MRM mode. The transition ions for molecular and product ions identification, MRM, cone voltage, and collision energy were optimized by Empower 3 Autotune Wizard software package. Analytical data were processed using Waters Empower 3 software (Waters, USA).

UHPLC-MS/MS Method

The concentrations of American elderberry compounds were determined by a Waters Acquity Ultra-High-Performance Liquid Chromatography (Waters, Milford, MA, USA) coupled with a XEVO TQ-XS tandem mass spectrometer (UHPLC-MS/MS, Waters) controlled by MassLynx software Ver 4.2. The compounds were separated by a CORTECS® C18+ analytical column with 1.6 µm particle size, 100 mm length x 2.1 mm internal diameter connected to CORTECS® UPLC C18+ VanGuard Pre-Column (1.6 µm particle size, 5 mm length x 2.1 mm internal diameter). Separation was achieved using a

linear gradient of 0.01% formic acid in water (A) and 0.01% formic acid in 100% acetonitrile (B). The gradient conditions are: 0–0.2 min, 2% B; 0.2–1.89 min, 2–80% (linear gradient) B; 1.89-1.92 min, 80–98% (linear gradient) B; 1.92–3.61 min (linear gradient), 98% B; 3.61–6.77 min, 2% B with a flow rate of 0.4 ml/min. The column temperature was set at 40˚C and the autosampler temperature was set at 10˚C. The system was first conditioned with 50 % acetonitrile and 50% of 0.01% formic acid, and the column was equilibrated with 2% acetonitrile and 98% of 0.01% formic acid solution before injection. The injection volume is 2 µl. The mass analyzer Xevo-TQXS was equipped with an electrospray ionization (ESI) source and operated in positive and negative ion mode. The acquisition parameters for compounds were carried out in the multi-reaction monitoring mode (MRM). Two fragment ions were monitored for quantification of analytes and qualifier as trace ions for confirmation (Table 0-2. Optimized MRM conditions for the analysis of elderberry compounds in UHPLC-MS/MS). The ionization energy, multi-reaction monitoring (MRM) transition ions (precursor and product ions), capillary and cone voltage (CV), desolvation gas flow, and collision energy (CE) were optimized by Waters IntelliStart™ optimization software package. The data was processed, quantified, and reviewed by TargetLynx software Ver 4.2. The optimized ionization, collision energy, and ion selections were described as in Table 0-2. Optimized MRM conditions for the analysis of elderberry compounds in UHPLC-MS/MS.

Method validation

The optimized method was validated for linearity, limit of detection (LOD), and limit of quantification (LOQ), carry-over, and matrix effects. Linearity of each compound was assessed by injection of seven-point calibration curves ranging from 5 to 500 ng mL^{-1}

for analysis in HPLC-MS/MS and from 0.1 to 100 ng mL^{-1} for analysis in UHPLC-MS/MS. LOD and LOQ values were calculated using the following equation:

$$LOD = \frac{3.3 \times Concentration}{Signal/Noise} \qquad \text{(Equation 1)}$$

$$LOQ = \frac{10 \times Concentration}{Signal/Noise} \qquad \text{(Equation 2)}$$

Carry-over was assessed by injecting five solvent-blank samples after the highest calibration standard concentration. To assess the matrix effect (ME) and recovery (RE) of compound in HPLC-MS/MS analysis[135], a standard mixture solution (100 ng mL^{-1}) was added to the 800-fold diluted elderberry juice extract and calculated as

$$ME = [((Css - Cns)/Cstd) -1] \times 100, \qquad \text{(Equation 3)}$$

$$RE = [(Css - Cns)/Cstd] \times 100, \qquad \text{(Equation 4)}$$

where C_{ss}, C_{ns} and C_{std} represent the estimated concentration of the spiked sample, a non-spiked sample, and a spiked standard concentration in the solvent, respectively. To assess the matrix effect in UHPLC-MS/MS analysis, a standard mixture solution (10 ng mL^{-1}) was added to the 1,600-fold diluted elderberry juice extract. The matrix effect and recovery rate of the compound were calculated using equations (3) and (4), respectively.

Statistical analysis

Quantification of analytes in American elderberry juices was performed in three analytical replicates. The results were expressed as mean ± SD. One-way ANOVA was performed using the statistical program R (ver. 4.5.1) to assess significant differences in analyte concentrations between cultivars. Statistical significance was defined at *p*-value of < 0.001. Multivariate analysis was performed using Metaboanlyst ver. 6.0 (https://www.metaboanalyst.ca/).

Table 0-1. Optimized multiple reaction monitoring (MRM) conditions for the analysis of neochlorogenic acid and chlorogenic acid in HPLC-MS/MS

Compound name	MW (g/mol)	Ion mode	RT (min)	Q1 (*m/z*)	Q2 (*m/z*)	Cone (V)	Collision (eV)
Neochlorogenic acid	354.10	ES^-	5.71	352.95	191.3	40	20
Chlorogenic acid	354.10	ES^-	6.07	352.95	191.3	40	20

*Q1 = Molecular ion, Q2 = Product ion (quantifier)

Table 0-2. Optimized MRM conditions for the analysis of elderberry compounds in UHPLC-MS/MS

Compound Name	MW (g/mol)	Ion mode	RT (min)	Q1 (*m/z*)	Q2 (*m/z*)	Cone (V)	Collision (eV)	Q3 (*m/z*)	Cone (V)	Collision (eV)
Cyanidin 3,5-*O*-diglucoside	611.16	ES^+	2.06	611.235	449.152	44	18	287.078	44	36
Cyanidin 3-*O*-sophoroside	611.16	ES^+	2.07	611.235	136.928	50	70	287.078	50	28
Cyanidin 3-*O*-sambubioside	581.15	ES^+	2.09	581.220	287.080	44	28	136.93	44	68
Cyanidin 3-*O*-galactoside / Cyanidin 3-O-glucoside	449.11	ES^+	2.10	449.185	287.085	34	26	136.995	34	54
Cyanidin 3-*O*-rutinoside	595.17	ES^+	2.10	595.181	287.078	58	28	136.929	58	72
Pelargonidin 3-*O*-glucoside	433.40	ES^+	2.14	432.900	271.104	32	30	120.995	32	54
3-4, Dihydroxybenzoic acid	154.03	ES^-	2.15	152.998	108.856	12	14	80.857	12	22
Peonidin 3-*O*-glucoside	463.40	ES^+	2.16	463.202	301.122	28	18	286.034	28	44
Catechin	290.08	ES^-	2.22	289.110	245.037	40	16	202.876	40	20
Epicatechin	290.27	ES^-	2.24	289.110	245.037	46	16	108.897	46	24
Caffeic acid	180.40	ES^+	2.30	181.064	88.986	18	28	162.998	18	8
Delphinidin 3-*O*-rutinoside	611.16	ES^+	2.30	611.171	303.016	50	30	228.991	50	70
Rutin (quercetin-3-rutinoside)	610.50	ES^-	2.30	609.341	300.145	78	36	271.007	78	64
Myricetin	318.23	ES^-	2.33	317.070	150.000	6	28	178.86	6	20
Isoquercetin / hyperoside	464.40	ES^-	2.34	463.177	300.165	60	26	270.964	60	44
Kaempferol 3-*O*-rutinoside	594.50	ES^+	2.35	595.277	287.065	30	20	449.191	30	12
Isorhamnetin 3-rutinoside	624.50	ES^-	2.36	623.330	314.857	74	32	270.95	74	56
Kaempferol 3-glucoside	448.40	ES^+	2.39	449.177	287.082	26	12	153.002	26	48
Isorhamnetin 3-*O*-glucoside	478.40	ES^-	2.40	477.177	314.061	68	28	242.907	68	44
p-Coumaric acid	164.16	ES^-	2.41	163.000	118.941	16	14	92.834	16	26
Ferulic acid	194.18	ES^-	2.45	193.020	133.898	10	16	177.893	10	12
Luteolin	286.24	ES^+	2.61	287.080	134.989	42	32	153.016	42	28

Quercetin	302.23	ES^-	2.62	301.070	150.876	48	22	178.859	48	20
Naringenin	272.25	ES^+	2.72	273.090	153.010	46	20	147.024	46	18
Kaempferol	286.24	ES^+	2.75	287.080	120.997	46	30	153.016	46	32
Isorhamnetin	316.26	ES^-	2.79	315.100	300.000	56	22	150.89	56	28

*Q1 = Molecular ion, Q2 = Product ion (quantifier), Q3 = Trace ion (qualifier)

RESULTS

The analytes in this study were analyzed using HPLC–MS/MS and UHPLC–MS/MS platforms. Based on the calculated limits of detection (LOD) and quantification (LOQ), the UHPLC–MS/MS system demonstrated better sensitivity and overall performance (Table 0-3. Calculated LOD and LOQ of selected analytes as measured in HPLC-MS/MS and UHPLC-MS/MS). However, chlorogenic acid (CGA) and neochlorogenic acid (NCGA) were not detected by UHPLC–MS/MS, likely due to the differences in column chemistry and mobile-phase composition. Furthermore, evidence of matrix effect (ME) was observed on several analytes when analyzed by HPLC-MS/MS (data not shown). To minimize this effect, samples were further diluted. Because dilution reduces analyte concentration, the use of a more sensitive analytical platform was essential to maintain the detection capability. This approach effectively reduced MEs to below 20% for most analytes, except for quercetin (Table 0-4 and Table 0-5). Nevertheless, all quantitative results were corrected by the estimated MEs value. All compounds except CGA and NCGA were quantified using UHPLC–MS/MS, while these two phenolic acids were analyzed using HPLC–MS/MS.

Method optimization for each analyte was performed with Waters IntelliStart™ software to generate product ions and optimize multiple reaction monitoring (MRM) parameters (Table 0-1). The method optimized for CGA and NCGA was performed using the AutoTune Wizard package in Empower3 software, and the optimized method parameters are presented in Table 0-2. An example of ion spectra generated for cyanidin 3,5-*O*-diglucoside by Waters IntelliStart™ software is shown in Figure 0-1. Ion spectra

generated by the Waters Intellistart software package of the molecular ion *m/z* 611.235 and product ions at *m/z* 449.152 and *m/z* 287.078 for the analysis of cyanidin 3,5-*O*-diglucoside in positive ion mode.. The molecular ion *m/z* 611.235 was detected in positive ionization mode, corresponding to the protonated ion $[M]^+$ of cyanidin 3,5-*O*-diglucoside. Fragmentation of this precursor ion produced product ions at *m/z* 449.152 and *m/z* 287.078, corresponding to the sequential loss of one and two glucose moieties, respectively. The fragment *m/z* 287.078 corresponds to the aglycone cyanidin, which is a characteristic of cyanidin-based anthocyanins. This fragmentation pattern is consistent with previous reports that characterized cyanidin derivatives in dried red hybrid-tea rose petals using high-mass-accuracy, multi-dimensional fragmentation analysis by liquid chromatography–electrospray ionization–ion trap–time of flight mass spectrometry (LC–ESI–IT–TOF–MS)[136].

Two cyanidin isomers, cyanidin 3-*O*-galactoside and cyanidin 3-*O*-glucoside, could not be chromatographically separated due to the identical retention time and fragmentation patterns; hence, the quantification of these analytes should be considered as the sum of two isomeric compounds. Similarly, quercetin derivatives, isoquercetin and hyperoside, which differ only in the attached sugar moiety, were not chromatographically resolved under the current analytical conditions, and their quantification was likewise reported as the sum of the two isomeric compounds.

Table 0-3. Calculated LOD and LOQ of selected analytes as measured in HPLC-MS/MS and UHPLC-MS/MS

Compound name	HPLC-MS/MS		UHPLC-MS/MS	
	LOD*	LOQ*	LOD*	LOQ*
3-4, Dihydroxybenzoic acid	1.26	4.15	1.36	4.50
Caffeic acid	0.38	1.26	0.51	1.68
p-Coumaric acid	1.32	4.34	0.24	0.80
Quercetin	0.72	2.37	0.14	0.43
Kaempferol	0.18	0.58	0.02	0.05
Naringenin	0.08	0.26	0.02	0.06
Cyanidin 3,5-O-diglucoside	3.13	10.34	0.06	0.21

*LOD and LOQ concentrations are in $\mu g\ L^{-1}$

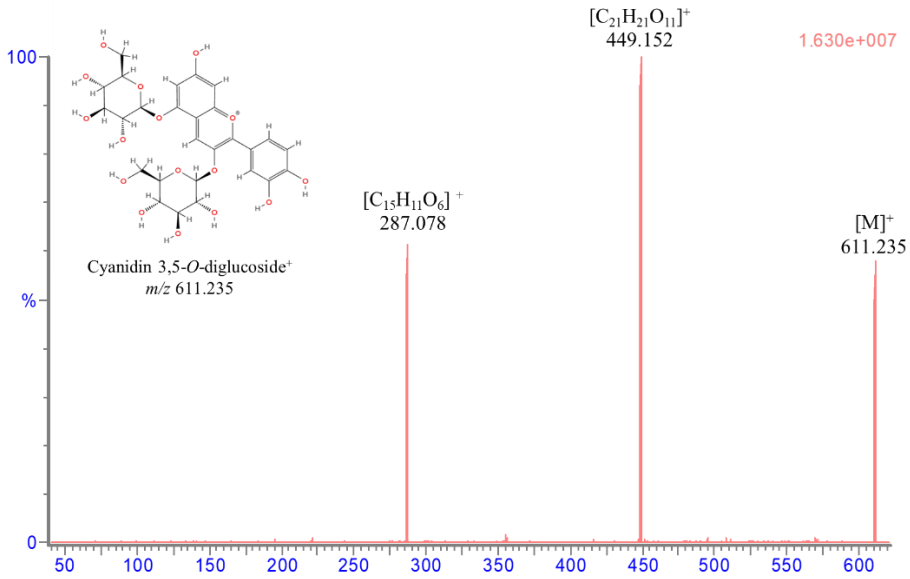

Figure 0-1. Ion spectra generated by the Waters Intellistart software package of the molecular ion *m/z* 611.235 and product ions at *m/z* 449.152 and *m/z* 287.078 for the analysis of cyanidin 3,5-*O*-diglucoside in positive ion mode.

Table 0-4. Calculated LOD, LOQ, and mean recovery of matrix effect of analytes for spike concentrations of 100 µg L^{-1} measured by HPLC-MS/MS

No	Compound name	LOD (µg L^{-1})	LOQ (µg L^{-1})	ME (%)	RE (%)	R^2
1	Neochlorogenic acid	3.39	11.21	-8.44 ± 7.24	91.56 ± 7.24	0.999
2	Chlorogenic acid	3.66	12.10	-1.78 ± 21.09	106.24 ± 21.09	0.998

*+ ME implies ion enhancement, – ME implies ion suppression

**Data presented as mean ± SD

Table 0-5. Calculated LOD, LOQ, and mean recoveries of matrix effect of analytes for spike concentrations of 10 µg L^{-1} measured by UHPLC-MS/MS

No	Compound name	LOD (µg L^{-1})	LOQ (µg L^{-1})	ME (%)	RE (%)	R^2
1	Cyanidin 3,5-*O*-diglucoside	60.69	200.26	-1.42 ± 9.99	98.58 ± 9.99	0.9996
2	Cyanidin 3-*O*-sophoroside	24.56	81.04	-9.01 ± 9.55	90.99 ± 9.55	0.9999
3	Cyanidin 3-*O*-sambubioside	41.63	137.39	-11.91 ± 9	88.09 ± 9	0.9999
4	Cyanidin 3-*O*-galactoside / Cyanidin 3-O-glucoside	46.38	153.04	-7.02 ± 10.14	92.98 ± 10.14	0.9998
5	Cyanidin 3-*O*-rutinoside	55.54	183.25	-17.26 ± 3.19	82.74 ± 3.19	0.9995
6	Pelargonidin 3-*O*-glucoside	5.06	16.66	-5.21 ± 2.55	94.79 ± 2.55	0.9994
7	3-4, Dihydroxybenzoic acid	1360.54	4489.79	-2.27 ± 4.26	97.73 ± 4.26	0.9993
8	Peonidin 3-*O*-glucoside	43.76	144.40	-8.22 ± 1.84	91.78 ± 1.84	0.9996
9	Catechin	329.44	1087.17	-12.76 ± 19.09	87.24 ± 19.09	0.9966
10	Epicatechin	319.79	1055.30	-8.96 ± 6.95	91.04 ± 6.95	0.9989
11	Caffeic acid	511.18	1686.90	4.61 ± 5.31	104.61 ± 5.31	0.9990
12	Delphinidin 3-*O*-rutinoside	56.10	185.14	-5.8 ± 27.02	94.2 ± 27.02	0.9983
13	Rutin (quercetin-3-rutinoside)	0.21	0.69	10.54 ± 23.51	110.54 ± 23.51	0.9988
14	Myricetin	155.34	512.62	3.94 ± 13.21	96.06 ± 13.21	0.9937
15	Isoquercetin/hyperoside	0.03	0.13	1.73 ± 2.13	101.73 ± 2.13	0.9990
16	Kaempferol 3-*O*-rutinoside	0.03	0.13	-4.85 ± 4.73	95.15 ± 4.73	0.9995
17	Isorhamnetin 3-rutinoside	4.34	14.30	-1.46 ± 3.76	98.54 ± 3.76	0.9988
18	Kaempferol 3-glucoside	0.80	2.64	-1.94 ± 2.79	98.06 ± 2.79	0.9996
19	Isorhamnetin 3-*O*-glucoside	1.34	4.43	-6.39 ± 2.37	93.61 ± 2.37	0.9984
20	p-Coumaric acid	240.61	793.98	-10.1 ± 4.52	91.32 ± 4.52	0.9994
21	Ferulic acid	6.06	20.03	-4.37 ± 1.24	95.63 ± 1.24	0.9999
22	Luteolin	97.57	321.95	-7.27 ± 3.52	92.73 ± 3.52	0.9988
23	Quercetin	132.48	437.20	39.1 ± 21.31	139.1 ± 21.31	0.9982

24	Naringenin	14.11	46.59	-7.41 ± 3.23	92.59 ± 3.23	0.9989
25	Kaempferol	18.45	60.88	-9.08 ± 14.3	90.92 ± 14.3	0.9989
26	Isorhamnetin	5.38	17.73	19.24 ± 6.84	119.24 ± 6.84	0.9989

*+ ME implies ion enhancement, – ME implies ion suppression

A B

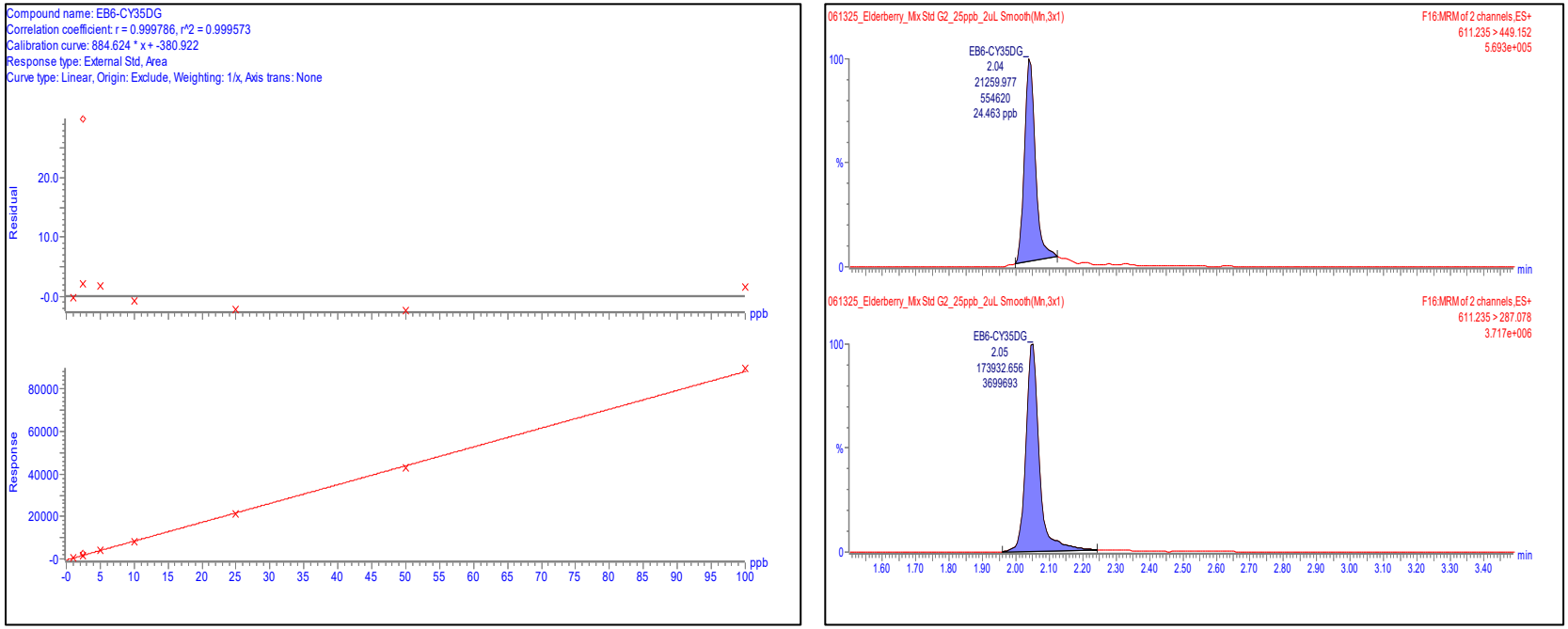

Figure 0-2. Analysis of compound cyanidin 3,5-*O*-diglucoside. A. Standard calibration curve ($R^2 = 0.9996$). B. Ion chromatogram of compound at RT 2.05 min.

For quantification of analytes in American elderberry juices, seven-point calibration curves ranging from 5 to 500 μg L^{-1} for analysis in HPLC-MS/MS and from 0.1 to 100 μg L^{-1} for analysis in UHPLC-MS/MS were used. Standard calibration curves showed good linear correlations (R^2 values >0.998) between integrated peak areas and known compound concentrations. An example of a standard calibration curve is shown in Figure 0-2A with an integrated peak at RT 2.05 min for the quantification of compound cyanidin 3,5-*O*-diglucoside (Figure 0-2B).

An attempt to quantify myricetin in American elderberry juices was carried out using both HPLC-MS/MS and UHPLC-MS/MS systems; however, the compound exhibited poor stability and was found to be degraded relatively quickly, even in stock standard solutions. This instability is consistent with a previous report describing the susceptibility of myricetin and related flavonols to oxidation under ambient conditions[137]. Therefore, the quantification of myricetin was excluded from the analysis.

Juices from 21 American elderberry cultivars were analyzed and quantified for their concentrations of three major classes of compounds: anthocyanins, phenolic acids, and flavonoids. The results were presented in Figure 0-3, Figure 0-4, and Figure 0-5 for the quantification of anthocyanins, phenolic acids, and flavonoids, respectively. The results showed that cyanidin-3-O-rutinoside was detected only in accession 1199, with a concentration of 2.54 ± 0.12 mg/L. Cyanidin-3-*O*-sophoroside was found to be the highest in accession 1896. Cyanidin-3-*O*-glucoside was detected in 5 accessions, with the highest concentration found in accession 1199, followed by accession 2083. Phenolic acid compounds were found to be the most abundant in accession 1196, although CGA and NCGA were not detected in this accession. In contrast, the flavonoid compound

isorhamnetin 3-rutinoside was found to be the highest in cultivar Ozark. Compounds pelargonidin 3-*O*-glucoside, peonidin 3-*O*-glucoside, catechin, epicatechin, and luteolin were not detected in any of the samples. Concentration of bioactive in the juice of American elderberry is presented in Table A 5, Table A 6, and Table A 7.

An unsupervised multivariate analysis, principal component analysis (PCA), was performed to explore overall patterns in the metabolite profile of American elderberry (Figure 6A). The PCA results showed separation among cultivars, indicating differential metabolic profiles between groups. Two principal components (PCs) explained 69.1% of the total variability, with the first principal component (PC1) explaining 48.1% of the data variability and the second PC (PC2) accounting for 21% of the data variability. A supervised model, partial least-squares discriminant analysis (PLS-DA)[37], was applied to further resolve group-specific differences (Figure 6B). PLS-DA model revealed significant discrimination among American elderberry cultivars, with two components explaining 61.1% of the total variance (PC1: 44.3%; PC2: 16.8%). Notably, accession 1896 clustered distinctly from the other cultivars, suggesting substantial differences in its metabolite composition. Cultivar Ozark also clustered separately from the other cultivars, indicating a distinct metabolite composition. This observation is consistent with previous studies employing untargeted metabolomic approaches, which similarly reported unique chemical profiles for Ozark compared to other American elderberry genotypes[26,124]

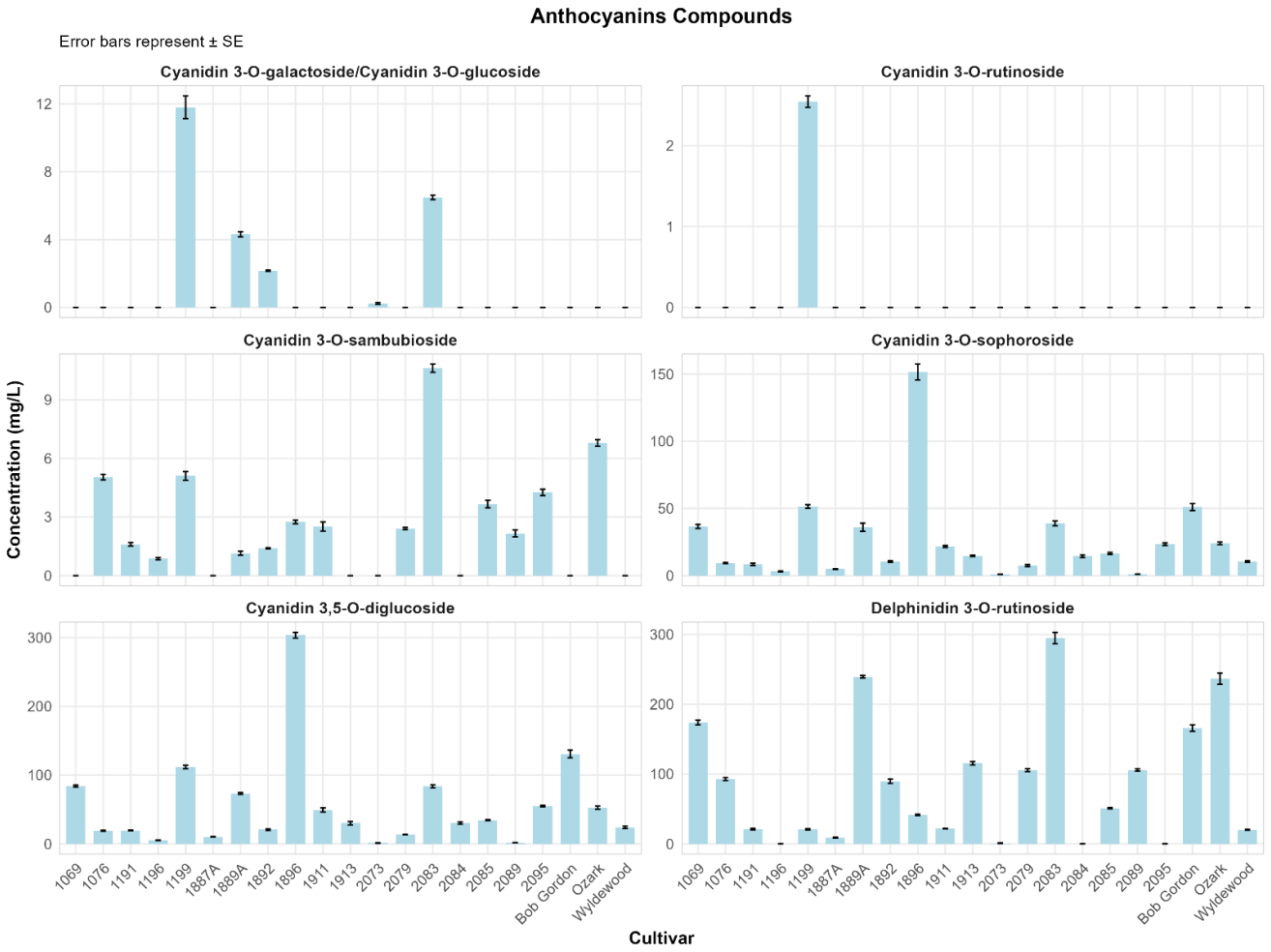

Figure 0-3. Mean concentration (mg L^{-1}) of anthocyanin compounds quantified in the juice of American elderberry cultivars measured by UHPLC-MS/MS. Results were presented as mean value ± standard error (n=3).

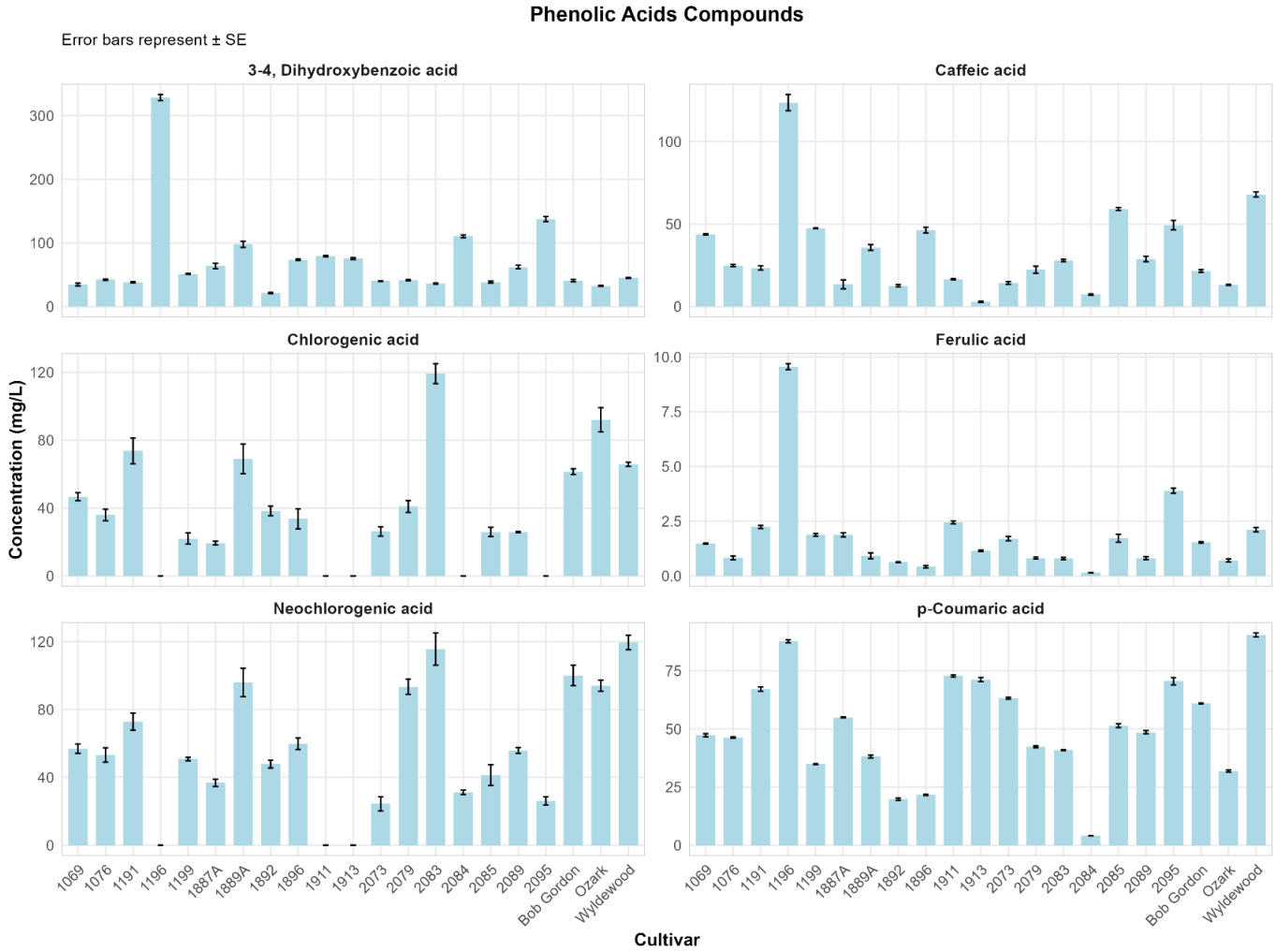

Figure 0-4. Mean concentration (mg L^{-1}) of phenolic acid compounds quantified in the juice of American elderberry cultivars measured by UHPLC-MS/MS and HPLC-MS/MS. Results were presented as mean value ± standard error (n=3).

Figure 0-5. Mean concentration (mg L^{-1}) of flavonoid compounds quantified in the juice of American elderberry cultivars measured by UHPLC-MS/MS. Results were presented as mean value ± standard error (n=3).

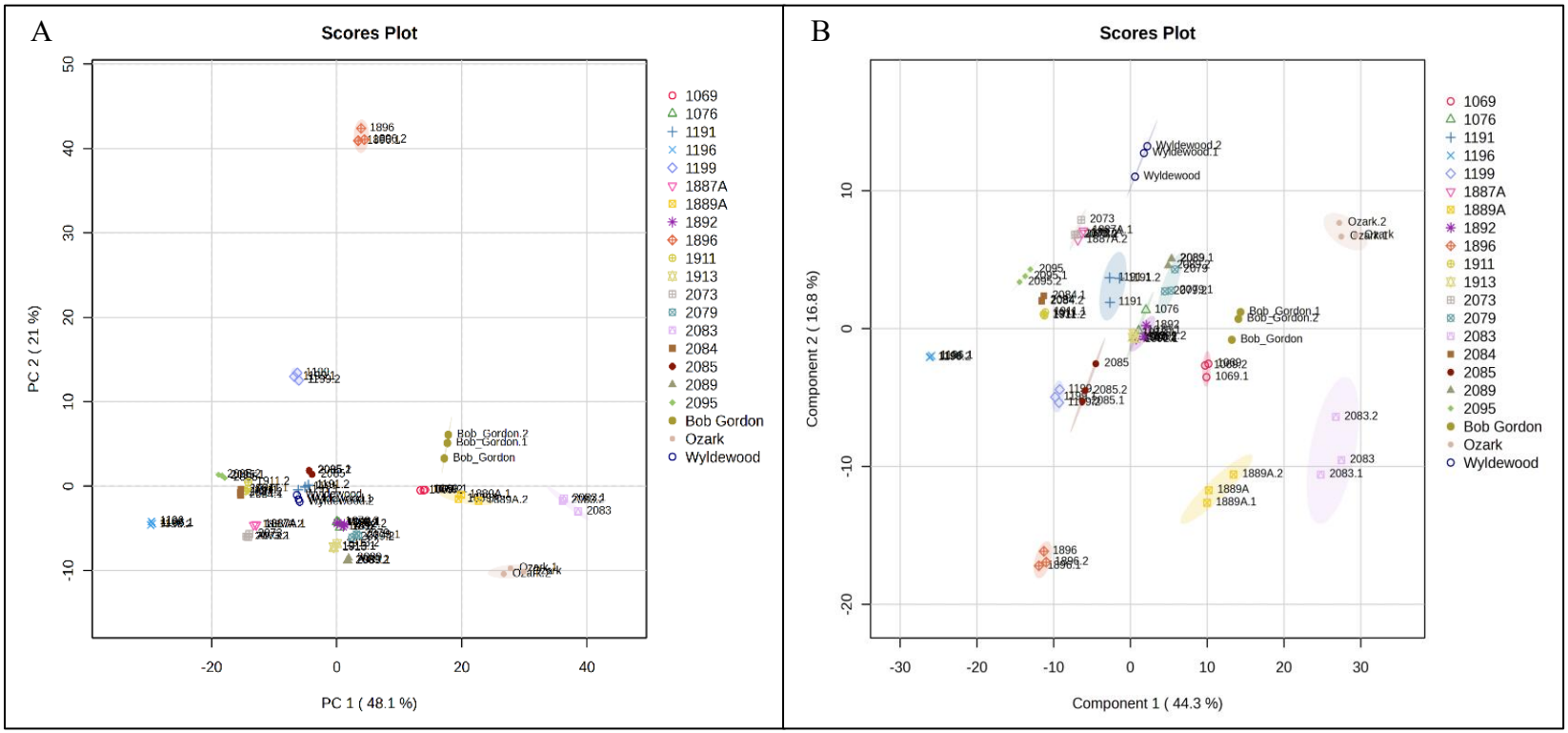

Figure 0-6. Multivariate analysis of compounds in various cultivars of American elderberry juices. **A**. PCA scores plot and **B.** PLS-DA scores plot of compounds in juices of 21 American elderberry cultivars revealed differences in the metabolomic profiles between cultivars. Circles with the same color represent analytical replicates (n=3). The colored ellipses indicate 95% confidence regions of each group.

DISCUSSION

This study aimed to establish a rapid, high-throughput method for quantifying classes of bioactive metabolites in American elderberry juices. Both HPLC-MS/MS and UHPLC-MS/MS systems were evaluated for their analytical performance. The UHPLC-MS/MS setup demonstrated a higher sensitivity with better chromatographic resolution and shorter run times compared to the HPLC-MS/MS system. The smaller particle size in the UHPLC column improved the column efficiency, resulting in lower baseline noise and higher signal-to-noise ratios. The sensitivity and selectivity of UHPLC-MS/MS at low detection levels enable precise quantification of analytes in complex matrices with minimal sample preparation.

Complex sample matrices are known to interfere with analytical measurements. The matrix effect (ME) refers to the direct or indirect alteration of an analyte's response caused by co-eluting, unintended components present in the sample. These interferences can either suppress or enhance ionization efficiency in the mass spectrometer, leading to inaccurate quantification if not properly monitored[132,133,138]. In this study, a 1600-fold dilution of the samples minimized the matrix effect, as shown in Table 0-5 with range of recovery rates of 82.74% ± 3.19 to 139.1% ± 21.31.

Compounds neochlorogenic acid and chlorogenic acid exhibit inconsistent peak formation under UHPLC conditions but are detected under chromatographic conditions in an HPLC system. Chlorogenic acids (pKa = 3.5) are weak acids with carboxyl (-COOH) and phenolic hydroxyl groups (-OH) that can be deprotonated at moderately acidic pH conditions. The lower acid concentration in the aqueous mobile phase (0.01% Formic acid)

of UHPLC systems might promote deprotonation of these phenolic acids. As these compounds become more anionic, their interaction with the C18 stationary phase weakens, leading to a reduction in compound retention in the column, and elution occurs earlier from the column near the solvent peak. This behavior is consistent with previous reports showing that acidified mobile phase improves retention and peak shape of phenolic acids[139,140].

This study presents a comprehensive quantification of metabolites in American elderberry (*Sambucus nigra* subsp. *canadensis*) juices from 18 propagated accessions and three established cultivars. A streamlined and validated workflow was developed to quantify 20 bioactive metabolites using a UHPLC–MS/MS system and two additional metabolites using HPLC–MS/MS. The study also addressed matrix effects inherent to complex juice samples, which were effectively mitigated through sample dilution while maintaining detection sensitivity on the UHPLC–MS/MS platform. This approach enabled accurate and reproducible quantification of target analytes and established a robust analytical framework for metabolomic evaluation of specialty crops.

Among the metabolites analyzed, anthocyanin compounds such as cyanidin-3,5-O-diglucoside, cyanidin-3-O-sophoroside, and cyanidin-3-O-sambubioside were consistently detected across all American elderberry juices, indicating that cyanidin-based anthocyanins represent the predominant pigments in elderberry. This finding aligns with previous reports describing cyanidin derivatives as the major anthocyanins responsible for the characteristic coloration of elderberry fruits[7,8].

The instability of myricetin observed in this study underscores the importance of considering the compound's stability in metabolomic analysis. The stability of compounds should also be carefully evaluated during product development, as degradation of

metabolites can alter both chemical composition and bioactivity of a product. Future studies should incorporate stabilization strategies, such as acidifying extraction solvents, to preserve sensitive compounds. Furthermore, despite the excellent performance of the developed analytical methods and high compound recovery, compounds such as pelargonidin 3-*O*-glucoside, peonidin 3-*O*-glucoside, catechin, epicatechin, and luteolin were not detected in any of the samples, suggesting that these compounds may be present in low concentrations. The dilution factor used in this analysis may have reduced their levels below the detection limit. However, if additional dilution reduces analyte concentrations to the point where they fall near or below the detection threshold, this suggests that their native abundance in the juices may be too low to exert a meaningful biological or bioactive effect.

Quantification of the bioactive metabolites in juices from 21 American elderberry cultivars revealed apparent genotype-dependent variation in metabolite composition. Similar genotype-dependent differences have been reported in a previous study of European elderberry (*Sambucus nigra* subsp. *nigra*)[141,142]. This finding underscores the potential for targeted breeding and cultivar selection to enhance desirable phytochemical traits, such as antioxidant capacity[15], antiviral bioactivity[116], color stability, and overall nutritional quality.

A previous study by Johnson et al. (2017) reported that quercetin 3-rutinoside was the most abundant polyphenol in juices from three American elderberry cultivars, with concentrations ranging from 47 ± 13 to 1,140 ± 107 mg/L. In our study, quercetin 3-rutinoside was likewise the dominant polyphenol across cultivars; however, its concentrations were lower overall, ranging from 0.6 ± 0.27 to 268.1 ± 8.06 mg/L. Johnson

et al. (2017) suggested that differences in genotype, growing year, and environmental conditions can substantially influence the accumulation of phenolic compounds in elderberry juices. Such factors likely contribute to the variation observed between studies, as metabolite biosynthesis in elderberry is highly responsive to environmental cues and cultivar-specific traits.

CONCLUSION

This study established and validated a high-throughput LC–MS/MS workflow for the targeted quantification of phenolic metabolites in American elderberry (*Sambucus nigra* subsp. *canadensis*) juices from 21 cultivars. Using a combination of UHPLC–MS/MS and HPLC–MS/MS platforms, 22 metabolites were successfully quantified across three major compound classes, anthocyanins, flavonoids, and phenolic acids, with excellent recovery rates. The optimized UHPLC–MS/MS method demonstrated superior sensitivity, precision, and efficiency, while strategic sample dilution effectively minimized matrix effects, ensuring accurate quantification in complex juice matrices.

Multivariate statistical analysis revealed apparent genotype-dependent variation between cultivars. American elderberry accessions 1896 and 2083, and the cultivar Ozark, were observed to have distinct chemical compositions, distinguishing them from other cultivars. In contrast, accession 1199 exhibited a high accumulation of cyanidin-based anthocyanins, suggesting its potential as a valuable source of natural pigment for colorant or functional food applications.

CHAPTER 4. SUMMARY AND FUTURE DIRECTION

This project establishes a comprehensive, high-throughput analytical framework for characterizing and quantifying bioactive metabolites in American elderberry using advanced UHPLC–MS/MS platforms. The study expands scientific understanding of elderberry phytochemistry, particularly its antioxidant and antiviral potential. Metabolomic profiling revealed substantial variation in the composition of polyphenols, flavonoids, and anthocyanins across cultivars, confirming strong genotype-dependent differences. However, environmental factors, including growing conditions, harvest year, pest or virus infection, and site-specific variables, can also influence metabolite accumulation. Future multi-year analyses will be essential to better predict the stability and production of bioactive compounds across diverse environments.

Comprehensive profiles of bioactive compounds for individual cultivars provide critical information for optimizing decision-making across the entire American elderberry supply chain. For growers, knowing the phytochemical strengths of each cultivar supports informed decisions on which to plant, allowing them to target cultivars with higher levels of bioactive compounds, stronger antioxidant activity, or enhanced antiviral potential. This, in turn, helps buyers by ensuring access to raw materials with verified chemical quality, enabling them to selectively source fruit from high-value cultivars and maintain consistency in product formulation. Processing facilities can leverage this chemical information to optimize extraction procedures, standardize product quality, and develop value-added ingredients enriched in specific bioactive compounds. Scientifically validated phytochemical profiles allow manufacturers and marketers to support evidence-based

health claims and clearly differentiate their products in the marketplace. Ultimately, consumers gain confidence in elderberry products supported by robust chemical analysis, ensuring transparency, reliability, and trust in nutraceuticals, functional beverages, and other health products derived from American elderberry.

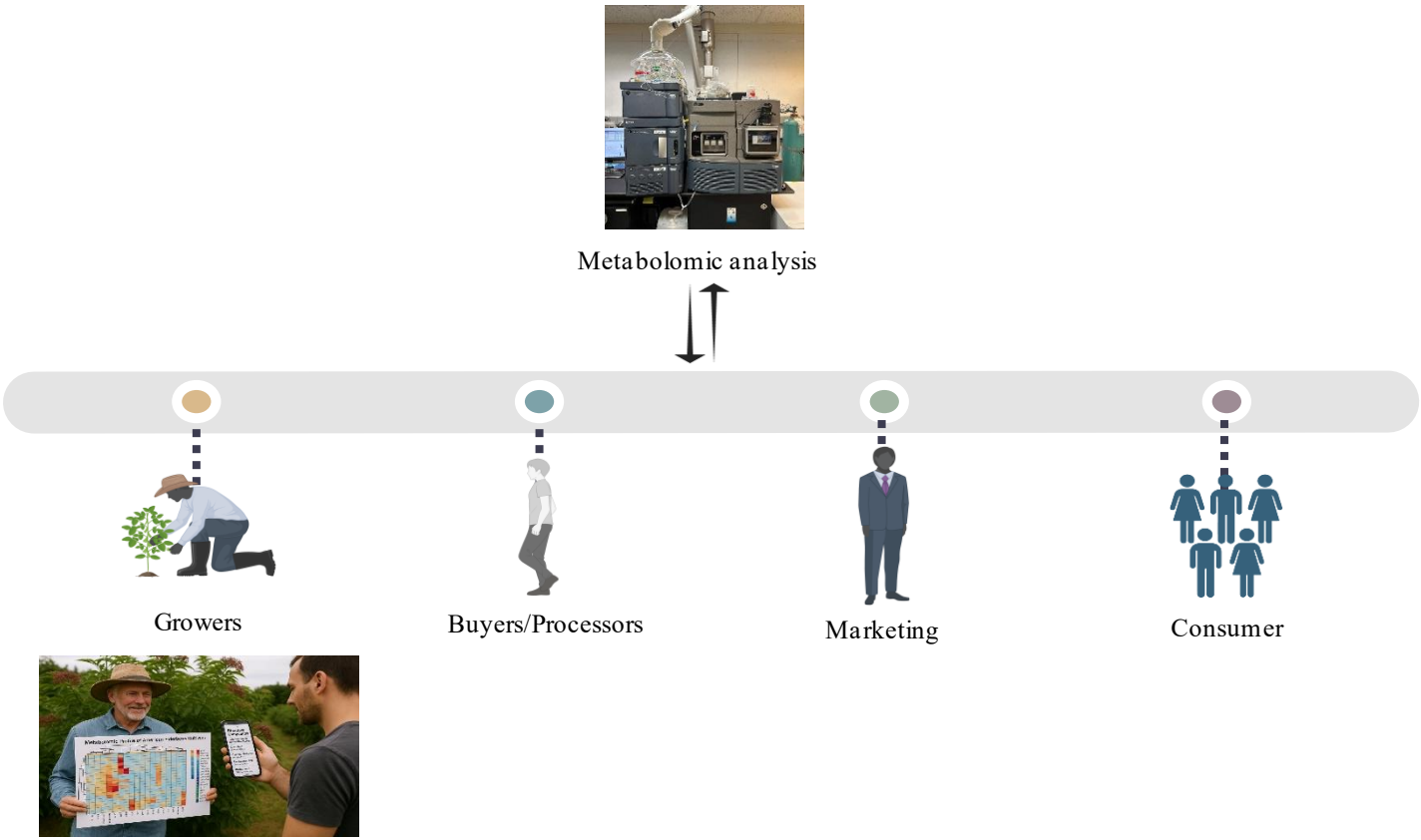

Figure 0-1. Schematic representation of the application of metabolomics analysis workflow

FUNDING AND ACKNOWLEDGEMENT

This work is supported by the USDA-NIFA-SCRI project, "Moving American Elderberry into Mainstream Production and Processing" [grant number 2021-51181-35860], the Missouri Department of Agriculture's Specialty Crop Block Grant Program, and the University of Missouri's Center for Agroforestry in cooperation with the USDA/ARS Dale Bumpers Small Farm Research Center [grant number 58-6020-6-001]. The authors would also like to thank the Center for Agroforestry at the University of Missouri for supporting part of this research.

APPENDIX

Table A 1. Annotation of peaks isolated from American elderberry juices in positive ion mode. Putative identifications were assigned through comparison with MS spectral data and accurate mass in METLIN library. Reported bioactivities of the compounds are summarized based on published references.

No.	Compounds	RT	Formula	Adducts	Theoretical Mass	Observed Mass	Δm (ppm)	Bioactivities	Ref
1	Spermine	0.45	$C_{10}H_{26}N_4$	$[M+H]^+$	202.21575	202.215	-2.6	Antioxidant, anticancer, antiaging	143–145
2	Niacinamide	0.57	$C_6H_6N_2O$	$[M+H]^+$	122.04801	122.048	-3.2	Anti-acne, antiaging and skin improvement effect	146,147
3	Niacin (Vit B3)	0.59	$C_6H_5NO_2$	$[M+H]^+$	123.03203	123.032	-3.9	Anti-dyslipidemia, anti-inflammatory	148,149
4	Picolinic acid	0.59	$C_6H_5NO_2$	$[M+H]^+$	123.03203	123.032	-3.9	Anticancer, antiviral	150–152
5	Betaine	0.63	$C_5H_{11}NO_2$	$[M+H]^+$	117.07898	117.078	-4.3	Antioxidant, anti-inflammatory	153,154
6	L-Valine	0.63	$C_5H_{11}NO_2$	$[M+H]^+$	117.07898	117.078	-4.3	Amino acid	155
7	3-Furoic acid	0.65	$C_5H_4O_3$	$[M-H]^-$	112.01605	112.017	4.3	Allosteric modulator	156
8	Citric acid	0.65	$C_6H_8O_7$	$[M-H]^-$	192.027	192.027	0.6	Antioxidant, anti-inflammation	41,157
9	Dehydrozingerone	0.65	$C_{11}H_{12}O_3$	$[M+H]^+$	192.07864	192.078	-3.7	Antioxidant, anti-inflammatory, antidepressant, antimicrobial, antidiabetic, anticancer	158–161

10	4-hydroxybenzaldehyde	0.76	C_7H6O_2	$[M+H]^+$	122.03678	122.036	-5.0	Antioxidant, wound healing, vasculoprotective agent	162,163
11	Salicylaldehyde	0.76	$C_7H_6O_2$	$[M+H]^+$	122.03678	122.036	-5.0	Antimicrobial	164
12	Tropolone	0.76	$C_7H_6O_2$	$[M+H]^+$	122.03678	122.036	-5.0	Anticancer, antimicrobial	165,166
13	Chromone	0.78	$C_9H_6O_2$	$[M+H]^+$	146.03678	146.036	-3.1	Antiallergic, anti-inflammatory, antidiabetic, anticancer, and antimicrobial	167,168
14	Coumarin	0.78	$C_9H_6O_2$	$[M+H]^+$	146.03678	146.036	-3.1	Anticancer, anti-inflammatory, antimicrobial	169,170
15	L-tyrosine	0.78	$C_9H_{11}NO_3$	$[M+H]^+$	181.07389	181.074	-1.9	Antidepressant, antioxidant	171,172
16	Pyroglutamic acid	0.79	$C_5H_7NO_3$	$[M+H]^+$	129.04259	129.042	-3.1	Antimicrobial, anti-inflammatory, neurogenic activities	173,174
17	Cotinine	0.91	$C_{10}H_{12}N_{2O}$	$[M+H]^+$	176.09496	176.094	-4.9	Neuroprotective	175
18	Castanospermine	1.02	$C_8H_{15}NO_4$	$[M+H]^+$	189.10011	189.1	-2.3	Antivirus, anticancer	143,176
19	Cearoin	1.57	$C_{14}H_{12}O_4$	$[M+H]^+$	244.07356	244.073	-0.9	Anticancer, anti-inflammatory, antimicrobial	177–179
20	Vanilloloside	1.58	$C_{14}H_{20}O_8$	$[M-H]^-$	316.11582	316.116	0.3	Antimicrobial, antioxidant, anticancer	180–182
21	Indoleacrylic acid	1.76	$C_{11}H_9NO_2$	$[M+H]^+$	187.06333	187.063	-2.4	Anti-inflammatory	183
22	3-hydroxycoumarin	2.33	$C_9H_6O_3$	$[M+H]^+$	162.03169	162.031	-2.9	Anticancer, anti-inflammatory, antimicrobial	169,170,184

23	Cinnamaldehyde	2.83	C_9H_8O	$[M+H]^+$	132.05751	132.057	-3.8	Antimicrobial, antidiabetic, antioxidant	185,186
24	Ethyl p-coumarate	2.85	$C_{11}H_{12}O_3$	$[M+H]^+$	192.07864	192.078	-3.7	Antifungal, antioxidant	187,188
25	Herniarin	2.85	$C_{10}H_8O_3$	$[M+H]^+$	176.04734	176.047	-2.7	Anticancer, anti-inflammatory, neuroprotective	189,189
26	Hymechrome	2.85	$C_{10}H_8O_3$	$[M+H]^+$	176.04734	176.047	-2.7	Anticancer	190
27	Myristicin	2.85	$C_{11}H_{12}O_3$	$[M+H]^+$	192.07864	192.078	-3.7	Anticancer, antimicrobial, anti-inflammatory, antioxidant	191–193
28	5,7-Dihydroxychromone	3.23	$C_9H_6O_4$	$[M+H]^+$	178.02661	178.026	-2.4	Antioxidant, antidiabetic, anticancer	194–196
29	7,8-Dihydroxycoumarin (Daphnetin)	3.23	$C_9H_6O_4$	$[M+H]^+$	178.02661	178.026	-2.4	Neuroprotective, antioxidant, anti-inflammatory, anticancer	197,198
30	Allamandin	3.74	$C_{15}H_{16}O_7$	$[M+H]^+$	308.0896	308.089	-1.3	Antiviral, anticancer	199–201
31	Epiafzelechin trimethyl ether	4.05	$C_{18}H_{20}O_5$	$[M+H]^+$	316.13107	316.131	-0.8	Anticancer	202
32	Aurentiacin	4.58	$C_{18}H_{18}O_4$	$[M+H]^+$	298.12051	298.12	-1.0	Anti-inflamatory, antimicrobial	203,204
33	Monocerin	5.09	$C_{16}H_{20}O_6$	$[M+H]^+$	308.12599	308.125	-3.3	Antimicrobial	205
34	Lucenin 2	5.13	$C_{27}H_{30}O_{16}$	$[M+H]^+$	610.15338	610.154	0.3	Anti-inflammatory, antioxidant	206
35	p-Cymene	5.47	$C_{10}H_{14}$	$[M+H]^+$	134.10955	134.109	-2.7	Antioxidant, anti-inflammatory, anticancer, antimicrobial	207–210
36	Kuwanon L	6.46	$C_{35}H_{30}O_{11}$	$[M+H]^+$	626.17881	626.175	-6.0	Antiviral, anti-inflammatory, antimicrobial	211–213

37	Tamarixetin	6.46	$C_{16}H_{12}O_7$	$[M+H]^+$	316.0583	316.058	-0.9	Anticancer, anti-inflammatory, anti-oxidation, organ protection, prevention of obesity	[214–216]
38	Anethole	8.67	$C_{10}H_{12}O$	$[M+H]^+$	148.08882	148.088	-3.6	Antimicrobial, antioxidant, anti-inflammatory	[217,218]
39	Cuminaldehyde	8.67	$C_{10}H_{12}O$	$[M+H]^+$	148.08882	148.088	-3.6	Antimicrobial, antioxidant, anticancer	[219,220]
40	Estragole	8.67	$C_{10}H_{12}O$	$[M+H]^+$	148.08882	148.088	-3.6	Antioxidant, anticancer	[221]

Table A 2. Annotation of peaks isolated from American elderberry juices with putative identifications assigned through comparison with mass spectral reference data in MSDIAL library (>70% identification score cut off).

No.	Compounds	Formula	Adducts	RT	Theoretical Mass	Observed Mass	Δm (ppm)
1	Arginine	$C_6H_{14}N_4O_2$	$[M+H]^+$	0.53	175.1191	175.1190	-0.69
2	L-histidine	$C_6H_9N_3O_2$	$[M+H]^+$	0.53	156.0775	156.0773	-1.28
3	Cis-4-hydroxy-d-proline	$C_5H_9NO_3$	$[M+H]^+$	0.60	132.0654	132.0654	0.00
4	2-Hydroxycinnamic acid, predominantly trans	$C_9H_8O_3$	$[M+H]^+$	0.79	165.0551	165.0552	0.12
5	Adenosine	$C_{10}H_{13}N_5O_4$	$[M+H]^+$	0.79	268.1043	268.1040	-1.04
6	Metalaxyl-M-TP CGA108906	$C_{14}H_{17}NO_6$	$[M+H]^+$	0.81	296.1134	296.1129	-1.72
7	Serotonin	$C_{10}H_{12}N_2O$	$[M+H]^+$	0.93	177.1023	177.1022	-0.56
8	Oxadixyl	$C_{14}H_{18}N_2O_4$	$[M+H]^+$	0.99	279.1343	279.1339	-1.22
9	Piperidine	$C_5H_{11}N$	$[M+H]^+$	1.00	86.0964	86.0964	0.12
10	Coniferaldehyde	$C_{10}H_{10}O_3$	$[M+H]^+$	1.11	179.0703	179.0703	0.28
11	DL-4-Hydroxyphenyllactic acid	$C_9H_{10}O_4$	$[M+H]^+$	1.14	183.0655	183.0652	-1.42
12	Gamma-Glutamyltyrosine	$C_{14}H_{18}N_2O_6$	$[M+H]^+$	1.22	311.1229	311.1238	2.86
13	Hesperidin	$C_{28}H_{34}O_{15}$	$[M+H]^+$	1.38	611.1881	611.1900	3.09
14	Kaempferol 3-O-sophoroside	$C_{27}H_{30}O_{16}$	$[M+H]^+$	1.41	611.1605	611.1606	0.29
15	Pantothenate	$C_9H_{17}NO_5$	$[M+H]^+$	1.43	220.1178	220.1179	0.27
16	D-Pantothenic acid	$C_9H_{17}NO_5$	$[M+H]^+$	1.52	220.1180	220.1185	2.23
17	Taxifolin-3-glucoside	$C_{21}H_{22}O_{12}$	$[M+H]^+$	1.55	467.1191	467.1180	-2.42
18	Indole-3-carboxyaldehyde	C_9H_7NO	$[M+H]^+$	1.76	146.0601	146.0606	3.29
19	Tryptophan	$C_{11}H_{12}N_2O_2$	$[M+H]^+$	1.76	205.0973	205.0980	3.51
20	Desethylatrazine	$C_6H_{10}ClN_5$	$[M+H]^+$	1.82	188.0704	188.0697	-3.72
21	Adenine	$C_5H_5N_5$	$[M+H]^+$	1.94	136.0619	136.0618	-1.03
22	5'-s-methylthioadenosine	$C_{11}H_{15}N_5O_3S$	$[M+H]^+$	1.94	298.0967	298.0974	2.05

23	Cis-Cinnamic acid	$C_9H_8O_2$	$[M+H]^+$	2.07	149.0597	149.0597	0.13
24	Paeonol	$C_9H_{10}O_3$	$[M+H]^+$	2.11	167.0705	167.0703	-1.08
25	3-hydroxy-1-(4-hydroxyphenyl)propan-1-one	$C_9H_{10}O_3$	$[M+H]^+$	2.15	167.0704	167.0703	-0.54
26	3',5'-Dimethoxy-4'-hydroxyacetophenone	$C_{10}H_{12}O_4$	$[M+H]^+$	2.16	197.0808	197.0808	0.20
27	NCGC00168941-08!(1S,3R,4R,5R)-3-[(e)-3-(3,4-dihydroxyphenyl)prop-2-enoyl]oxy-1,4,5-trihydroxycyclohexane-1-carboxylic acid	$C_{16}H_{18}O_9$	$[M+H]^+$	2.33	355.1026	355.1020	-1.72
28	NCGC00385551-01!5-[(2S,3R,4S,5S,6R)-6-[[(2R,3R,4R)-3,4-dihydroxy-4-(hydroxymethyl)oxolan-2-yl]oxymethyl]-3,4,5-trihydroxyoxan-2-yl]oxy-4-(3,4-dihydroxyphenyl)-7-hydroxychromen-2-one	$C_{26}H_{28}O_{15}$	$[M+H]^+$	2.45	581.1505	581.1500	-0.84
29	2,4,6-trihydroxyacetophenone	$C_8H_8O_4$	$[M+H]^+$	2.47	169.0495	169.0500	3.25
30	NCGC00380393-01_C15H20O4_Pentaleno[1,6a-c]pyran-9-carboxylic acid, 1,3,4,5,6,7,7a,9a-octahydro-4,6,6-trimethyl-3-oxo-, (4S,4ar,7as,9ar)-	$C_{15}H_{20}O_4$	$[M+H]^+$	2.56	265.1436	265.1430	-2.04
31	5-hydroxy-3-[(2S,3R,4R,5S)-3-hydroxy-5-(hydroxymethyl)-4-[(2S,3R,4S,5S,6R)-3,4,5-trihydroxy-6-(hydroxymethyl)oxan-2-yl]oxyoxolan-2-yl]oxy-2-(4-hydroxyphenyl)-7-[(2S,3R,4R,5R,6S)-3,4,5-trihydroxy-6-methyloxan-2-yl]oxychromen-4-one	$C_{32}H_{38}O_{19}$	$[M+H]^+$	2.70	727.2099	727.2080	-2.60
32	Lonicerin	$C_{27}H_{30}O_{15}$	$[M+H]^+$	2.72	595.1677	595.1660	-2.76
33	Quercetin-3,4'-O-di-beta-glucoside	$C_{27}H_{30}O_{17}$	$[M+H]^+$	2.75	627.1553	627.1556	0.40
34	3,4-Dihydroxymandelic acid	$C_8H_8O_5$	$[M+H]^+$	2.98	185.0440	185.0445	2.43
35	7-[(2S,3R,4S,5S,6R)-6-[[(2S,3R,4R)-3,4-dihydroxy-4-(hydroxymethyl)oxolan-2-yl]oxymethyl]-3,4,5-trihydroxyoxan-2-yl]oxy-5-hydroxy-3-(4-hydroxyphenyl)-6-methoxychromen-4-one	$C_{27}H_{30}O_{15}$	$[M+H]^+$	3.31	595.1677	595.1658	-3.18
36	Myricetin-3-rutinoside	$C_{27}H_{30}O_{17}$	$[M+H]^+$	3.31	627.1590	627.1590	0.00

37	Kaempferal-3-O-glc-1-3-rham-1-6-glucoside	$C_{33}H_{40}O_{20}$	$[M+H]^+$	3.42	757.2187	757.2190	0.40
38	4-Methyl-6,7-dihydroxycoumarin	$C_{10}H_8O_4$	$[M+H]^+$	3.70	193.0498	193.0500	0.83
39	NCGC00169080-02_C15H18O3_Azuleno[6,5-b]furan-2,6(3H,4H)-dione, 3a,7,7a,8,9,9a-hexahydro-5,8-dimethyl-3-methylene-, (3ar,7as,8S,9ar)-	$C_{15}H_{18}O_3$	$[M+H]^+$	3.81	247.1331	247.1330	-0.28
40	Piliformic-acid	$C_{11}H_{18}O_4$	$[M+H]^+$	4.10	215.1276	215.1278	1.12
41	NCGC00381208-01_C20H24O6_(3ar,4S,6E,9Z,11as)-4-Hydroxy-6,10-dimethyl-3-methylene-2,8-dioxo-2,3,3a,4,5,8,11,11a-octahydrocyclodeca[b]furan-11-yl (2Z)-2-methyl-2-butenoate	$C_{20}H_{24}O_6$	$[M+H]^+$	4.14	361.1646	361.1650	1.02
42	6a,7,8-trihydroxy-3-methyl-3,4,5,6,7,12a-hexahydro-2H-benzo[a]anthracene-1,12-dione	$C_{19}H_{20}O_5$	$[M+H]^+$	4.19	329.1393	329.1378	-4.44
43	NCGC00385777-01_C19H32O8_(2R)-4-[(1S)-1-Hydroxy-2,6,6-trimethyl-4-oxo-2-cyclohexen-1-yl]-2-butanyl beta-D-glucopyranoside	$C_{19}H_{32}O_8$	$[M+H]^+$	4.20	389.2177	389.2170	-1.64
44	6-methylcoumarin	$C_{10}H_8O_2$	$[M+H]^+$	4.22	161.0593	161.0600	4.16
45	NCGC00169108-02!3-[6-[[(2R,3R,4R,5S,6S)-3,5-dihydroxy-6-methyl-4-[(2S,3R,4R,5R,6S)-3,4,5-trihydroxy-6-methyloxan-2-yl]oxyoxan-2-yl]oxymethyl]-3,4,5-trihydroxyoxan-2-yl]oxy-2-(3,4-dihydroxyphenyl)-5,7-dihydroxychromen-4-one	$C_{33}H_{40}O_{20}$	$[M+H]^+$	4.29	757.2189	757.2180	-1.20
46	5,7-dihydroxy-2-(3,4,5-trihydroxyphenyl)-4H-chromen-4-one	$C_{15}H_{10}O_7$	$[M+H]^+$	4.30	303.0501	303.0500	-0.20
47	Quercetin-3-O-vicianoside	$C_{26}H_{28}O_{16}$	$[M+H]^+$	4.33	597.1453	597.1450	-0.40
48	2-Norbornene-5,6-dicarboxylic anhydride	$C_9H_8O_3$	$[M+H]^+$	4.42	165.0549	165.0546	-2.00
49	Methyl trans-cinnamic acid	$C_{10}H_{10}O_2$	$[M+H]^+$	4.42	163.0758	163.0754	-2.27
50	Gibberellic acid	$C_{19}H_{22}O_6$	$[M+H]^+$	4.42	347.1498	347.1489	-2.62

51	NCGC00386049-01!3-[(2S,3R,4S,5R,6S)-3,4-dihydroxy-6-methyl-5-[(2S,3R,4S,5S,6R)-3,4,5-trihydroxy-6-(hydroxymethyl)oxan-2-yl]oxyoxan-2-yl]oxy-2-(3,4-dihydroxyphenyl)-5,7-dihydroxychromen-4-one	$C_{27}H_{30}O_{16}$	$[M+H]^+$	4.91	611.1610	611.1600	-1.70
52	Delphinidin 3-galactoside	$C_{21}H_{21}O_{12}$	$[M]^+$	4.94	465.1029	465.1022	-1.59
53	3-[4,5-dihydroxy-6-(hydroxymethyl)-3-[(2S,3R,4R,5R,6S)-3,4,5-trihydroxy-6-methyloxan-2-yl]oxyoxan-2-yl]oxy-5-hydroxy-2-(4-hydroxyphenyl)-7-[3,4,5-trihydroxy-6-(hydroxymethyl)oxan-2-yl]oxychromen-4-one	$C_{33}H_{40}O_{20}$	$[M+H]^+$	5.01	757.2206	757.2186	-2.65
54	Cyanidin-3-O-sambubioside-5-O-glucoside	$C_{32}H_{39}O_{20}$	$[M]^+$	5.19	743.2015	743.2024	1.14
55	[6-[2-(3,4-dihydroxyphenyl)-8-hydroxy-4-oxochromen-7-yl]oxy-3,4,5-trihydroxyoxan-2-yl]methyl (E)-3-(4-hydroxyphenyl)prop-2-enoate	$C_{30}H_{26}O_{13}$	$[M+H]^+$	5.22	595.1455	595.1446	-1.55
56	Cyanidin-3-O-(6''-O-(E-p-coum)-2''-O-(beta-xylopyranosyl)-beta-glucopyranoside)-5-O-beta-glucopyranoside	$C_{41}H_{45}O_{22}$	$[M]^+$	5.28	889.2414	889.2402	-1.30
57	NCGC00385836-01!3-[[(2R,3S,4S,5R,6S)-6-[2-(3,4-dihydroxyphenyl)-5,7-dihydroxy-4-oxochromen-3-yl]oxy-3,4,5-trihydroxyoxan-2-yl]methoxy]-3-oxopropanoic acid	$C_{24}H_{22}O_{15}$	$[M+H]^+$	5.57	551.1044	551.1030	-2.43
58	NCGC00385924-01_C15H18O4_(3as,10ar,10br)-6,10a-Dimethyl-3-methylene-3,3a,4,5,7,8,10a,10b-octahydrofuro[3',2':6,7]cyclohepta[1,2-b]pyran-2,9-dione	$C_{15}H_{18}O_4$	$[M+H]^+$	5.57	263.1277	263.1280	1.25
59	Petunidin-3-O-beta-glucoside	$C_{22}H_{23}O_{12}$	$[M]^+$	6.29	479.1193	479.1179	-2.92
60	Delta-Tridecalactone	$C_{13}H_{24}O_2$	$[M+H]^+$	6.79	213.1846	213.1849	1.59
61	E-Resveratrol trimethyl ether	$C_{17}H_{18}O_3$	$[M+H]^+$	6.90	271.1324	271.1329	1.92
62	NCGC00015870-35!2-(3,4-dihydroxyphenyl)-3,5,7-trihydroxychromen-4-one	$C_{15}H_{10}O_7$	$[M+H]^+$	8.06	303.0503	303.0500	-1.09

63	(2E)-1-(2,4-dihydroxyphenyl)-3-(4-hydroxyphenyl)-2-propen-1-one	$C_{15}H_{12}O_4$	$[M+H]^+$	9.93	257.0813	257.0800	-4.98
64	2-naphthalenol	$C_{10}H_8O$	$[M+H]^+$	10.98	145.0649	145.0648	-0.90
65	(4ar,5as,9R)-9-ethynyl-9a,11b-dimethylhexadecahydrocyclopenta[1,2]phenanthro[8a,9-b]oxirene-3,9-diol	$C_{21}H_{30}O_3$	$[M+H]^+$	11.91	331.2201	331.2200	-0.36
66	Alpha-Cyperone	$C_{15}H_{22}O$	$[M+H]^+$	22.61	219.1747	219.1743	-1.96
67	Phthalic anhydride	$C_8H_4O_3$	$[M+H]^+$	23.10	149.0235	149.0233	-1.07
68	Tri(butoxyethyl)phosphate	$C_{18}H_{39}O_7P$	$[M+H]^+$	23.60	399.2518	399.2506	-2.98
69	1-Oleoyl-sn-glycero-3-phosphocholine	$C_{26}H_{52}NO_7P$	$[M+H]^+$	24.21	522.3585	522.3560	-4.67
70	1-palmitoyl-2-hydroxy-sn-glycero-3-phosphoethanolamine	$C_{21}H_{44}NO_7P$	$[M+H]^+$	24.26	454.2933	454.2928	-1.19
71	Velvione	$C_{16}H_{28}O$	$[M+H]^+$	25.77	237.2212	237.2213	0.25
72	4-((17S)-3-(((2R,4S,6R)-5-(((4S,6R)-5-(((4S,5S,6R)-4,5-dihydroxy-6-methyltetrahydro-2H-pyran-2-yl)oxy)-4-hydroxy-6-methyltetrahydro-2H-pyran-2-yl)oxy)-4-hydroxy-6-methyltetrahydro-2H-pyran-2-yl)oxy)-12,14-dihydroxy-10,13-dimethylhexadecahydro-1H-cyclopenta[a]phenanthren-17-yl)furan-2(5H)-one	$C_{41}H_{64}O_{14}$	$[M+H]^+$	28.41	781.4309	781.4300	-1.18
73	Stearamide	$C_{18}H_{37}NO$	$[M+H]^+$	31.49	284.2953	284.2940	-4.40
74	Dehydrocorydaline nitrate	$C_{22}H_{24}N_2O_7$	$[M+H]^+$	32.75	429.1702	429.1700	-0.44
75	Lutein	$C_{40}H_{56}O_2$	$[M]^+$	32.75	568.4297	568.4300	0.53
76	Erucamide	$C_{22}H_{43}NO$	$[M+H]^+$	32.90	338.3421	338.3424	1.00
77	Deoxycholic acid	$C_{24}H_{40}O_4$	$[M+H]^+$	33.03	393.2984	393.3000	4.04
78	Artesunate	$C_{19}H_{28}O_8$	$[M+H]^+$	34.25	385.1794	385.1800	1.43
79	M-Cumenyl methylcarbamate	$C_{11}H_{15}NO_2$	$[M+H]^+$	34.29	194.1175	194.1176	0.31
80	2-(4-oxoquinazolin-3(4H)-yl)ethyl isobutyrate	$C_{14}H_{16}N_2O_3$	$[M+H]^+$	34.33	261.1313	261.1300	-4.94
81	Toddalolactone	$C_{16}H_{20}O_6$	$[M+H]^+$	34.62	309.1307	309.1300	-2.30

82	Datiscetin-3-O-rutinoside	$C_{27}H_{30}O_{15}$	$[M+H]^+$	5.85	595.1666	595.1658	-1.44
83	Delta-Aminolevulinic acid	$C_5H_9NO_3$	$[M-H]^-$	0.58	130.0505	130.0508	2.69
84	(S)-malate	$C_4H_6O_5$	$[M-H]^-$	0.67	133.0140	133.0142	1.13
85	Citrate	$C_6H_8O_7$	$[M-H]^-$	0.78	191.0190	191.0196	2.88
86	Citramalate	$C_5H_8O_5$	$[M-H]^-$	0.83	147.0287	147.0294	4.35
87	3-hydroxy-3-methylglutarate	$C_6H_{10}O_5$	$[M-H]^-$	0.89	161.0445	161.0451	3.29
88	Catechol	$C_6H_6O_2$	$[M-H]^-$	0.99	109.0295	109.0291	-3.30
89	4-hydroxybenzoate	$C_7H_6O_3$	$[M-H]^-$	1.04	137.0240	137.0246	4.60
90	L-phenylalanine	$C_9H_{11}NO_2$	$[M-H]^-$	1.24	164.0717	164.0715	-1.10
91	Trans-Cinnamic acid	$C_9H_8O_2$	$[M-H]^-$	1.24	147.0452	147.0453	0.95
92	P-Coumaraldehyde	$C_9H_8O_2$	$[M-H]^-$	2.10	147.0452	147.0454	1.97
93	4-hydroxybenzoic acid	$C_7H_6O_3$	$[M-H]^-$	2.28	137.0244	137.0242	-1.53
94	D-(-)-quinic acid	$C_7H_{12}O_6$	$[M-H]^-$	2.33	191.0561	191.0564	1.57
95	2-Isopropylmalic acid	$C_7H_{12}O_5$	$[M-H]^-$	2.41	175.0607	175.0608	0.80
96	Trans-4-Coumaric acid	$C_9H_8O_3$	$[M-H]^-$	2.60	163.0401	163.0399	-1.04
97	4-coumarate	$C_9H_8O_3$	$[M-H]^-$	2.65	163.0400	163.0400	0.18
98	M-xylene-4-sulfonic acid	$C_8H_{10}O_3S$	$[M-H]^-$	3.31	185.0278	185.0278	0.00
99	2-Hydroxy-4-methylpentanoic acid	$C_6H_{12}O_3$	$[M-H]^-$	3.68	131.0713	131.0715	1.30
100	3-phenyllactic acid	$C_9H_{10}O_3$	$[M-H]^-$	6.07	165.0557	165.0559	0.91

Table A 3. The half maximal inhibitory concentration (IC_{50}) concentration of American elderberry putative compounds against HIV virus strains NL4-2 and BaL

No.	Compound name	NL4-3		BaL	
		Mean (µM)	SEM	Mean(µM)	SEM
1	Caffeic acid	97.14	13.97	>100	0.00
2	Cryptochlorogenic acid	>100	0.00	>100	0.00
3	Catechin hydrate	NI	NI	NI	NI
4	Chlorogenic acid	NI	NI	NI	NI
5	p-Coumaric acid	NI	NI	NI	NI
6	Cyanidin 3,5-*O*-diglucoside	NI	NI	NI	NI
7	Cyanidin 3-*O*-galactoside	55.95	3.57	>100	0.00
8	Cyanidin 3-*O*-glucoside	65.77	11.68	>100	0.00
9	Cyanidin 3-*O*-rutinoside	>100	0.00	>100	0.00
10	Cyanidin 3-*O*-sambubioside	51.28	2.10	>100	0.00
11	Cyanidin 3-*O*-sophoroside	53.31	5.10	87.37	2.88
12	Delphinidin 3-*O*-rutinoside	34.92	1.25	97.52	9.13
13	3-4, Dihydroxybenzoic acid	NI	NI	NI	NI
14	Epicatechin	NI	NI	NI	NI
15	Ferulic acid	NI	NI	NI	NI
16	Gallic acid	6.24	0.12	6.24	0.12
17	Hyperoside	NI	NI	NI	NI
18	Isorhamnetin	0.64	0.01	2.22	0.69
19	Isorhamnetin 3-rutinoside	NI	NI	NI	NI
20	Kaempferol	2.45	0.28	8.73	0.70
21	Kaempferol 3-glucoside	NI	NI	NI	NI
22	Kaempferol 3-*O*-rutinoside	NI	NI	NI	NI
23	Luteolin	1.32	0.05	1.77	0.02
24	Myricetin	3.11	0.12	2.97	1.39
25	Naringenin	NI	NI	NI	NI
26	Neochlorogenic acid	NI	NI	NI	NI
27	Pelargonidin 3-*O*-glucoside	NI	NI	NI	NI
28	Peonidin 3-*O*-glucoside	NI	NI	NI	NI
29	Quercetin	2.49	0.24	3.84	0.56
30	Quercetin-3-β-D-glucoside	>100	0.00	>100	0.00
31	Rutin	NI	NI	NI	NI
32	Isorhamnetin 3-*O*-glucoside	NI	NI	NI	NI

*NI = No inhibition.

**Compounds with an IC_{50} concentration greater than 100µM were found to have no inhibitory on the growth of *S. aureus* (n=2).

Table A 4. The half maximal inhibitory concentration (IC_{50}) concentration of American elderberry putative compounds against *S. aureus*

No.	Compounds	IC_{50} (µM)	SEM
1	Caffeic acid	NI	NI
2	4-caffeoylquinic acid (cryptochlorogenic acid)	NI	NI
3	Catechin hydrate	NI	NI
4	Chlorogenic acid (5-caffeoylquinic acid)	NI	NI
5	p-Coumaric acid	NI	NI
6	Cyanidin 3,5-*O*-diglucoside	NI	NI
7	Cyanidin 3-*O*-galactoside	21.95	0.37
8	Cyanidin 3-*O*-glucoside	10.27	0.52
9	Cyanidin 3-*O*-rutinoside	8.44	0.01
10	Cyanidin 3-*O*-sambubioside	16.78	0.92
11	Cyanidin 3-*O*-sophoroside	32.36	9.19
12	Delphinidin 3-*O*-rutinoside	22.00	2.66
13	3-4, Dihydroxybenzoic zcid	NI	NI
14	(-)-Epicatechin	NI	NI
15	Ferulic acid	NI	NI
16	Gallic acid	NI	NI
17	Hyperoside (Quercetin 3-galactoside)	NI	NI
18	Isorhamnetin	NI	NI
19	Isorhamnetin 3-rutinoside	NI	NI
20	Kaempferol	NI	NI
21	Kaempferol 3-glucoside	NI	NI
22	Kaempferol 3-*O*-rutinoside	NI	NI
23	Luteolin	NI	NI
24	Myricetin	NI	NI
25	Naringenin	NI	NI
26	Neochlorogenic acid (3-caffeoylquinic acid)	NI	NI
27	Pelargonidin 3-*O*-glucoside	46.45	5.78
28	Peonidin 3-*O*-glucoside	28.65	2.25
29	Quercetin	>100	0.00
30	Quercetin-3-β-D-glucoside (hirsutrin)	NI	NI
31	Rutin (Quercetin-3-rutinoside)	NI	NI
32	Isorhamnetin 3-*O*-glucoside	NI	NI
33	Vancomycin (control +)	2.16	0.42

*NI = No inhibition.

**Compounds with an IC_{50} concentration greater than 100µM were found to have no inhibitory activity on the growth of *S. aureus* (n=2).

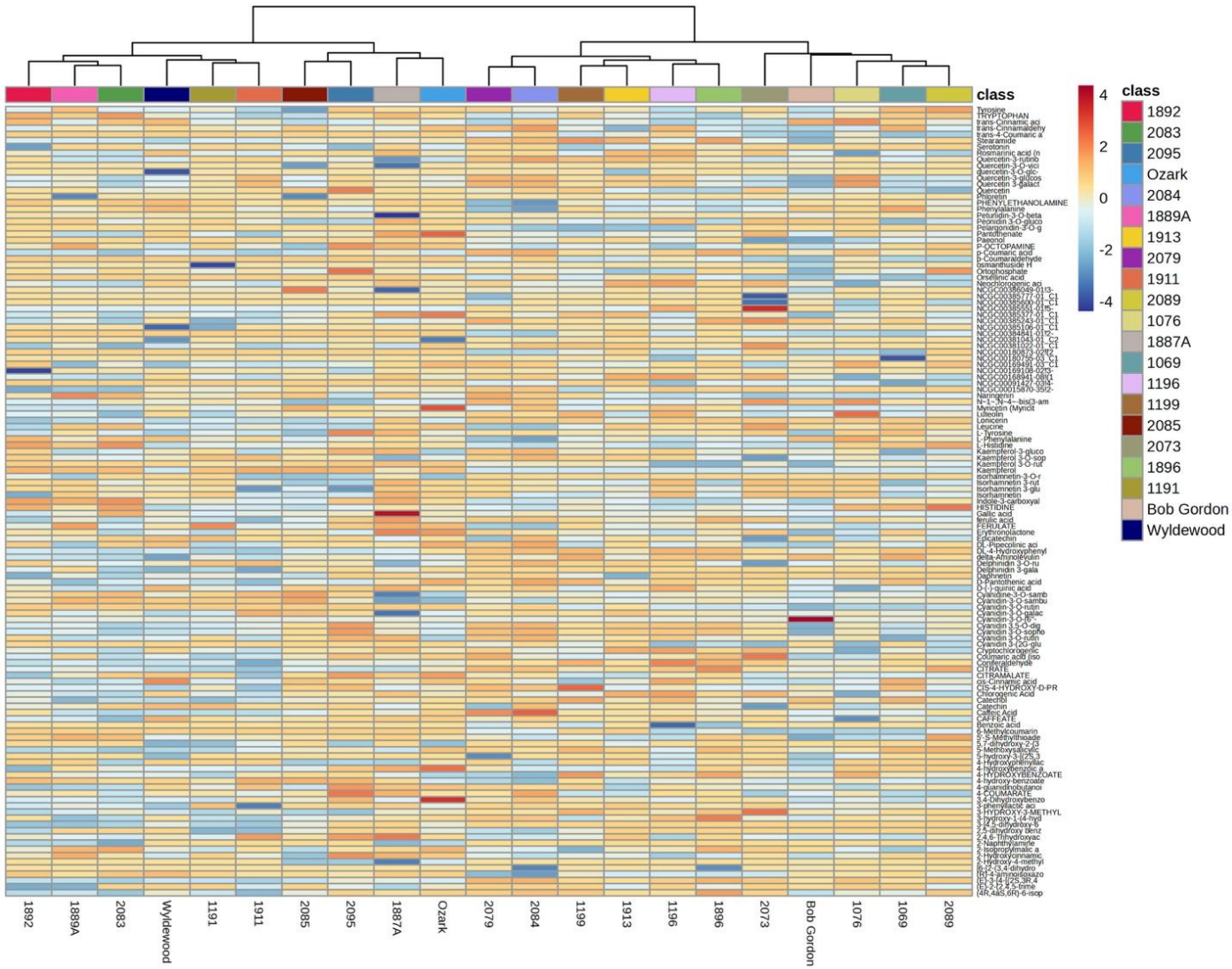

Figure A 1. The heatmap relative intensity of 127 putatively identified compounds in the juices of 21 American elderberry genotypes.

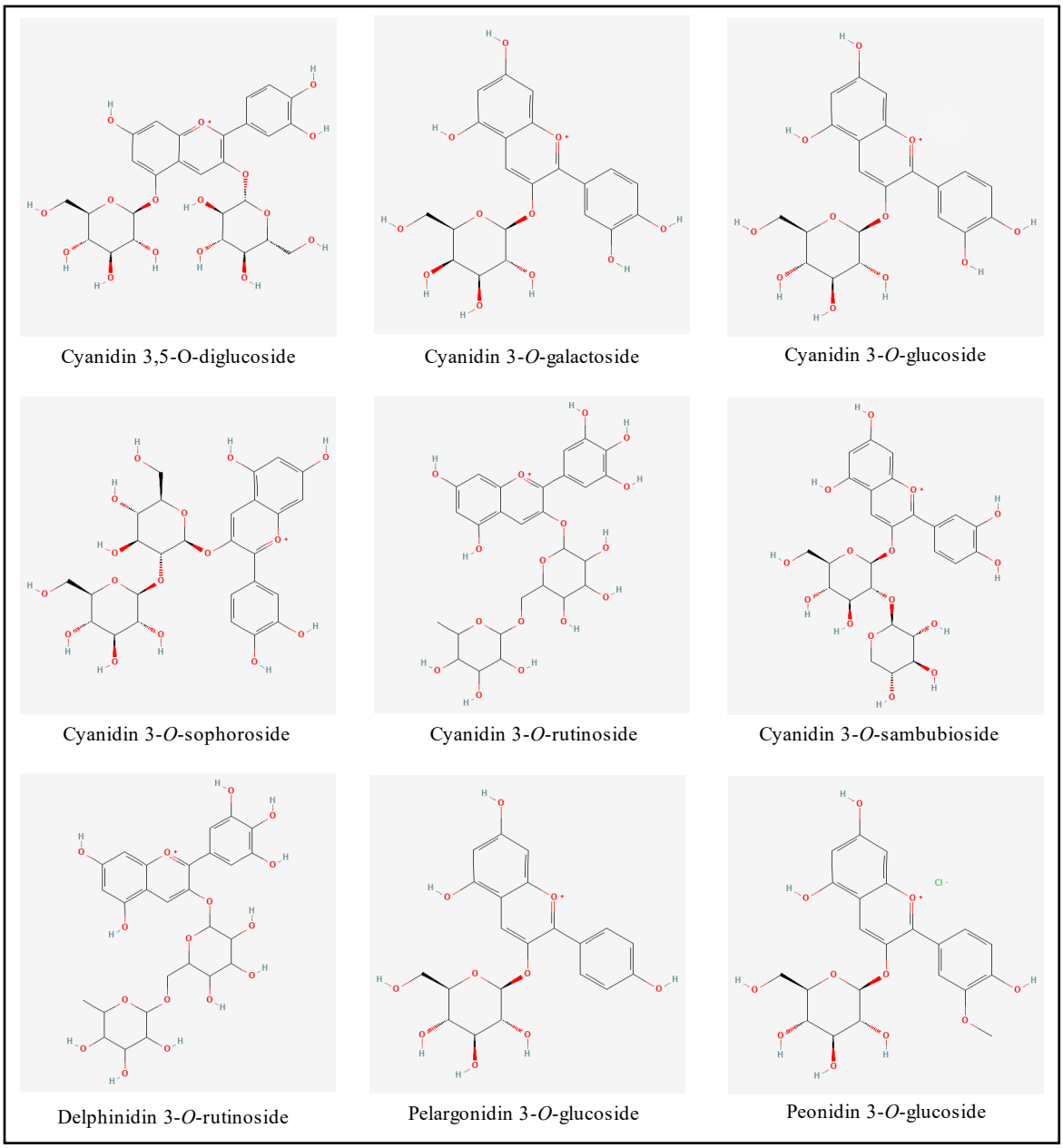

Figure A 2. Chemical structure of nine anthocyanin compounds putatively identified in American elderberry juices.

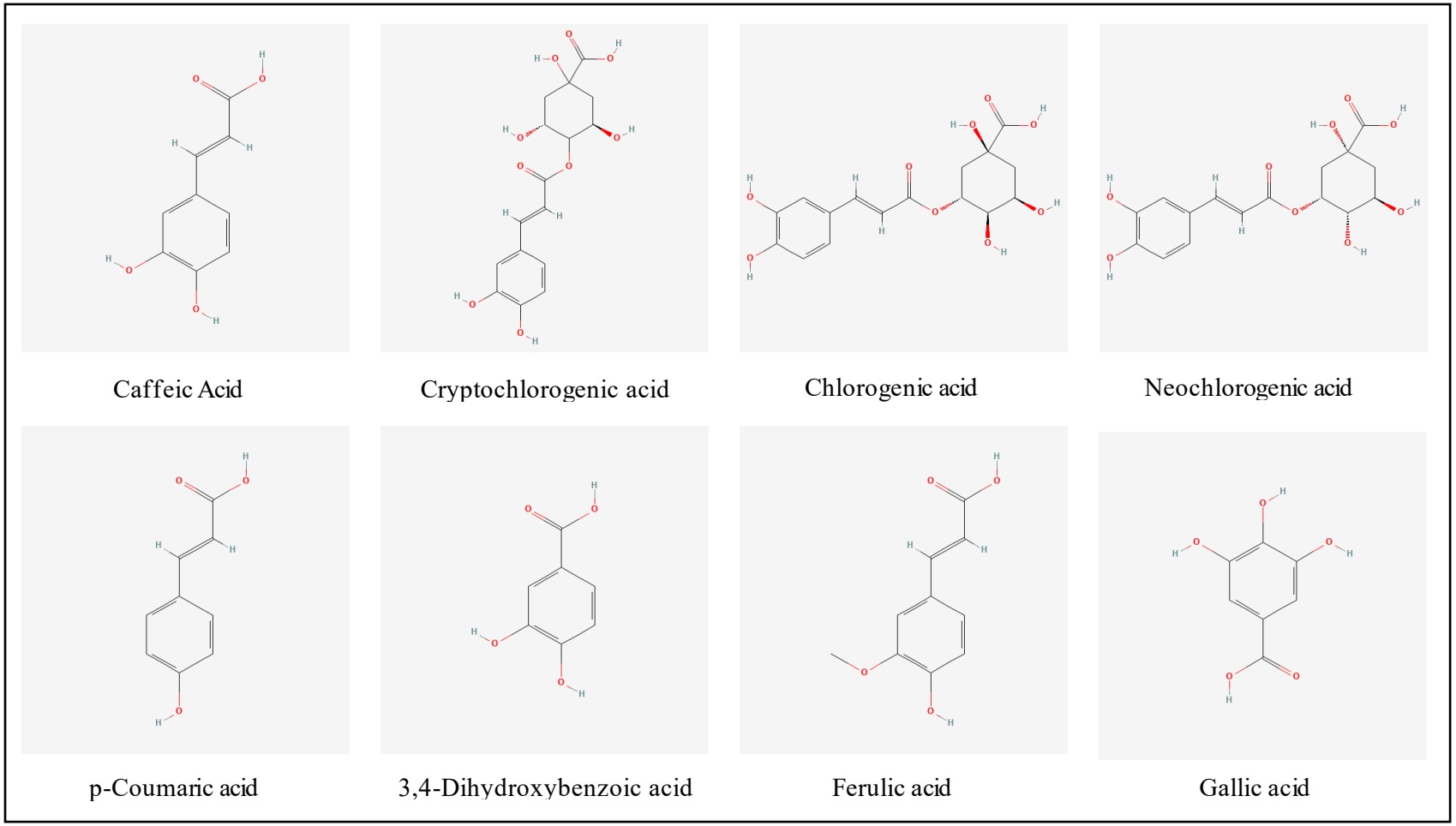

Figure A 3. Chemical structure of eight polyphenol compounds putatively identified in American elderberry juices.

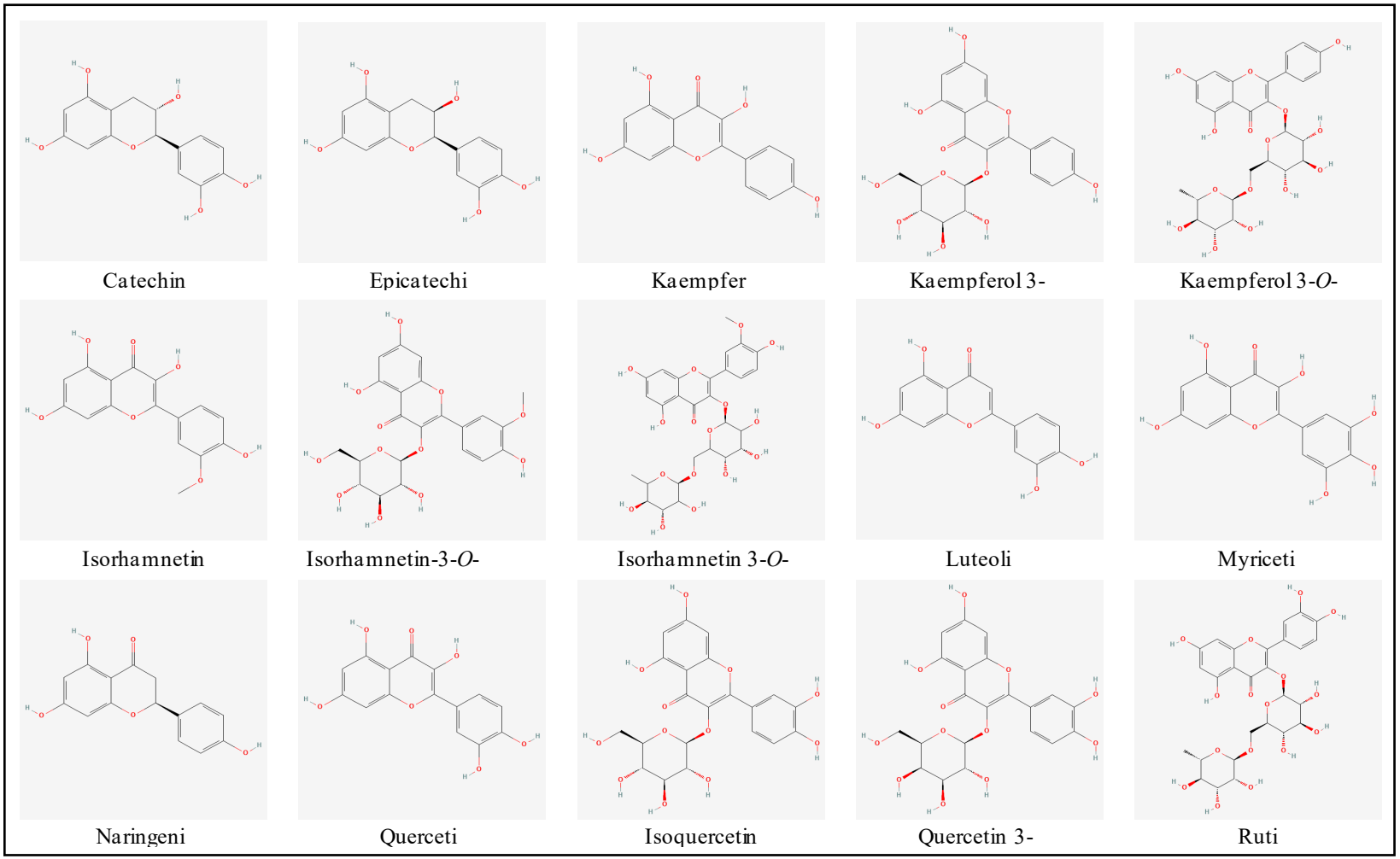

Figure A 4. Chemical structure of 15 flavonoid compounds putatively identified in American elderberry juices.

A.

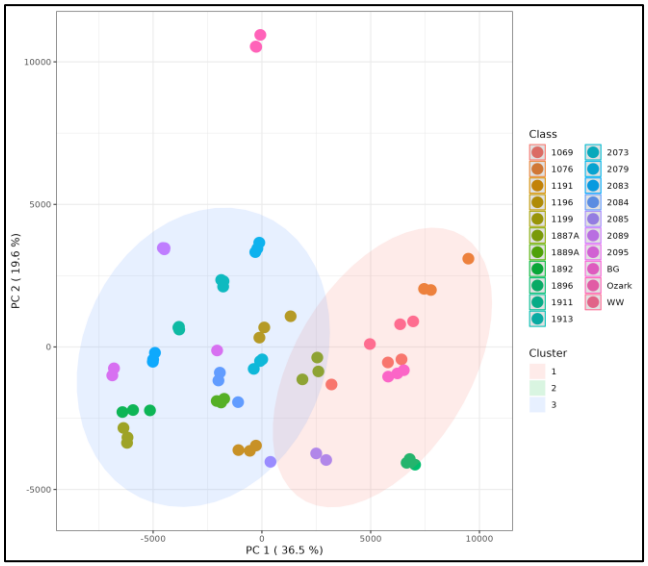

B.

Cluster	Members
Cluster 1	1191 , 1191.1 , 1191.2 , 1196 , 1196.1 , 1196.2 , 1199 , 1199.1 , 1199.2 , 1889A , 1889A.1 , 1889A.2 , 1892 , 1892.1 , 1892.2 , 1911 , 1911.1 , 1911.2 , 1913 , 1913.1 , 1913.2 , 2073 , 2073.1 , 2073.2 , 2079 , 2079.1 , 2079.2 , 2083 , 2083.1 , 2083.2 , 2084 , 2084.1 , 2084.2 , 2085.1 , 2089 , 2089.1 , 2089.2 , 2095 , 2095.1 , 2095.2
Cluster 2	Ozark , Ozark.1 , Ozark.2
Cluster 3	1069 , 1069.1 , 1069.2 , 1076 , 1076.1 , 1076.2 , 1887A , 1887A.1 , 1887A.2 , 1896 , 1896.1 , 1896.2 , 2085 , 2085.2 , BG , BG.1 , BG.2 , WW , WW.1 , WW.2

Figure A 5. K-means clustering analysis of metabolomic data from American elderberry genotypes. A. Metabolomic abundance data were subjected to k-means clustering (K=3) resulting in the grouping of genotypes based on similarity in metabolomic profiles. Each color represents a distinct of cluster. B. List of genotypes assigned to each cluster group.

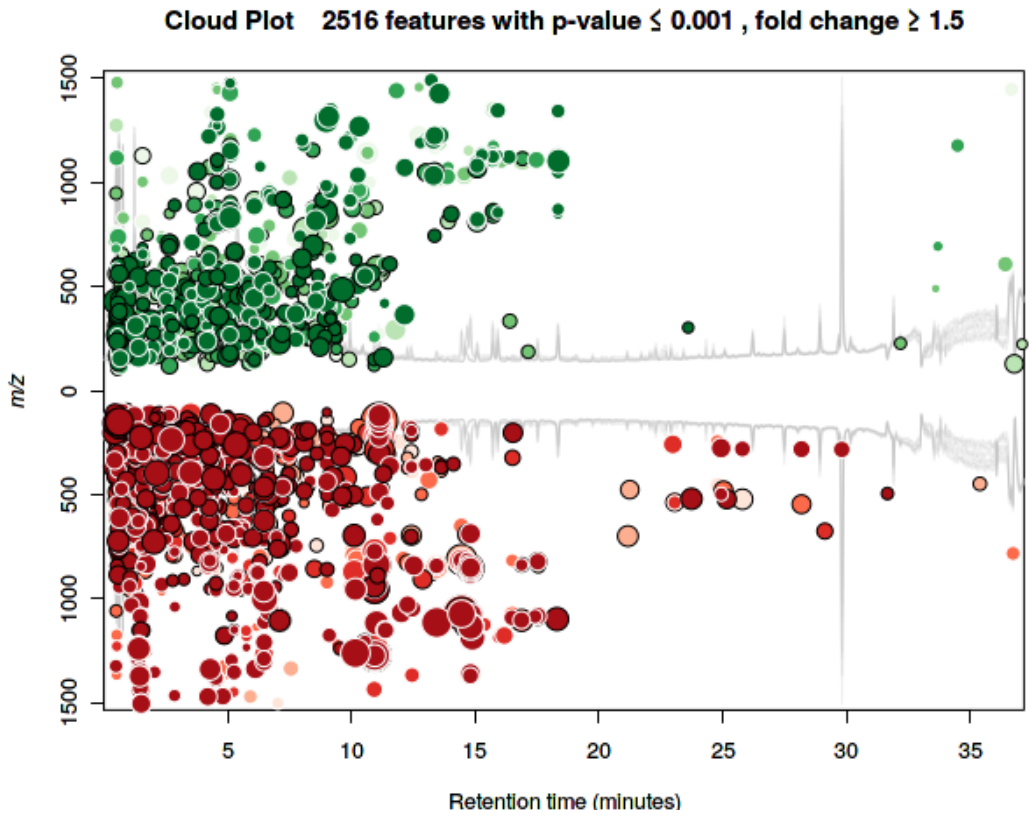

Figure A 6. Metabolomic cloudplot representation generated from XCMS platform for the analysis of the juice of American elderberry accession 1896 and 1191 showed 2561 features with p-value ≤0.001, and fold-change ≥1.5. Each circle represents a feature detected on the samples. Green color represented metabolomic feature that is up-regulated, while red color represented metabolomic feature that is down-regulated. Fold-change of a feature was presented as a radius of a circle.

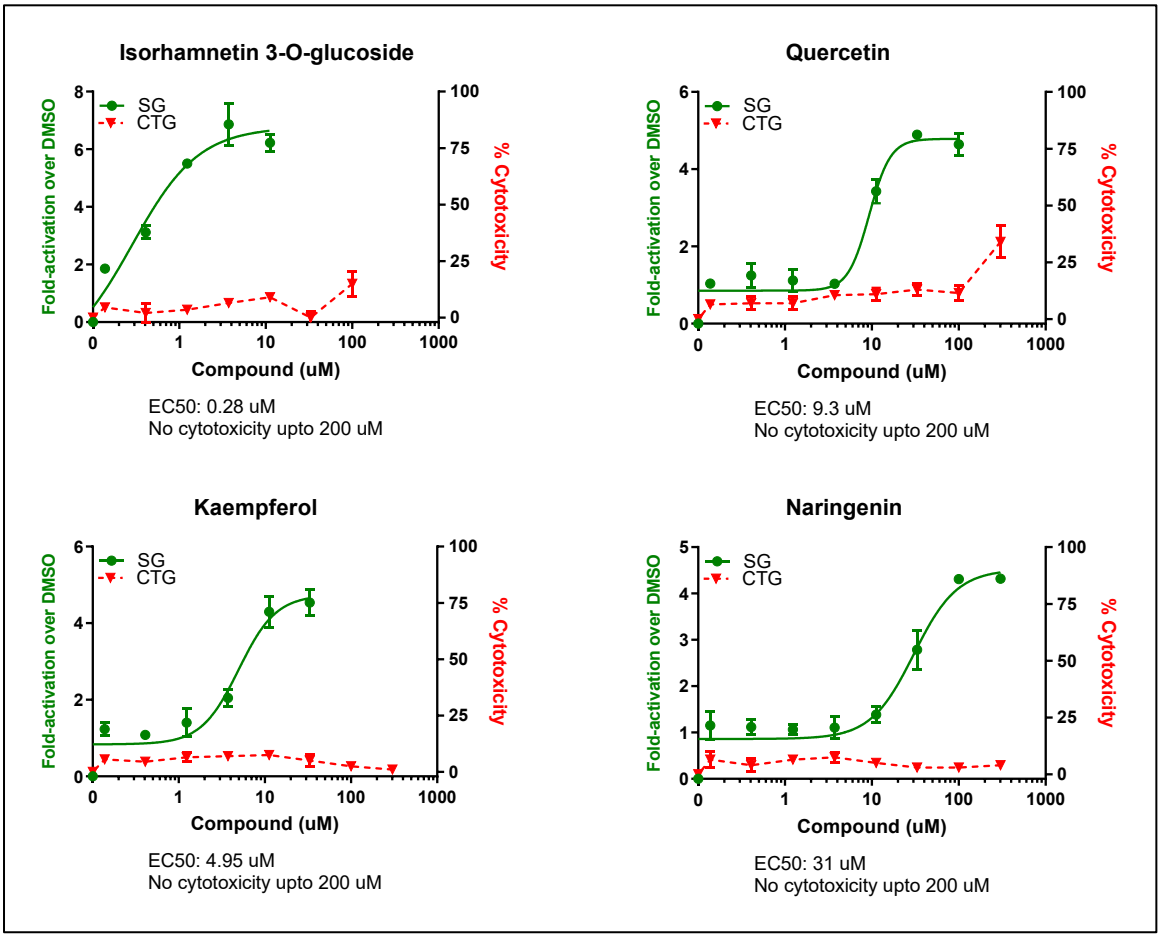

Figure A 7. Representative American elderberry compound cytotoxicity in ARE assay in HepG2 cell line (n=2).

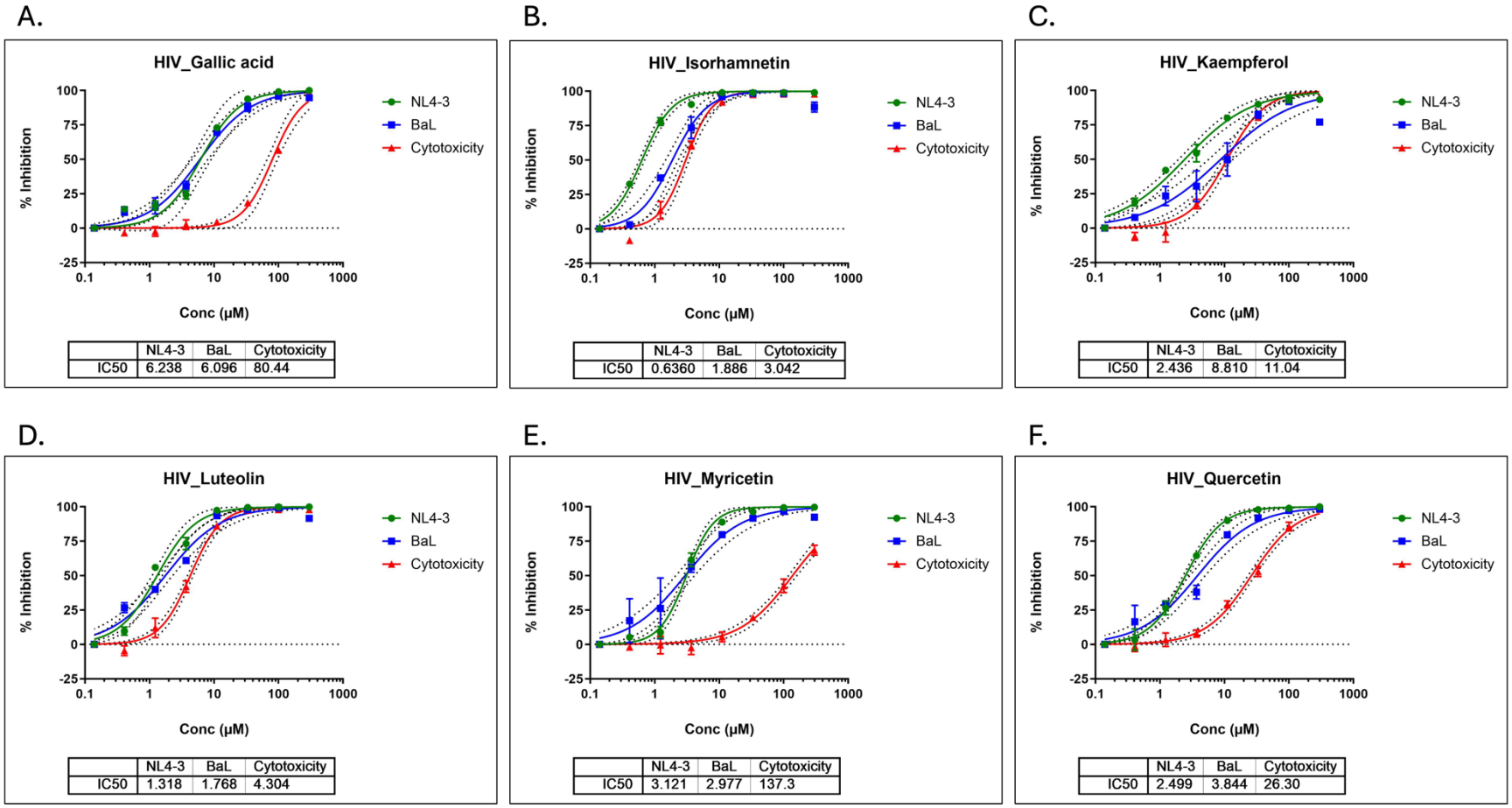

Figure A 8. Antiviral activity of American elderberry compounds against HIV strains NL4-3 and BaL (n=2). A. Gallic acid. B. Isorhamnetin. C. Kaempferol. D. Luteolin. E. Myricetin. F. Quercetin

Table A 5. Concentration of bioactive compounds in the juice of American elderberry accession 1892, 2083, 2073, 1076, 1069, and 2095

No.	Elderberry Compound	ACC 1892	ACC 2083	ACC 2073	ACC 1076	ACC 1887A	ACC 1069	ACC 2095
1	Caffeic acid	12.67 ± 1.26	27.97 ± 1.21	14.44 ± 1.49	24.90 ± 1.15	13.58 ± 4.66	43.81 ± 0.61	49.43 ± 4.82
2	Chlorogenic acid	38.30 ± 4.97	119.26 ± 10.23	26.22 ± 4.81	35.93 ± 5.88	19.35 ± 1.92	46.72 ± 4.06	nd*
3	p-Coumaric acid	19.79 ± 0.88	40.89 ± 0.36	63.26 ± 0.75	46.33 ± 0.47	55.00 ± 0.36	47.31 ± 1.16	70.51 ± 2.73
4	Cyanidin 3,5-O-diglucoside	20.65 ± 1.87	83.52 ± 3.89	1.30 ± 0.65	19.00 ± 1.12	10.29 ± 0.32	84.01 ± 2.66	55.14 ± 1.88
5	Cyanidin 3-O-galactoside/ Cyanidin 3-O-glucoside	2.17 ± 0.06	6.49 ± 0.22	0.24 ± 0.09	nd*	nd*	nd*	nd*
6	Cyanidin 3-O-rutinoside	nd*	nd*	nd*	nd*	nd*	nd*	nd*
7	Cyanidin 3-O-sambubioside	1.40 ± 0.05	10.62 ± 0.36	nd*	5.04 ± 0.24	nd*	nd*	4.26 ± 0.28
8	Cyanidin 3-O-sophoroside	10.52 ± 0.94	38.88 ± 3.25	0.96 ± 0.28	9.32 ± 0.66	4.88 ± 0.41	36.58 ± 2.58	23.45 ± 1.63
9	Delphinidin 3-O-rutinoside	89.65 ± 5.20	294.83 ± 14.36	0.96 ± 0.64	92.87 ± 3.39	8.80 ± 0.88	173.80 ± 5.83	nd*
10	3-4, Dihydroxybenzoic acid	21.45 ± 1.84	36.47 ± 1.81	40.23 ± 0.78	42.40 ± 1.74	64.00 ± 7.36	34.86 ± 3.59	137.70 ± 6.74
11	Ferulic acid	0.63 ± 0.04	0.80 ± 0.09	1.71 ± 0.17	0.83 ± 0.15	1.88 ± 0.17	1.48 ± 0.05	3.89 ± 0.20
12	Isorhamnetin	0.17 ± 0.00	1.49 ± 0.16	0.40 ± 0.05	0.27 ± 0.01	0.56 ± 0.06	0.57 ± 0.07	0.04 ± 0.01
13	Isorhamnetin 3-rutinoside	5.82 ± 0.25	60.41 ± 0.80	0.86 ± 0.12	7.77 ± 0.42	6.65 ± 0.15	41.46 ± 0.56	nd*
14	Kaempferol	2.52 ± 0.49	4.07 ± 0.14	2.26 ± 0.14	2.11 ± 0.25	nd*	3.69 ± 0.41	nd*
15	Kaempferol 3-glucoside	0.56 ± 0.02	0.70 ± 0.04	nd*	nd*	nd*	1.26 ± 0.10	nd*
16	Kaempferol 3-O-rutinoside	4.09 ± 0.13	8.96 ± 0.32	0.13 ± 0.03	2.91 ± 0.25	nd*	10.76 ± 0.55	nd*
17	Naringenin	0.12 ± 0.03	0.09 ± 0.04	0.21 ± 0.01	0.13 ± 0.01	0.27 ± 0.02	0.08 ± 0.01	0.06 ± 0.02
18	Neochlorogenic acid	47.77 ± 3.98	115.61 ± 16.50	24.37 ± 7.20	53.17 ± 7.27	36.70 ± 3.71	56.90 ± 4.69	26.08 ± 4.23
19	Quercetin	16.10 ± 0.86	71.30 ± 1.68	3.62 ± 0.69	31.13 ± 3.50	8.55 ± 1.19	25.89 ± 2.50	1.65 ± 0.46
20	Isoquercetin	7.47 ± 0.41	19.32 ± 0.56	0.42 ± 0.05	7.31 ± 0.10	2.92 ± 0.21	12.22 ± 0.38	0.05 ± 0.03
21	Rutin (quercetin-3-rutinoside)	79.12 ± 1.18	268.10 ± 8.06	1.43 ± 0.34	85.23 ± 3.80	7.35 ± 0.09	158.66 ± 2.91	nd*
22	Isorhamnetin 3-O-glucoside	0.74 ± 0.06	3.38 ± 0.28	1.16 ± 0.10	0.88 ± 0.11	2.03 ± 0.26	3.91 ± 0.16	nd*

*nd = not detected/below limit of detection. **data presented as mean ± SD (mg L^{-1})

Table A 6. Concentration of bioactive compounds in the juice of American elderberry cultivar Ozark, 1196, 1199, 2084, 2085, 1889A, and 1913

No.	Elderberry Compound	Ozark	ACC 1196	ACC 1199	ACC 2084	ACC 2085	ACC 1889A	ACC 1913
1	Caffeic acid	13.22 ± 0.61	123.64 ± 8.53	47.50 ± 0.43	7.34 ± 0.69	50.23 ± 14.42	35.86 ± 3.10	2.96 ± 0.71
2	Chlorogenic acid	92.05 ± 12.42	nd*	22.04 ± 5.73	nd*	36.87 ± 15.94	69.01 ± 15.06	nd*
3	p-Coumaric acid	31.91 ± 0.76	87.73 ± 1.13	34.90 ± 0.34	4.06 ± 0.07	46.83 ± 6.58	38.10 ± 1.05	71.26 ± 1.49
4	Cyanidin 3,5-O-diglucoside	52.84 ± 4.08	5.21 ± 0.66	111.72 ± 4.62	30.43 ± 2.90	47.22 ± 22.42	73.15 ± 2.22	29.95 ± 4.29
5	Cyanidin 3-O-galactoside/ Cyanidin 3-O-glucoside	nd*	nd*	11.80 ± 1.16	nd*	1.34 ± 2.32	4.31 ± 0.25	nd*
6	Cyanidin 3-O-rutinoside	nd*	nd*	2.54 ± 0.12	nd*	nd*	nd*	nd*
7	Cyanidin 3-O-sambubioside	6.79 ± 0.30	0.86 ± 0.09	5.11 ± 0.38	nd*	2.75 ± 1.54	1.15 ± 0.18	nd*
8	Cyanidin 3-O-sophoroside	24.09 ± 1.66	3.18 ± 0.57	51.44 ± 2.36	14.46 ± 1.64	22.64 ± 9.41	36.02 ± 5.32	14.74 ± 0.79
9	Delphinidin 3-O-rutinoside	236.71 ± 13.95	0.00 ± 0.00	20.79 ± 1.52	0.00 ± 0.00	112.24 ± 107.37	239.44 ± 3.18	115.35 ± 4.16
10	3-4, Dihydroxybenzoic acid	32.81 ± 1.41	328.54 ± 8.55	51.60 ± 1.18	110.54 ± 3.83	55.76 ± 28.31	97.95 ± 8.33	75.68 ± 2.54
11	Ferulic acid	0.72 ± 0.12	9.56 ± 0.24	1.88 ± 0.11	0.15 ± 0.02	1.25 ± 0.52	0.92 ± 0.23	1.15 ± 0.06
12	Isorhamnetin	0.44 ± 0.02	0.04 ± 0.01	0.44 ± 0.03	0.03 ± 0.01	0.08 ± 0.01	0.10 ± 0.01	0.40 ± 0.04
13	Isorhamnetin 3-rutinoside	111.91 ± 2.89	nd*	1.26 ± 0.10	nd*	0.73 ± 1.27	2.21 ± 0.16	42.10 ± 1.88
14	Kaempferol	1.36 ± 0.05	nd*	6.71 ± 0.33	nd*	5.56 ± 3.46	1.59 ± 0.18	1.04 ± 0.09
15	Kaempferol 3-glucoside	nd*	nd*	nd*	nd*	0.74 ± 0.13	0.46 ± 0.14	0.50 ± 0.04
16	Kaempferol 3-O-rutinoside	15.42 ± 0.47	nd*	nd*	nd*	2.93 ± 0.59	3.94 ± 0.38	3.64 ± 0.23
17	Naringenin	0.11 ± 0.03	0.31 ± 0.01	0.17 ± 0.02	0.19 ± 0.02	0.14 ± 0.02	0.12 ± 0.01	0.12 ± 0.02
18	Neochlorogenic acid	94.02 ± 5.68	nd*	50.80 ± 1.72	31.19 ± 2.22	52.81 ± 30.20	95.83 ± 14.48	nd*
19	Quercetin	8.85 ± 0.56	1.44 ± 0.20	52.88 ± 2.64	1.90 ± 0.76	57.10 ± 11.76	43.25 ± 0.92	14.16 ± 0.56
20	Isoquercetin	10.76 ± 0.40	0.00 ± 0.00	7.48 ± 0.20	0.29 ± 0.03	9.02 ± 3.34	12.72 ± 0.25	17.79 ± 0.17
21	Rutin (quercetin-3-rutinoside)	216.70 ± 3.85	0.60 ± 0.27	15.17 ± 0.56	1.13 ± 0.32	116.21 ± 88.21	221.64 ± 5.55	113.83 ± 0.70
22	Isorhamnetin 3-O-glucoside	3.14 ± 0.19	nd*	0.70 ± 0.05	nd*	0.14 ± 0.24	0.40 ± 0.04	4.58 ± 0.06

nd = not detected/below limit of detection. **data presented as mean ± SD (mg L^{-1})

Table A 7. Concentration of bioactive compounds in the juice of American elderberry accession 2079, 1911, 1896, 2089, Bob Gordon, and Wyldewood. *nd = not detected/below limit of detection. **data presented as mean ± SD (mg L^{-1})

No.	Elderberry Compound	ACC 2079	ACC 1911	ACC 1896	ACC 1191	ACC 2089	Bob Gordon	Wyldewood
1	Caffeic acid	22.43 ± 3.63	16.68 ± 0.59	46.36 ± 3.00	23.51 ± 2.17	28.89 ± 2.80	21.64 ± 1.38	67.95 ± 2.65
2	Chlorogenic acid	40.96 ± 6.02	nd*	33.67 ± 10.26	73.71 ± 13.10	25.86 ± 0.56	61.47 ± 2.92	65.78 ± 2.18
3	p-Coumaric acid	42.35 ± 0.73	72.80 ± 0.78	21.61 ± 0.48	67.14 ± 1.58	48.63 ± 1.14	61.00 ± 0.27	90.46 ± 1.56
4	Cyanidin 3,5-O-diglucoside	13.61 ± 0.39	49.26 ± 5.14	303.44 ± 7.44	19.47 ± 0.65	1.75 ± 0.22	130.83 ± 9.82	23.95 ± 2.80
5	Cyanidin 3-O-galactoside/ Cyanidin 3-O-glucoside	nd*	nd*	nd*	nd*	nd*	nd*	nd*
6	Cyanidin 3-O-rutinoside	nd*	nd*	nd*	nd*	nd*	nd*	nd*
7	Cyanidin 3-O-sambubioside	2.41 ± 0.08	2.51 ± 0.40	2.75 ± 0.16	1.60 ± 0.15	2.17 ± 0.30	nd*	nd*
8	Cyanidin 3-O-sophoroside	7.50 ± 1.38	21.71 ± 1.32	151.50 ± 10.22	8.33 ± 1.46	1.12 ± 0.18	51.03 ± 4.34	10.52 ± 0.92
9	Delphinidin 3-O-rutinoside	105.57 ± 3.44	21.87 ± 0.63	41.45 ± 1.41	21.20 ± 1.72	105.84 ± 2.62	165.76 ± 7.93	20.11 ± 1.06
10	3-4, Dihydroxybenzoic acid	41.69 ± 1.49	79.43 ± 1.65	74.01 ± 1.95	38.27 ± 1.46	62.39 ± 4.75	40.96 ± 3.02	45.30 ± 1.18
11	Ferulic acid	0.81 ± 0.08	2.45 ± 0.10	0.42 ± 0.10	2.23 ± 0.12	0.81 ± 0.11	1.54 ± 0.06	2.11 ± 0.17
12	Isorhamnetin	0.04 ± 0.01	0.07 ± 0.01	0.65 ± 0.03	0.08 ± 0.01	1.00 ± 0.05	0.63 ± 0.05	0.68 ± 0.03
13	Isorhamnetin 3-rutinoside	0.48 ± 0.05	0.88 ± 0.00	3.35 ± 0.17	0.13 ± 0.00	47.22 ± 1.40	39.89 ± 0.33	4.37 ± 0.29
14	Kaempferol	nd*	nd*	2.92 ± 0.27	6.65 ± 0.22	2.79 ± 0.39	2.91 ± 0.19	3.50 ± 0.40
15	Kaempferol 3-glucoside	0.40 ± 0.70	nd*	0.32 ± 0.04	0.62 ± 0.02	0.37 ± 0.04	nd*	nd*
16	Kaempferol 3-O-rutinoside	1.30 ± 0.20	nd*	nd*	0.88 ± 0.06	2.50 ± 0.25	9.20 ± 0.08	0.00 ± 0.00
17	Naringenin	0.14 ± 0.05	0.09 ± 0.03	0.17 ± 0.03	0.18 ± 0.03	0.13 ± 0.03	0.10 ± 0.01	0.32 ± 0.02
18	Neochlorogenic acid	93.39 ± 7.76	nd*	59.77 ± 5.83	72.83 ± 8.70	55.81 ± 2.89	100.06 ± 10.46	119.46 ± 7.40
19	Quercetin	21.92 ± 1.12	13.34 ± 1.12	105.97 ± 3.09	59.05 ± 3.18	25.19 ± 2.00	28.85 ± 0.30	28.98 ± 2.31
20	Isoquercetin	6.54 ± 0.23	2.55 ± 0.11	16.14 ± 0.58	9.93 ± 0.14	5.85 ± 0.50	20.81 ± 0.25	4.18 ± 0.27
21	Rutin (quercetin-3-rutinoside)	96.97 ± 4.44	18.17 ± 0.77	31.40 ± 0.76	15.27 ± 0.12	100.16 ± 2.73	159.10 ± 1.70	15.90 ± 0.97
22	Isorhamnetin 3-O-glucoside	nd*	nd*	1.13 ± 0.07	nd*	5.07 ± 0.35	4.23 ± 0.08	1.33 ± 0.07

REFERENCES

(1) Applequist, W. L. A Brief Review of Recent Controversies in the Taxonomy and Nomenclature of Sambucus Nigra Sensu Lato. *Acta Hortic.* **2015**, No. 1061, 25–33. https://doi.org/10.17660/ActaHortic.2015.1061.1.

(2) Salamon, I.; Grulova, D. Elderberry (Sambucus Nigra): From Natural Medicine in Ancient Times to Protection against Witches in the Middle Ages - a Brief Historical Overview. *Acta Hortic.* **2015**, No. 1061, 35–39. https://doi.org/10.17660/ActaHortic.2015.1061.2.

(3) Moerman, D. E. Ethnobotany in Native North America. *Encyclopaedia of the History of Science, Technology, and Medicine in Non-Western Cultures*; Selin, H., Ed.; Springer Netherlands: Dordrecht, 2016; pp 1729–1736. https://doi.org/10.1007/978-94-007-7747-7_8580.

(4) Mohlenbrock, R. H. USDA, NRCS 1989 Midwest Wetland Flora @USDA NRCS PLANTS.

(5) Cernusca, M.; Gold, M.; Godsey, L. Elderberry Market Research. **2011**.

(6) Thomas, A. L.; Byers, P. L.; Avery, Jr., J. D.; Kaps, M.; Gu, S. Horticultural Performance of Eight American Elderberry Genotypes at Three Missouri Locations. *Acta Hortic.* **2015**, No. 1061, 237–244. https://doi.org/10.17660/ActaHortic.2015.1061.26.

(7) Appenteng, M. K.; Krueger, R.; Johnson, M. C.; Ingold, H.; Bell, R.; Thomas, A. L.; Greenlief, C. M. Cyanogenic Glycoside Analysis in American Elderberry. *Molecules* **2021**, *26* (5), 1384. https://doi.org/10.3390/molecules26051384.

(8) Liu, D.; He, X.-Q.; Wu, D.-T.; Li, H.-B.; Feng, Y.-B.; Zou, L.; Gan, R.-Y. Elderberry (Sambucus Nigra L.): Bioactive Compounds, Health Functions, and Applications. *J. Agric. Food Chem.* **2022**, *70* (14), 4202–4220. https://doi.org/10.1021/acs.jafc.2c00010.

(9) Kiprovski, B.; Malenčić, Đ.; Ljubojević, M.; Ognjanov, V.; Veberic, R.; Hudina, M.; Mikulic-Petkovsek, M. Quality Parameters Change during Ripening in Leaves and Fruits of Wild Growing and Cultivated Elderberry (Sambucus Nigra) Genotypes. *Sci. Hortic.* **2021**, *277*, 109792. https://doi.org/10.1016/j.scienta.2020.109792.

(10) Domínguez, R.; Zhang, L.; Rocchetti, G.; Lucini, L.; Pateiro, M.; Munekata, P. E. S.; Lorenzo, J. M. Elderberry (Sambucus Nigra L.) as Potential Source of Antioxidants. Characterization, Optimization of Extraction Parameters and Bioactive Properties. *Food Chem.* **2020**, *330*, 127266. https://doi.org/10.1016/j.foodchem.2020.127266.

(11) Mikulic-Petkovsek, M.; Samoticha, J.; Eler, K.; Stampar, F.; Veberic, R. Traditional Elderflower Beverages: A Rich Source of Phenolic Compounds with High Antioxidant Activity. *J. Agric. Food Chem.* **2015**, *63* (5), 1477–1487. https://doi.org/10.1021/jf506005b.

(12) Johnson, M. C.; Dela Libera Tres, M.; Thomas, A. L.; Rottinghaus, G. E.; Greenlief, C. M. Discriminant Analyses of the Polyphenol Content of American Elderberry Juice from Multiple Environments Provide Genotype Fingerprint. *J. Agric. Food Chem.* **2017**, *65* (20), 4044–4050. https://doi.org/10.1021/acs.jafc.6b05675.

(13) Osman, A. G.; Avula, B.; Katragunta, K.; Ali, Z.; Chittiboyina, A. G.; Khan, I. A. Elderberry Extracts: Characterization of the Polyphenolic Chemical Composition, Quality Consistency, Safety, Adulteration, and Attenuation of Oxidative Stress- and

Inflammation-Induced Health Disorders. *Molecules* **2023**, *28* (7), 3148. https://doi.org/10.3390/molecules28073148.

(14) Pahlke, G.; Ahlberg, K.; Oertel, A.; Janson-Schaffer, T.; Grabher, S.; Mock, H.; Matros, A.; Marko, D. Antioxidant Effects of Elderberry Anthocyanins in Human Colon Carcinoma Cells: A Study on Structure–Activity Relationships. *Mol. Nutr. Food Res.* **2021**, *65* (17), 2100229. https://doi.org/10.1002/mnfr.202100229.

(15) Przybylska-Balcerek, A.; Szablewski, T.; Szwajkowska-Michałek, L.; Świerk, D.; Cegielska-Radziejewska, R.; Krejpcio, Z.; Suchowilska, E.; Tomczyk, Ł.; Stuper-Szablewska, K. Sambucus Nigra Extracts–Natural Antioxidants and Antimicrobial Compounds. *Molecules* **2021**, *26* (10), 2910. https://doi.org/10.3390/molecules26102910.

(16) Jiang, J. M.; Zong, Y.; Chuang, D. Y.; Lei, W.; Lu, C.-H.; Gu, Z.; Fritsche, K. L.; Thomas, A. L.; Lubahn, D. B.; Simonyi, A.; Sun, G. Y. Effects of Elderberry Juice from Different Genotypes on Oxidative and Inflammatory Responses in Microglial Cells. *Acta Hortic.* **2015**, No. 1061, 281–288. https://doi.org/10.17660/ActaHortic.2015.1061.31.

(17) Olejnik, A.; Kowalska, K.; Olkowicz, M.; Rychlik, J.; Juzwa, W.; Myszka, K.; Dembczyński, R.; Białas, W. Anti-Inflammatory Effects of Gastrointestinal Digested Sambucus Nigra L. Fruit Extract Analysed in Co-Cultured Intestinal Epithelial Cells and Lipopolysaccharide-Stimulated Macrophages. *J. Funct. Foods* **2015**, *19*, 649–660. https://doi.org/10.1016/j.jff.2015.09.064.

(18) Gleńsk, M.; Czapińska, E.; Woźniak, M.; Ceremuga, I.; Włodarczyk, M.; Terlecki, G.; Ziółkowski, P.; Seweryn, E. Triterpenoid Acids as Important Antiproliferative Constituents of European Elderberry Fruits. *Nutr. Cancer* **2017**, *69* (4), 643–651. https://doi.org/10.1080/01635581.2017.1295085.

(19) Pereira, D. I.; Amparo, T. R.; Almeida, T. C.; Costa, F. S. F.; Brandão, G. C.; Santos, O. D. H. D.; Da Silva, G. N.; Bianco De Souza, G. H. Cytotoxic Activity of Butanolic Extract from *Sambucus Nigra* L. Flowers *in Natura* and Vehiculated in Micelles in Bladder Cancer Cells and Fibroblasts. *Nat. Prod. Res.* **2022**, *36* (4), 1100–1104. https://doi.org/10.1080/14786419.2020.1851220.

(20) Porter, R. S.; Bode, R. F. A Review of the Antiviral Properties of Black Elder (Sambucus Nigra L.) Products: Antiviral Properties of Black Elder (Sambucus Nigra L.). *Phytother. Res.* **2017**, *31* (4), 533–554. https://doi.org/10.1002/ptr.5782.

(21) Álvarez, C.; Barriga, A.; Albericio, F.; Romero, M.; Guzmán, F. Identification of Peptides in Flowers of Sambucus Nigra with Antimicrobial Activity against Aquaculture Pathogens. *Molecules* **2018**, *23* (5), 1033. https://doi.org/10.3390/molecules23051033.

(22) Salvador, Â.; Król, E.; Lemos, V.; Santos, S.; Bento, F.; Costa, C.; Almeida, A.; Szczepankiewicz, D.; Kulczyński, B.; Krejpcio, Z.; Silvestre, A.; Rocha, S. Effect of Elderberry (Sambucus Nigra L.) Extract Supplementation in STZ-Induced Diabetic Rats Fed with a High-Fat Diet. *Int. J. Mol. Sci.* **2016**, *18* (1), 13. https://doi.org/10.3390/ijms18010013.

(23) Macarrón, R.; Hertzberg, R. P. Design and Implementation of High Throughput Screening Assays. *Mol. Biotechnol.* **2011**, *47* (3), 270–285. https://doi.org/10.1007/s12033-010-9335-9.

(24) Macarron, R.; Banks, M. N.; Bojanic, D.; Burns, D. J.; Cirovic, D. A.; Garyantes, T.; Green, D. V. S.; Hertzberg, R. P.; Janzen, W. P.; Paslay, J. W.; Schopfer, U.; Sittampalam, G. S. Impact of High-Throughput Screening in Biomedical Research. *Nat. Rev. Drug Discov.* **2011**, *10* (3), 188–195. https://doi.org/10.1038/nrd3368.

(25) Cai, Z.; Stubblefield, K.; Thomas, A. L.; Aguilar, F. X. From Niche to Mainstream: US Consumer Trends and Preferences for Elderberry Products. *HortScience* **2024**, *59* (12), 1723–1729. https://doi.org/10.21273/HORTSCI18180-24.

(26) Thomas, A. L.; Byers, P. L.; Gu, S.; Avery, Jr., J. D.; Kaps, M.; Datta, A.; Fernando, L.; Grossi, P.; Rottinghaus, G. E. Occurrence of Polyphenols, Organic Acids, and Sugars among Diverse Elderberry Genotypes Grown in Three Missouri (USA) Locations. *Acta Hortic.* **2015**, No. 1061, 147–154. https://doi.org/10.17660/ActaHortic.2015.1061.14.

(27) Lee, J.; Finn, C. E. Anthocyanins and Other Polyphenolics in American Elderberry (*Sambucus Canadensis*) and European Elderberry (*S. Nigra*) Cultivars. *J. Sci. Food Agric.* **2007**, *87* (14), 2665–2675. https://doi.org/10.1002/jsfa.3029.

(28) Johnson, M. C.; Dela Libera Tres, M.; Thomas, A. L.; Rottinghaus, G. E.; Greenlief, C. M. Discriminant Analyses of the Polyphenol Content of American Elderberry Juice from Multiple Environments Provide Genotype Fingerprint. *J. Agric. Food Chem.* **2017**, *65* (20), 4044–4050. https://doi.org/10.1021/acs.jafc.6b05675.

(29) Tsugawa, H.; Rai, A.; Saito, K.; Nakabayashi, R. Metabolomics and Complementary Techniques to Investigate the Plant Phytochemical Cosmos. *Nat. Prod. Rep.* **2021**, *38* (10), 1729–1759. https://doi.org/10.1039/D1NP00014D.

(30) Mudge, E.; Applequist, W. L.; Finleya, J.; Patience, L.; Townesmithb, A. K.; Walkerb, K. M.; Browna. Variation of Select Flavonols and Chlorogenic Acid Content of Elderberry Collected throughout the Eastern United States. **2016**.

(31) Byers, P. L.; Thomas, A. L.; Millican, M. 'Wyldewood' Elderberry. *HortScience* **2010**, *45* (2), 312–313. https://doi.org/10.21273/HORTSCI.45.2.312.

(32) Byers, P. L.; Thomas, A. L. 'Bob Gordon' Elderberry. *Journal of the American Pomological Society* **2011**, *65* (2), 52–55.

(33) Özyürek, M.; Güçlü, K.; Tütem, E.; Başkan, K. S.; Erçağ, E.; Esin Çelik, S.; Baki, S.; Yıldız, L.; Karaman, Ş.; Apak, R. A Comprehensive Review of CUPRAC Methodology. *Anal. Methods* **2011**, *3* (11), 2439. https://doi.org/10.1039/c1ay05320e.

(34) Wu, K. C.; McDonald, P. R.; Liu, J. J.; Chaguturu, R.; Klaassen, C. D. Implementation of a High-Throughput Screen for Identifying Small Molecules to Activate the Keap1-Nrf2-ARE Pathway. *PLoS ONE* **2012**, *7* (10), e44686. https://doi.org/10.1371/journal.pone.0044686.

(35) Platt, E. J.; Wehrly, K.; Kuhmann, S. E.; Chesebro, B.; Kabat, D. Effects of CCR5 and CD4 Cell Surface Concentrations on Infections by Macrophagetropic Isolates of Human Immunodeficiency Virus Type 1. *J. Virol.* **1998**, *72* (4), 2855–2864. https://doi.org/10.1128/JVI.72.4.2855-2864.1998.

(36) Sarzotti-Kelsoe, M.; Bailer, R. T.; Turk, E.; Lin, C.; Bilska, M.; Greene, K. M.; Gao, H.; Todd, C. A.; Ozaki, D. A.; Seaman, M. S.; Mascola, J. R.; Montefiori, D. C. Optimization and Validation of the TZM-Bl Assay for Standardized Assessments of Neutralizing Antibodies against HIV-1. *J. Immunol. Methods* **2014**, *409*, 131–146. https://doi.org/10.1016/j.jim.2013.11.022.

(37) Silva, E.; Perez Da Graça, J.; Porto, C.; Martin Do Prado, R.; Nunes, E.; Corrêa Marcelino-Guimarães, F.; Conrado Meyer, M.; Jorge Pilau, E. Untargeted Metabolomics Analysis by UHPLC-MS/MS of Soybean Plant in a Compatible Response to Phakopsora Pachyrhizi Infection. *Metabolites* **2021**, *11* (3), 179. https://doi.org/10.3390/metabo11030179.
(38) Bai, J.; Zhang, Y.; Tang, C.; Hou, Y.; Ai, X.; Chen, X.; Zhang, Y.; Wang, X.; Meng, X. Gallic Acid: Pharmacological Activities and Molecular Mechanisms Involved in Inflammation-Related Diseases. *Biomed. Pharmacother.* **2021**, *133*, 110985. https://doi.org/10.1016/j.biopha.2020.110985.
(39) Vincent, S.; Stanely, S. P.; Ponnian, S. M. P. Protective Effects of 3, 4-dihydroxybenzoic Acid on Myocardial Infarction Induced by Isoproterenol in Rats. *J. Biochem. Mol. Toxicol.* **2024**, *38* (8), e23773. https://doi.org/10.1002/jbt.23773.
(40) Satari, A.; Ghasemi, S.; Habtemariam, S.; Asgharian, S.; Lorigooini, Z. Rutin: A Flavonoid as an Effective Sensitizer for Anticancer Therapy; Insights into Multifaceted Mechanisms and Applicability for Combination Therapy. *Evid. Based Complement. Alternat. Med.* **2021**, *2021*, 1–10. https://doi.org/10.1155/2021/9913179.
(41) Jeszka-Skowron, M.; Krawczyk, M.; Zgoła-Grześkowiak, A. Determination of Antioxidant Activity, Rutin, Quercetin, Phenolic Acids and Trace Elements in Tea Infusions: Influence of Citric Acid Addition on Extraction of Metals. *J. Food Compos. Anal.* **2015**, *40*, 70–77. https://doi.org/10.1016/j.jfca.2014.12.015.
(42) Li, Y. Q.; Zhou, F. C.; Gao, F.; Bian, J. S.; Shan, F. Comparative Evaluation of Quercetin, Isoquercetin and Rutin as Inhibitors of α-Glucosidase. *J. Agric. Food Chem.* **2009**, *57* (24), 11463–11468. https://doi.org/10.1021/jf903083h.
(43) Ganeshpurkar, A.; Saluja, A. K. The Pharmacological Potential of Rutin. *Saudi Pharm. J.* **2017**, *25* (2), 149–164. https://doi.org/10.1016/j.jsps.2016.04.025.
(44) Miladinovic, B.; Faria, M. Â.; Ribeiro, M.; Sobral, M. M. C.; Ferreira, I. M. P. L. V. O. Delphinidin-3-Rutinoside from Blackcurrant Berries (Ribes Nigrum): In Vitro Antiproliferative Activity and Interactions with Other Phenolic Compounds. *Molecules* **2023**, *28* (3), 1286. https://doi.org/10.3390/molecules28031286.
(45) Xie, J.; Cui, H.; Xu, Y.; Xie, L.; Chen, W. Delphinidin-3- *O* -Sambubioside: A Novel Xanthine Oxidase Inhibitor Identified from Natural Anthocyanins. *Food Qual. Saf.* **2021**, *5*, fyaa038. https://doi.org/10.1093/fqsafe/fyaa038.
(46) Magnani, C.; Isaac, V. L. B.; Correa, M. A.; Salgado, H. R. N. Caffeic Acid: A Review of Its Potential Use in Medications and Cosmetics. *Anal Methods* **2014**, *6* (10), 3203–3210. https://doi.org/10.1039/C3AY41807C.
(47) Ma, X.; Okyere, S. K.; Hu, L.; Wen, J.; Ren, Z.; Deng, J.; Hu, Y. Anti-Inflammatory Activity and Mechanism of Cryptochlorogenic Acid from Ageratina Adenophora. *Nutrients* **2022**, *14* (3), 439. https://doi.org/10.3390/nu14030439.
(48) Zhou, Y. The Protective Effects of Cryptochlorogenic Acid on β-Cells Function in Diabetes in Vivo and Vitro via Inhibition of Ferroptosis. *Diabetes Metab. Syndr. Obes. Targets Ther.* **2020**, *Volume 13*, 1921–1931. https://doi.org/10.2147/DMSO.S249382.
(49) Lou, Z.; Wang, H.; Zhu, S.; Ma, C.; Wang, Z. Antibacterial Activity and Mechanism of Action of Chlorogenic Acid. *J. Food Sci.* **2011**, *76* (6). https://doi.org/10.1111/j.1750-3841.2011.02213.x.

(50) Naveed, M.; Hejazi, V.; Abbas, M.; Kamboh, A. A.; Khan, G. J.; Shumzaid, M.; Ahmad, F.; Babazadeh, D.; FangFang, X.; Modarresi-Ghazani, F.; WenHua, L.; XiaoHui, Z. Chlorogenic Acid (CGA): A Pharmacological Review and Call for Further Research. *Biomed. Pharmacother.* **2018**, *97*, 67–74. https://doi.org/10.1016/j.biopha.2017.10.064.

(51) Gao, X.; Zhang, S.; Wang, L.; Yu, L.; Zhao, X.; Ni, H.; Wang, Y.; Wang, J.; Shan, C.; Fu, Y. Anti-Inflammatory Effects of Neochlorogenic Acid Extract from Mulberry Leaf (Morus Alba L.) Against LPS-Stimulated Inflammatory Response through Mediating the AMPK/Nrf2 Signaling Pathway in A549 Cells. *Molecules* **2020**, *25* (6), 1385. https://doi.org/10.3390/molecules25061385.

(52) Navarro-Orcajada, S.; Matencio, A.; Vicente-Herrero, C.; García-Carmona, F.; López-Nicolás, J. M. Study of the Fluorescence and Interaction between Cyclodextrins and Neochlorogenic Acid, in Comparison with Chlorogenic Acid. *Sci. Rep.* **2021**, *11* (1), 3275. https://doi.org/10.1038/s41598-021-82915-9.

(53) Liang, Z.; Liang, H.; Guo, Y.; Yang, D. Cyanidin 3-O-Galactoside: A Natural Compound with Multiple Health Benefits. *Int. J. Mol. Sci.* **2021**, *22* (5), 2261. https://doi.org/10.3390/ijms22052261.

(54) Lee, J. H.; Choung, M.-G. Identification and Characterisation of Anthocyanins in the Antioxidant Activity-Containing Fraction of Liriope Platyphylla Fruits. *Food Chem.* **2011**, *127* (4), 1686–1693. https://doi.org/10.1016/j.foodchem.2011.02.037.

(55) Olivas-Aguirre, F.; Rodrigo-García, J.; Martínez-Ruiz, N.; Cárdenas-Robles, A.; Mendoza-Díaz, S.; Álvarez-Parrilla, E.; González-Aguilar, G.; De La Rosa, L.; Ramos-Jiménez, A.; Wall-Medrano, A. Cyanidin-3-O-Glucoside: Physical-Chemistry, Foodomics and Health Effects. *Molecules* **2016**, *21* (9), 1264. https://doi.org/10.3390/molecules21091264.

(56) Lee, S. G.; Vance, T. M.; Nam, T.-G.; Kim, D.-O.; Koo, S. I.; Chun, O. K. Contribution of Anthocyanin Composition to Total Antioxidant Capacity of Berries. *Plant Foods Hum. Nutr.* **2015**, *70* (4), 427–432. https://doi.org/10.1007/s11130-015-0514-5.

(57) Devi, K. P.; Malar, D. S.; Nabavi, S. F.; Sureda, A.; Xiao, J.; Nabavi, S. M.; Daglia, M. Kaempferol and Inflammation: From Chemistry to Medicine. *Pharmacol. Res.* **2015**, *99*, 1–10. https://doi.org/10.1016/j.phrs.2015.05.002.

(58) Periferakis, A.; Periferakis, K.; Badarau, I. A.; Petran, E. M.; Popa, D. C.; Caruntu, A.; Costache, R. S.; Scheau, C.; Caruntu, C.; Costache, D. O. Kaempferol: Antimicrobial Properties, Sources, Clinical, and Traditional Applications. *Int. J. Mol. Sci.* **2022**, *23* (23), 15054. https://doi.org/10.3390/ijms232315054.

(59) Lee, S.-J.; Hong, S.; Yoo, S.-H.; Kim, G.-W. Cyanidin-3-O-Sambubioside from Acanthopanax Sessiliflorus Fruit Inhibits Metastasis by Downregulating MMP-9 in Breast Cancer Cells MDA-MB-231. *Planta Med.* **2013**, *79* (17), 1636–1640. https://doi.org/10.1055/s-0033-1350954.

(60) Ojeda, D.; Jiménez-Ferrer, E.; Zamilpa, A.; Herrera-Arellano, A.; Tortoriello, J.; Alvarez, L. Inhibition of Angiotensin Convertin Enzyme (ACE) Activity by the Anthocyanins Delphinidin- and Cyanidin-3-O-Sambubiosides from Hibiscus Sabdariffa. *J. Ethnopharmacol.* **2010**, *127* (1), 7–10. https://doi.org/10.1016/j.jep.2009.09.059.

(61) Shen, Y.; Song, X.; Li, L.; Sun, J.; Jaiswal, Y.; Huang, J.; Liu, C.; Yang, W.; Williams, L.; Zhang, H.; Guan, Y. Protective Effects of P-Coumaric Acid against Oxidant and Hyperlipidemia-an in Vitro and in Vivo Evaluation. *Biomed. Pharmacother.* **2019**, *111*, 579–587. https://doi.org/10.1016/j.biopha.2018.12.074.
(62) Boz, H. *P* -Coumaric Acid in Cereals: Presence, Antioxidant and Antimicrobial Effects. *Int. J. Food Sci. Technol.* **2015**, *50* (11), 2323–2328. https://doi.org/10.1111/ijfs.12898.
(63) Kong, C.; Jeong, C.; Choi, J.; Kim, K.; Jeong, J. Antiangiogenic Effects of *P* -Coumaric Acid in Human Endothelial Cells. *Phytother. Res.* **2013**, *27* (3), 317–323. https://doi.org/10.1002/ptr.4718.
(64) Ou, S.; Kwok, K. Ferulic Acid: Pharmaceutical Functions, Preparation and Applications in Foods. *J. Sci. Food Agric.* **2004**, *84* (11), 1261–1269. https://doi.org/10.1002/jsfa.1873.
(65) Zhu, H.; Liang, Q.-H.; Xiong, X.-G.; Chen, J.; Wu, D.; Wang, Y.; Yang, B.; Zhang, Y.; Zhang, Y.; Huang, X. Anti-Inflammatory Effects of the Bioactive Compound Ferulic Acid Contained in *Oldenlandia Diffusa* on Collagen-Induced Arthritis in Rats. *Evid. Based Complement. Alternat. Med.* **2014**, *2014* (1), 573801. https://doi.org/10.1155/2014/573801.
(66) Amini, A. M.; Muzs, K.; Spencer, J. Pe.; Yaqoob, P. Pelargonidin-3- O -Glucoside and Its Metabolites Have Modest Anti-Inflammatory Effects in Human Whole Blood Cultures. *Nutr. Res.* **2017**, *46*, 88–95. https://doi.org/10.1016/j.nutres.2017.09.006.
(67) Duarte, L. J.; Chaves, V. C.; Nascimento, M. V. P. D. S.; Calvete, E.; Li, M.; Ciraolo, E.; Ghigo, A.; Hirsch, E.; Simões, C. M. O.; Reginatto, F. H.; Dalmarco, E. M. Molecular Mechanism of Action of Pelargonidin-3- O -Glucoside, the Main Anthocyanin Responsible for the Anti-Inflammatory Effect of Strawberry Fruits. *Food Chem.* **2018**, *247*, 56–65. https://doi.org/10.1016/j.foodchem.2017.12.015.
(68) Gowd, V.; Karim, N.; Xie, L.; Shishir, M. R. I.; Xu, Y.; Chen, W. In Vitro Study of Bioaccessibility, Antioxidant, and α-Glucosidase Inhibitory Effect of Pelargonidin-3-O-Glucoside after Interacting with Beta-Lactoglobulin and Chitosan/Pectin. *Int. J. Biol. Macromol.* **2020**, *154*, 380–389. https://doi.org/10.1016/j.ijbiomac.2020.03.126.
(69) Isemura, M. Catechin in Human Health and Disease. *Molecules* **2019**, *24* (3), 528. https://doi.org/10.3390/molecules24030528.
(70) Johnson, R.; Bryant, S.; Huntley, A. L. Green Tea and Green Tea Catechin Extracts: An Overview of the Clinical Evidence. *Maturitas* **2012**, *73* (4), 280–287. https://doi.org/10.1016/j.maturitas.2012.08.008.
(71) Daussin, F. N.; Heyman, E.; Burelle, Y. Effects of (−)-Epicatechin on Mitochondria. *Nutr. Rev.* **2021**, *79* (1), 25–41. https://doi.org/10.1093/nutrit/nuaa094.
(72) Navarrete-Yañez, V.; Garate-Carrillo, A.; Rodriguez, A.; Mendoza-Lorenzo, P.; Ceballos, G.; Calzada-Mendoza, C.; Hogan, M. C.; Villarreal, F.; Ramirez-Sanchez, I. Effects of (−)-Epicatechin on Neuroinflammation and Hyperphosphorylation of Tau in the Hippocampus of Aged Mice. *Food Funct.* **2020**, *11* (12), 10351–10361. https://doi.org/10.1039/D0FO02438D.
(73) Qu, Z.; Liu, A.; Li, P.; Liu, C.; Xiao, W.; Huang, J.; Liu, Z.; Zhang, S. Advances in Physiological Functions and Mechanisms of (−)-Epicatechin. *Crit. Rev. Food Sci. Nutr.* **2021**, *61* (2), 211–233. https://doi.org/10.1080/10408398.2020.1723057.

(74) Imran, M.; Rauf, A.; Abu-Izneid, T.; Nadeem, M.; Shariati, M. A.; Khan, I. A.; Imran, A.; Orhan, I. E.; Rizwan, M.; Atif, M.; Gondal, T. A.; Mubarak, M. S. Luteolin, a Flavonoid, as an Anticancer Agent: A Review. *Biomed. Pharmacother.* **2019**, *112*, 108612. https://doi.org/10.1016/j.biopha.2019.108612.
(75) Lin, Y.; Shi, R.; Wang, X.; Shen, H.-M. Luteolin, a Flavonoid with Potentials for Cancer Prevention and Therapy. **2009**.
(76) Lu, P.; Zhang, T.; Ren, Y.; Rao, H.; Lei, J.; Zhao, G.; Wang, M.; Gong, D.; Cao, Z. A Literature Review on the Antiviral Mechanism of Luteolin. *Nat. Prod. Commun.* **2023**, *18* (4), 1934578X2311715. https://doi.org/10.1177/1934578X231171521.
(77) Zima, V.; Radilová, K.; Kožíšek, M.; Albiñana, C. B.; Karlukova, E.; Brynda, J.; Fanfrlík, J.; Flieger, M.; Hodek, J.; Weber, J.; Majer, P.; Konvalinka, J.; Machara, A. Unraveling the Anti-Influenza Effect of Flavonoids: Experimental Validation of Luteolin and Its Congeners as Potent Influenza Endonuclease Inhibitors. *Eur. J. Med. Chem.* **2020**, *208*, 112754. https://doi.org/10.1016/j.ejmech.2020.112754.
(78) Habtemariam, S. α-Glucosidase Inhibitory Activity of Kaempferol-3- *O* -Rutinoside. *Nat. Prod. Commun.* **2011**, *6* (2), 1934578X1100600. https://doi.org/10.1177/1934578X1100600211.
(79) Wang, Y.; Tang, C.; Zhang, H. Hepatoprotective Effects of Kaempferol 3-O-Rutinoside and Kaempferol 3-O-Glucoside from Carthamus Tinctorius L. on CCl4-Induced Oxidative Liver Injury in Mice. *J. Food Drug Anal.* **2015**, *23* (2), 310–317. https://doi.org/10.1016/j.jfda.2014.10.002.
(80) Boots, A. W.; Haenen, G. R. M. M.; Bast, A. Health Effects of Quercetin: From Antioxidant to Nutraceutical. *Eur. J. Pharmacol.* **2008**, *585* (2–3), 325–337. https://doi.org/10.1016/j.ejphar.2008.03.008.
(81) Li, Y.; Yao, J.; Han, C.; Yang, J.; Chaudhry, M.; Wang, S.; Liu, H.; Yin, Y. Quercetin, Inflammation and Immunity. *Nutrients* **2016**, *8* (3), 167. https://doi.org/10.3390/nu8030167.
(82) Rauf, A.; Imran, M.; Khan, I. A.; ur-Rehman, M.; Gilani, S. A.; Mehmood, Z.; Mubarak, M. S. Anticancer Potential of Quercetin: A Comprehensive Review. *Phytother. Res.* **2018**, *32* (11), 2109–2130. https://doi.org/10.1002/ptr.6155.
(83) Qiu, P.; Chen, J.; Wu, J.; Wang, Q.; Hu, Y.; Li, X.; Shi, H.; Wang, X. The Effect of Anthocyanin from *Dioscorea Alata* L. after Purification, Identification on Antioxidant Capacity in Mice. *Food Sci. Nutr.* **2023**, *11* (10), 6106–6115. https://doi.org/10.1002/fsn3.3547.
(84) Zhang, C.-P.; Li, W.-H.; Liu, J.-R.; Li, G.-D.; Zhang, H.-P.; Wei, J.-F.; Chen, H.-S.; Zhao, J.-L.; Wang, Y.-F.; Lv, Q.; Liu, M. The Effective Analysis for Blue Honeysuckle Extract in the Treatment of Hepatocellular Carcinoma. *Evid. Based Complement. Alternat. Med.* **2022**, *2022*, 1–13. https://doi.org/10.1155/2022/9601020.
(85) Laganà, G.; Barreca, D.; Smeriglio, A.; Germanò, M. P.; D'Angelo, V.; Calderaro, A.; Bellocco, E.; Trombetta, D. Evaluation of Anthocyanin Profile, Antioxidant, Cytoprotective, and Anti-Angiogenic Properties of Callistemon Citrinus Flowers. *Plants* **2020**, *9* (8), 1045. https://doi.org/10.3390/plants9081045.
(86) Seo, J.; Jo, S.; Jung, Y. S.; Mijan, M.; Cha, J.; Hong, S.; Byun, S.; Lim, T. *Rosa Gallica* and Its Active Compound, Cyanidin-3, 5- *O* -diglucoside, Improve Skin

Hydration via the GLK Signaling Pathway. *BioFactors* **2023**, *49* (2), 415–427. https://doi.org/10.1002/biof.1922.

(87) Wang, Q.; Wei, H.; Zhou, S.; Li, Y.; Zheng, T.; Zhou, C.; Wan, X. Hyperoside: A Review on Its Sources, Biological Activities, and Molecular Mechanisms. *Phytother. Res.* **2022**, *36* (7), 2779–2802. https://doi.org/10.1002/ptr.7478.

(88) Ma, C.; Jiang, Y.; Zhang, X.; Chen, X.; Liu, Z.; Tian, X. Isoquercetin Ameliorates Myocardial Infarction through Anti-Inflammation and Anti-Apoptosis Factor and Regulating TLR4-NF-κB Signal Pathway. *Mol. Med. Rep.* **2018**. https://doi.org/10.3892/mmr.2018.8709.

(89) Yang, Q.; Kang, Z.; Zhang, J.; Qu, F.; Song, B. Neuroprotective Effects of Isoquercetin: An In Vitro and In Vivo Study. *Cell J. Yakhteh* **2021**, *23* (3). https://doi.org/10.22074/cellj.2021.7116.

(90) Riaz, A.; Rasul, A.; Hussain, G.; Zahoor, M. K.; Jabeen, F.; Subhani, Z.; Younis, T.; Ali, M.; Sarfraz, I.; Selamoglu, Z. Astragalin: A Bioactive Phytochemical with Potential Therapeutic Activities. *Adv. Pharmacol. Sci.* **2018**, *2018*, 1–15. https://doi.org/10.1155/2018/9794625.

(91) Gong, G.; Guan, Y.-Y.; Zhang, Z.-L.; Rahman, K.; Wang, S.-J.; Zhou, S.; Luan, X.; Zhang, H. Isorhamnetin: A Review of Pharmacological Effects. *Biomed. Pharmacother.* **2020**, *128*, 110301. https://doi.org/10.1016/j.biopha.2020.110301.

(92) Xu, Y.; Tang, C.; Tan, S.; Duan, J.; Tian, H.; Yang, Y. Cardioprotective Effect of Isorhamnetin against Myocardial Ischemia Reperfusion (I/R) Injury in Isolated Rat Heart through Attenuation of Apoptosis. *J. Cell. Mol. Med.* **2020**, *24* (11), 6253–6262. https://doi.org/10.1111/jcmm.15267.

(93) Vincent Brice Ayissi, O.; Borris Rt, G.; Paul Fewou, M. In Silico Identification of Apigenin and Narcissin (Food-Flavonoids) as Potential Targets Against SARS-CoV-2 Viral Proteins: Comparison with the Effect of Remdesivir. *J. Clin. Anesth. Pain Manag.* **2021**, *5* (1). https://doi.org/10.36959/377/356.

(94) Rigano, D.; Formisano, C.; Basile, A.; Lavitola, A.; Senatore, F.; Rosselli, S.; Bruno, M. Antibacterial Activity of Flavonoids and Phenylpropanoids from *Marrubium Globosum* Ssp . *Libanoticum*. *Phytother. Res.* **2007**, *21* (4), 395–397. https://doi.org/10.1002/ptr.2061.

(95) Yoo, G.; Oh, Y.; Yang, H.; Kim, T.; Sung, S.; Kim, S. Efficient Preparation of Narcissin from Opuntia Ficus-Indica Fruits by Combination of Response Surface Methodology and High-Speed Countercurrent Chromatography. *Pharmacogn. Mag.* **2018**, *14* (56), 338. https://doi.org/10.4103/pm.pm_422_17.

(96) Ahn, H. J.; You, H. J.; Park, M. S.; Li, Z.; Choe, D.; Johnston, T. V.; Ku, S.; Ji, G. E. Microbial Biocatalysis of Quercetin-3-Glucoside and Isorhamnetin-3-Glucoside in *Salicornia Herbacea* and Their Contribution to Improved Anti-Inflammatory Activity. *RSC Adv.* **2020**, *10* (9), 5339–5350. https://doi.org/10.1039/C9RA08059G.

(97) Chen, P.-N.; Chu, S.-C.; Chiou, H.-L.; Chiang, C.-L.; Yang, S.-F.; Hsieh, Y.-S. Cyanidin 3-Glucoside and Peonidin 3-Glucoside Inhibit Tumor Cell Growth and Induce Apoptosis In Vitro and Suppress Tumor Growth In Vivo. *Nutr. Cancer* **2005**, *53* (2), 232–243. https://doi.org/10.1207/s15327914nc5302_12.

(98) Sari, D.; Cairns, J.; Safitri, A.; Fatchiyah, F. Virtual Prediction of the Delphinidin-3-O-Glucoside and Peonidin-3-O-Glucoside as Anti-Inflammatory of TNF- and #945;

Signaling. *Acta Inform. Medica* **2019**, *27* (3), 152. https://doi.org/10.5455/aim.2019.27.152-157.

(99) Joshi, R.; Kulkarni, Y. A.; Wairkar, S. Pharmacokinetic, Pharmacodynamic and Formulations Aspects of Naringenin: An Update. *Life Sci.* **2018**, *215*, 43–56. https://doi.org/10.1016/j.lfs.2018.10.066.

(100) Stabrauskiene, J.; Kopustinskiene, D. M.; Lazauskas, R.; Bernatoniene, J. Naringin and Naringenin: Their Mechanisms of Action and the Potential Anticancer Activities. *Biomedicines* **2022**, *10* (7), 1686. https://doi.org/10.3390/biomedicines10071686.

(101) Song, X.; Tan, L.; Wang, M.; Ren, C.; Guo, C.; Yang, B.; Ren, Y.; Cao, Z.; Li, Y.; Pei, J. Myricetin: A Review of the Most Recent Research. *Biomed. Pharmacother.* **2021**, *134*, 111017. https://doi.org/10.1016/j.biopha.2020.111017.

(102) Sumner, L. W.; Amberg, A.; Barrett, D.; Beale, M. H.; Beger, R.; Daykin, C. A.; Fan, T. W.-M.; Fiehn, O.; Goodacre, R.; Griffin, J. L.; Hankemeier, T.; Hardy, N.; Harnly, J.; Higashi, R.; Kopka, J.; Lane, A. N.; Lindon, J. C.; Marriott, P.; Nicholls, A. W.; Reily, M. D.; Thaden, J. J.; Viant, M. R. Proposed Minimum Reporting Standards for Chemical Analysis: Chemical Analysis Working Group (CAWG) Metabolomics Standards Initiative (MSI). *Metabolomics* **2007**, *3* (3), 211–221. https://doi.org/10.1007/s11306-007-0082-2.

(103) Schymanski, E. L.; Jeon, J.; Gulde, R.; Fenner, K.; Ruff, M.; Singer, H. P.; Hollender, J. Identifying Small Molecules via High Resolution Mass Spectrometry: Communicating Confidence. *Environ. Sci. Technol.* **2014**, *48* (4), 2097–2098. https://doi.org/10.1021/es5002105.

(104) Meunier, M.; Schinkovitz, A.; Derbré, S. Current and Emerging Tools and Strategies for the Identification of Bioactive Natural Products in Complex Mixtures. *Nat. Prod. Rep.* **2024**, *41* (11), 1766–1786. https://doi.org/10.1039/D4NP00006D.

(105) Tautenhahn, R.; Patti, G. J.; Rinehart, D.; Siuzdak, G. XCMS Online: A Web-Based Platform to Process Untargeted Metabolomic Data. *Anal. Chem.* **2012**, *84* (11), 5035–5039. https://doi.org/10.1021/ac300698c.

(106) Domingo-Almenara, X.; Montenegro-Burke, J. R.; Ivanisevic, J.; Thomas, A.; Sidibé, J.; Teav, T.; Guijas, C.; Aisporna, A. E.; Rinehart, D.; Hoang, L.; Nordström, A.; Gómez-Romero, M.; Whiley, L.; Lewis, M. R.; Nicholson, J. K.; Benton, H. P.; Siuzdak, G. XCMS-MRM and METLIN-MRM: A Cloud Library and Public Resource for Targeted Analysis of Small Molecules. *Nat. Methods* **2018**, *15* (9), 681–684. https://doi.org/10.1038/s41592-018-0110-3.

(107) Tsugawa, H.; Cajka, T.; Kind, T.; Ma, Y.; Higgins, B.; Ikeda, K.; Kanazawa, M.; VanderGheynst, J.; Fiehn, O.; Arita, M. MS-DIAL: Data-Independent MS/MS Deconvolution for Comprehensive Metabolome Analysis. *Nat. Methods* **2015**, *12* (6), 523–526. https://doi.org/10.1038/nmeth.3393.

(108) Nguyen, T.; Nioi, P.; Pickett, C. B. The Nrf2-Antioxidant Response Element Signaling Pathway and Its Activation by Oxidative Stress. *J. Biol. Chem.* **2009**, *284* (20), 13291–13295. https://doi.org/10.1074/jbc.R900010200.

(109) Popović-Djordjević, J.; Quispe, C.; Giordo, R.; Kostić, A.; Katanić Stanković, J. S.; Tsouh Fokou, P. V.; Carbone, K.; Martorell, M.; Kumar, M.; Pintus, G.; Sharifi-Rad, J.; Docea, A. O.; Calina, D. Natural Products and Synthetic Analogues against HIV: A Perspective to Develop New Potential Anti-HIV Drugs. *Eur. J. Med. Chem.* **2022**, *233*, 114217. https://doi.org/10.1016/j.ejmech.2022.114217.

(110) Harnett, J.; Oakes, K.; Carè, J.; Leach, M.; Brown, D.; Cramer, H.; Pinder, T.-A.; Steel, A.; Anheyer, D. The Effects of Sambucus Nigra Berry on Acute Respiratory Viral Infections: A Rapid Review of Clinical Studies. *Adv. Integr. Med.* **2020**, *7* (4), 240–246. https://doi.org/10.1016/j.aimed.2020.08.001.

(111) Zakay-Rones, Z.; Thom, E.; Wollan, T.; Wadstein, J. Randomized Study of the Efficacy and Safety of Oral Elderberry Extract in the Treatment of Influenza A and B Virus Infections. *J. Int. Med. Res.* **2004**, *32* (2), 132–140. https://doi.org/10.1177/147323000403200205.

(112) Barak, V.; Halperin, T.; Kalickman, I. The Effect of Sambucol, a Black Elderberry-Based, Natural Product, on the Production of Human Cytokines: I. Inflammatory Cytokines. *Eur. Cytokine Netw.* **2001**, *12* (2), 290–296.

(113) Kinoshita, E.; Hayashi, K.; Katayama, H.; Hayashi, T.; Obata, A. Anti-Influenza Virus Effects of Elderberry Juice and Its Fractions. *Biosci. Biotechnol. Biochem.* **2012**, *76* (9), 1633–1638. https://doi.org/10.1271/bbb.120112.

(114) Torabian, G.; Valtchev, P.; Adil, Q.; Dehghani, F. Anti-Influenza Activity of Elderberry (Sambucus Nigra). *J. Funct. Foods* **2019**, *54*, 353–360. https://doi.org/10.1016/j.jff.2019.01.031.

(115) Krawitz, C.; Mraheil, M. A.; Stein, M.; Imirzalioglu, C.; Domann, E.; Pleschka, S.; Hain, T. Inhibitory Activity of a Standardized Elderberry Liquid Extract against Clinically-Relevant Human Respiratory Bacterial Pathogens and Influenza A and B Viruses. *BMC Complement. Altern. Med.* **2011**, *11* (1), 16. https://doi.org/10.1186/1472-6882-11-16.

(116) Porter, R. S.; Bode, R. F. A Review of the Antiviral Properties of Black Elder (*Sambucus Nigra* L.) Products: Antiviral Properties of Black Elder (*Sambucus Nigra* L.). *Phytother. Res.* **2017**, *31* (4), 533–554. https://doi.org/10.1002/ptr.5782.

(117) Wieland, L. S.; Piechotta, V.; Feinberg, T.; Ludeman, E.; Hutton, B.; Kanji, S.; Seely, D.; Garritty, C. Elderberry for Prevention and Treatment of Viral Respiratory Illnesses: A Systematic Review. *BMC Complement. Med. Ther.* **2021**, *21* (1), 112. https://doi.org/10.1186/s12906-021-03283-5.

(118) Setz, C.; Rauch, P.; Setz, M.; Breitenberger, S.; Plattner, S.; Schubert, U. Synergistic Antiviral Activity of European Black Elderberry Fruit Extract and Quinine Against SARS-CoV-2 and Influenza A Virus. *Nutrients* **2025**, *17* (7), 1205. https://doi.org/10.3390/nu17071205.

(119) Kowalinski, E.; Zubieta, C.; Wolkerstorfer, A.; Szolar, O. H. J.; Ruigrok, R. W. H.; Cusack, S. Structural Analysis of Specific Metal Chelating Inhibitor Binding to the Endonuclease Domain of Influenza pH1N1 (2009) Polymerase. *PLoS Pathog.* **2012**, *8* (8), e1002831. https://doi.org/10.1371/journal.ppat.1002831.

(120) Hayden, F. G.; Sugaya, N.; Hirotsu, N.; Lee, N.; De Jong, M. D.; Hurt, A. C.; Ishida, T.; Sekino, H.; Yamada, K.; Portsmouth, S.; Kawaguchi, K.; Shishido, T.; Arai, M.; Tsuchiya, K.; Uehara, T.; Watanabe, A. Baloxavir Marboxil for Uncomplicated Influenza in Adults and Adolescents. *N. Engl. J. Med.* **2018**, *379* (10), 913–923. https://doi.org/10.1056/NEJMoa1716197.

(121) Rogolino, D.; Naesens, L.; Bartoli, J.; Carcelli, M.; De Luca, L.; Pelosi, G.; Stokes, R. W.; Van Berwaer, R.; Vittorio, S.; Stevaert, A.; Cohen, S. M. Exploration of the 2,3-Dihydroisoindole Pharmacophore for Inhibition of the Influenza Virus PA

Endonuclease. *Bioorganic Chem.* **2021**, *116*, 105388. https://doi.org/10.1016/j.bioorg.2021.105388.

(122) Yuan, S.; Chu, H.; Singh, K.; Zhao, H.; Zhang, K.; Kao, R. Y. T.; Chow, B. K. C.; Zhou, J.; Zheng, B.-J. A Novel Small-Molecule Inhibitor of Influenza A Virus Acts by Suppressing PA Endonuclease Activity of the Viral Polymerase. *Sci. Rep.* **2016**, *6* (1), 22880. https://doi.org/10.1038/srep22880.

(123) Kuzuhara, T.; Iwai, Y.; Takahashi, H.; Hatakeyama, D.; Echigo, N. Green Tea Catechins Inhibit the Endonuclease Activity of Influenza A Virus RNA Polymerase. *PLoS Curr.* **2009**, *1*, RRN1052. https://doi.org/10.1371/currents.RRN1052.

(124) Dwikarina, A.; Bayati, M.; Efrat, N.; Roy, A.; Lei, Z.; Ho, K.-V.; Sumner, L.; Greenlief, M.; L.Thomas, A.; Applequist, W.; Townesmith, A.; Lin, C.-H. Exploring American Elderberry Compounds for Antioxidant, Antiviral, and Antibacterial Properties Through High-Throughput Screening Assays Combined with Untargeted Metabolomics. Biochemistry September 14, 2024. https://doi.org/10.1101/2024.09.13.611920.

(125) Kasote, D. M.; Lei, Z.; Kranawetter, C. D.; Conway-Anderson, A.; Sumner, B. W.; Sumner, L. W. A Novel UHPLC-MS/MS Based Method for Isomeric Separation and Quantitative Determination of Cyanogenic Glycosides in American Elderberry. *Metabolites* **2024**, *14* (7), 360. https://doi.org/10.3390/metabo14070360.

(126) Kivilompolo, M.; Obůrka, V.; Hyötyläinen, T. Comparison of GC–MS and LC–MS Methods for the Analysis of Antioxidant Phenolic Acids in Herbs. *Anal. Bioanal. Chem.* **2007**, *388* (4), 881–887. https://doi.org/10.1007/s00216-007-1298-8.

(127) Halket, J. M.; Waterman, D.; Przyborowska, A. M.; Patel, R. K. P.; Fraser, P. D.; Bramley, P. M. Chemical Derivatization and Mass Spectral Libraries in Metabolic Profiling by GC/MS and LC/MS/MS. *J. Exp. Bot.* **2005**, *56* (410), 219–243. https://doi.org/10.1093/jxb/eri069.

(128) Alkaraly, A. Z.; Kormod, L.; Abdelsalam, R. A.; Hadad, G. M.; El-Gendy, A. E. LC-UV and LC-MS/MS Detection and Quantification of Steroid Hormones in Edible Food Samples and Water Using Solid Phase Extraction. *Int. J. Environ. Anal. Chem.* **2023**, *103* (15), 3587–3603. https://doi.org/10.1080/03067319.2021.1912328.

(129) Bystrom, L. M.; Lewis, B. A.; Brown, D. L.; Rodriguez, E.; Obendorf, R. L. Characterisation of Phenolics by LC–UV/Vis, LC–MS/MS and Sugars by GC in Melicoccus Bijugatus Jacq. 'Montgomery' Fruits. *Food Chem.* **2008**, *111* (4), 1017–1024. https://doi.org/10.1016/j.foodchem.2008.04.058.

(130) Baldrey, S. F.; Brodie, R. R.; Morris, G. R.; Jenkins, E. H.; Brookes, S. T. Comparison of LC-UV and LC-MS-MS for the Determination of Taxol. *Chromatographia* **2002**, *55* (S1), S187–S192. https://doi.org/10.1007/BF02493378.

(131) Custodio-Mendoza, J. A.; Pokorski, P.; Aktaş, H.; Napiórkowska, A.; Kurek, M. A. Advances in Chromatographic Analysis of Phenolic Phytochemicals in Foods: Bridging Gaps and Exploring New Horizons. *Foods* **2024**, *13* (14), 2268. https://doi.org/10.3390/foods13142268.

(132) Williams, M. L.; Olomukoro, A. A.; Emmons, R. V.; Godage, N. H.; Gionfriddo, E. Matrix Effects Demystified: Strategies for Resolving Challenges in Analytical Separations of Complex Samples. *J. Sep. Sci.* **2023**, *46* (23), 2300571. https://doi.org/10.1002/jssc.202300571.

(133) Steiner, D.; Krska, R.; Malachová, A.; Taschl, I.; Sulyok, M. Evaluation of Matrix Effects and Extraction Efficiencies of LC–MS/MS Methods as the Essential Part for Proper Validation of Multiclass Contaminants in Complex Feed. *J. Agric. Food Chem.* **2020**, *68* (12), 3868–3880. https://doi.org/10.1021/acs.jafc.9b07706.

(134) Badawy, M. E. I.; El-Nouby, M. A. M.; Kimani, P. K.; Lim, L. W.; Rabea, E. I. A Review of the Modern Principles and Applications of Solid-Phase Extraction Techniques in Chromatographic Analysis. *Anal. Sci.* **2022**, *38* (12), 1457–1487. https://doi.org/10.1007/s44211-022-00190-8.

(135) Matuszewski, B. K.; Constanzer, M. L.; Chavez-Eng, C. M. Strategies for the Assessment of Matrix Effect in Quantitative Bioanalytical Methods Based on HPLC−MS/MS. *Anal. Chem.* **2003**, *75* (13), 3019–3030. https://doi.org/10.1021/ac020361s.

(136) Barnes, J. S.; Schug, K. A. Structural Characterization of Cyanidin-3,5-Diglucoside and Pelargonidin-3,5-Diglucoside Anthocyanins: Multi-Dimensional Fragmentation Pathways Using High Performance Liquid Chromatography-Electrospray Ionization-Ion Trap-Time of Flight Mass Spectrometry. *Int. J. Mass Spectrom.* **2011**, *308* (1), 71–80. https://doi.org/10.1016/j.ijms.2011.07.026.

(137) Lin, S.; Simal-Gandara, J.; Cao, H.; Xiao, J. The Stability and Degradation Products of Polyhydroxy Flavonols in Boiling Water. *Curr. Res. Food Sci.* **2023**, *6*, 100509. https://doi.org/10.1016/j.crfs.2023.100509.

(138) Fu, Y.; Li, W.; Picard, F. Assessment of Matrix Effect in Quantitative LC-MS Bioanalysis. *Bioanalysis* **2024**, *16* (12), 631–634. https://doi.org/10.4155/bio-2024-0047.

(139) Yang, F.; Gong, J. F.; Shen, L.; Zhang, C.; Kou, F. R.; Gao, J.; Li, Y.; Bing Xu, G. Development of an LC-MS/MS Method for Quantitative Analysis of Chlorogenic Acid in Human Plasma and Its Application to a Pharmacokinetic Study in Chinese Patients with Advanced Solid Tumor. *J. Pharm. Biomed. Anal.* **2020**, *177*, 112809. https://doi.org/10.1016/j.jpba.2019.112809.

(140) Wang, Y.; Wen, J.; Zheng, W.; Zhao, L.; Fu, X.; Wang, Z.; Xiong, Z.; Li, F.; Xiao, W. Simultaneous Determination of Neochlorogenic Acid, Chlorogenic Acid, Cryptochlorogenic Acid and Geniposide in Rat Plasma by UPLC-MS/MS and Its Application to a Pharmacokinetic Study after Administration of Reduning Injection. *Biomed. Chromatogr.* **2015**, *29* (1), 68–74. https://doi.org/10.1002/bmc.3241.

(141) Papagrigoriou, T.; Iliadi, P.; Mitić, M. N.; Mrmošanin, J. M.; Papanastasi, K.; Karapatzak, E.; Maloupa, E.; Gkourogianni, A. V.; Badeka, A. V.; Krigas, N.; Lazari, D. Wild-Growing and Conventionally or Organically Cultivated Sambucus Nigra Germplasm: Fruit Phytochemical Profile, Total Phenolic Content, Antioxidant Activity, and Leaf Elements. *Plants* **2023**, *12* (8), 1701. https://doi.org/10.3390/plants12081701.

(142) Kiprovski, B.; Malenčić, Đ.; Ljubojević, M.; Ognjanov, V.; Veberic, R.; Hudina, M.; Mikulic-Petkovsek, M. Quality Parameters Change during Ripening in Leaves and Fruits of Wild Growing and Cultivated Elderberry (Sambucus Nigra) Genotypes. *Sci. Hortic.* **2021**, *277*, 109792. https://doi.org/10.1016/j.scienta.2020.109792.

(143) Whitby, K.; Pierson, T. C.; Geiss, B.; Lane, K.; Engle, M.; Zhou, Y.; Doms, R. W.; Diamond, M. S. Castanospermine, a Potent Inhibitor of Dengue Virus Infection In

Vitro and In Vivo. *J. Virol.* **2005**, *79* (14), 8698–8706. https://doi.org/10.1128/JVI.79.14.8698-8706.2005.
(144) Pegg, A. E. The Function of Spermine: Function of Spermine. *IUBMB Life* **2014**, *66* (1), 8–18. https://doi.org/10.1002/iub.1237.
(145) Xu, T.-T.; Li, H.; Dai, Z.; Lau, G. K.; Li, B.-Y.; Zhu, W.-L.; Liu, X.-Q.; Liu, H.-F.; Cai, W.-W.; Huang, S.-Q.; Wang, Q.; Zhang, S.-J. Spermidine and Spermine Delay Brain Aging by Inducing Autophagy in SAMP8 Mice. *Aging* **2020**, *12* (7), 6401–6414. https://doi.org/10.18632/aging.103035.
(146) Marques, C.; Hadjab, F.; Porcello, A.; Lourenço, K.; Scaletta, C.; Abdel-Sayed, P.; Hirt-Burri, N.; Applegate, L. A.; Laurent, A. Mechanistic Insights into the Multiple Functions of Niacinamide: Therapeutic Implications and Cosmeceutical Applications in Functional Skincare Products. *Antioxidants* **2024**, *13* (4), 425. https://doi.org/10.3390/antiox13040425.
(147) Matts, P. J.; Oblong, J. E.; Bissett, D. L. A Review of the Range of Effects of Niacinamide in Human Skin. **2002**, *5* (4).
(148) Julius, U. Niacin as Antidyslipidemic Drug. *Can. J. Physiol. Pharmacol.* **2015**, *93* (12), 1043–1054. https://doi.org/10.1139/cjpp-2014-0478.
(149) Freitas, C. S.; Roveda, A. C.; Truzzi, D. R.; Garcia, A. C.; Cunha, T. M.; Cunha, F. Q.; Franco, D. W. Anti-Inflammatory and Anti-Nociceptive Activity of Ruthenium Complexes with Isonicotinic and Nicotinic Acids (Niacin) as Ligands. *J. Med. Chem.* **2015**, *58* (11), 4439–4448. https://doi.org/10.1021/acs.jmedchem.5b00133.
(150) Narayan, R.; Sharma, M.; Yadav, R.; Biji, A.; Khatun, O.; Kaur, S.; Kanojia, A.; Joy, C. M.; Rajmani, R.; Sharma, P. R.; Jeyasankar, S.; Rani, P.; Shandil, R. K.; Narayanan, S.; Rao, D. C.; Satchidanandam, V.; Das, S.; Agarwal, R.; Tripathi, S. Picolinic Acid Is a Broad-Spectrum Inhibitor of Enveloped Virus Entry That Restricts SARS-CoV-2 and Influenza A Virus in Vivo. *Cell Rep. Med.* **2023**, *4* (8), 101127. https://doi.org/10.1016/j.xcrm.2023.101127.
(151) Sharma, R.; Fatma, B.; Saha, A.; Bajpai, S.; Sistla, S.; Dash, P. K.; Parida, M.; Kumar, P.; Tomar, S. Inhibition of Chikungunya Virus by Picolinate That Targets Viral Capsid Protein. *Virology* **2016**, *498*, 265–276. https://doi.org/10.1016/j.virol.2016.08.029.
(152) Ogata, S.; Inoue, K.; Ida, C.; Okumura, K. Apoptosis Induced by the Esters of Picolinic Acid with Alkyl Groups in HL-60 Cells. **2018**, *25*.
(153) Zhang, M.; Zhang, H.; Li, H.; Lai, F.; Li, X.; Tang, Y.; Min, T.; Wu, H. Antioxidant Mechanism of Betaine without Free Radical Scavenging Ability. *J. Agric. Food Chem.* **2016**, *64* (42), 7921–7930. https://doi.org/10.1021/acs.jafc.6b03592.
(154) Zhao, G.; He, F.; Wu, C.; Li, P.; Li, N.; Deng, J.; Zhu, G.; Ren, W.; Peng, Y. Betaine in Inflammation: Mechanistic Aspects and Applications. *Front. Immunol.* **2018**, *9*, 1070. https://doi.org/10.3389/fimmu.2018.01070.
(155) Jian, H.; Miao, S.; Liu, Y.; Li, H.; Zhou, W.; Wang, X.; Dong, X.; Zou, X. Effects of Dietary Valine Levels on Production Performance, Egg Quality, Antioxidant Capacity, Immunity, and Intestinal Amino Acid Absorption of Laying Hens during the Peak Lay Period. *Animals* **2021**, *11* (7), 1972. https://doi.org/10.3390/ani11071972.
(156) Sampaio-Dias, I. E.; Reis-Mendes, A.; Costa, V. M.; García-Mera, X.; Brea, J.; Loza, M. I.; Pires-Lima, B. L.; Alcoholado, C.; Algarra, M.; Rodríguez-Borges, J. E.

Discovery of New Potent Positive Allosteric Modulators of Dopamine D 2 Receptors: Insights into the Bioisosteric Replacement of Proline to 3-Furoic Acid in the Melanostatin Neuropeptide. *J. Med. Chem.* **2021**, *64* (9), 6209–6220. https://doi.org/10.1021/acs.jmedchem.1c00252.

(157) Abdel-Salam, O. M. E.; Youness, E. R.; Mohammed, N. A.; Morsy, S. M. Y.; Omara, E. A.; Sleem, A. A. Citric Acid Effects on Brain and Liver Oxidative Stress in Lipopolysaccharide-Treated Mice. *J. Med. Food* **2014**, *17* (5), 588–598. https://doi.org/10.1089/jmf.2013.0065.

(158) Burmudžija, A. Z.; Muškinja, J. M.; Kosanić, M. M.; Ranković, B. R.; Novaković, S. B.; Đorđević, S. B.; Stanojković, T. P.; Baskić, D. D.; Ratković, Z. R. Cytotoxic and Antimicrobial Activity of Dehydrozingerone Based Cyclopropyl Derivatives. *Chem. Biodivers.* **2017**, *14* (8), e1700077. https://doi.org/10.1002/cbdv.201700077.

(159) Kuo, P.-C.; Cherng, C.-Y.; Jeng, J.-F.; Damu, A. G.; Teng, C.-M.; Lee, E.-J.; Wu, T.-S. Isolation of a Natural Antioxidant, Dehydrozingerone from Zingiber Officinale and Synthesis of Its Analogues for Recognition of Effective Antioxidant and Antityrosinase Agents. *Arch. Pharm. Res.* **2005**, *28* (5), 518–528. https://doi.org/10.1007/BF02977752.

(160) Lee, E. S.; Kang, J. S.; Kim, H. M.; Kim, S. J.; Kim, N.; Lee, J. O.; Kim, H. S.; Lee, E. Y.; Chung, C. H. Dehydrozingerone Inhibits Renal Lipotoxicity in High-fat Diet–Induced Obese Mice. *J. Cell. Mol. Med.* **2021**, *25* (18), 8725–8733. https://doi.org/10.1111/jcmm.16828.

(161) Moorkoth, S.; Prathyusha, N. S.; Manandhar, S.; Xue, Y.; Sankhe, R.; Pai, K. S. R.; Kumar, N. Antidepressant-like Effect of Dehydrozingerone from Zingiber Officinale by Elevating Monoamines in Brain: In Silico and in Vivo Studies. *Pharmacol. Rep.* **2021**, *73* (5), 1273–1286. https://doi.org/10.1007/s43440-021-00252-0.

(162) Chen, K.-Y.; Chen, Y.-J.; Cheng, C.-J.; Jhan, K.-Y.; Chiu, C.-H.; Wang, L.-C. 3-Hydroxybenzaldehyde and 4-Hydroxybenzaldehyde Enhance Survival of Mouse Astrocytes Treated with Angiostrongylus Cantonensis Young Adults Excretory/Secretory Products. *Biomed. J.* **2021**, *44* (6), S258–S266. https://doi.org/10.1016/j.bj.2020.11.008.

(163) Kang, C. W.; Han, Y. E.; Kim, J.; Oh, J. H.; Cho, Y. H.; Lee, E. J. 4-Hydroxybenzaldehyde Accelerates Acute Wound Healing through Activation of Focal Adhesion Signalling in Keratinocytes. *Sci. Rep.* **2017**, *7* (1), 14192. https://doi.org/10.1038/s41598-017-14368-y.

(164) Sharif, H. M. A.; Ahmed, D.; Mir, H. Antimicrobial Salicylaldehyde Schiff Bases: Synthesis, Characterization and Evaluation. **2015**.

(165) Mo, X.; Chen, Z.; Chu, B.; Liu, D.; Liang, Y.; Liang, F. Structure and Anticancer Activities of Four Cu(II) Complexes Bearing Tropolone. *Metallomics* **2019**, *11* (11), 1952–1964. https://doi.org/10.1039/C9MT00165D.

(166) Nakano, K.; Chigira, T.; Miyafusa, T.; Nagatoishi, S.; Caaveiro, J. M. M.; Tsumoto, K. Discovery and Characterization of Natural Tropolones as Inhibitors of the Antibacterial Target CapF from Staphylococcus Aureus. *Sci. Rep.* **2015**, *5* (1), 15337. https://doi.org/10.1038/srep15337.

(167) Reis, J.; Gaspar, A.; Milhazes, N.; Borges, F. Chromone as a Privileged Scaffold in Drug Discovery: Recent Advances: Miniperspective. *J. Med. Chem.* **2017**, *60* (19), 7941–7957. https://doi.org/10.1021/acs.jmedchem.6b01720.
(168) Mohsin, N. U. A.; Irfan, M.; Hassan, S. U.; Saleem, U. Current Strategies in Development of New Chromone Derivatives with Diversified Pharmacological Activities: A Review. *Pharm. Chem. J.* **2020**, *54* (3), 241–257. https://doi.org/10.1007/s11094-020-02187-x.
(169) Küpeli Akkol, E.; Genç, Y.; Karpuz, B.; Sobarzo-Sánchez, E.; Capasso, R. Coumarins and Coumarin-Related Compounds in Pharmacotherapy of Cancer. *Cancers* **2020**, *12* (7), 1959. https://doi.org/10.3390/cancers12071959.
(170) Barot, K. P.; Jain, S. V.; Kremer, L.; Singh, S.; Ghate, M. D. Recent Advances and Therapeutic Journey of Coumarins: Current Status and Perspectives. *Med. Chem. Res.* **2015**, *24* (7), 2771–2798. https://doi.org/10.1007/s00044-015-1350-8.
(171) Alabsi, A.; Khoudary, A. C.; Abdelwahed, W. The Antidepressant Effect of L-Tyrosine-Loaded Nanoparticles: Behavioral Aspects. *Ann. Neurosci.* **2016**, *23* (2), 89–99. https://doi.org/10.1159/000443575.
(172) Gülçin, İ. Comparison of in Vitro Antioxidant and Antiradical Activities of L-Tyrosine and L-Dopa. *Amino Acids* **2007**, *32* (3), 431–438. https://doi.org/10.1007/s00726-006-0379-x.
(173) Ai, L.; Fu, S.; Li, Y.; Zuo, M.; Huang, W.; Huang, J.; Jin, Z.; Chen, Y. Natural Products-Based: Synthesis and Antifungal Activity Evaluation of Novel L-Pyroglutamic Acid Analogues. *Front. Plant Sci.* **2022**, *13*, 1102411. https://doi.org/10.3389/fpls.2022.1102411.
(174) Gang, F.; Zhu, F.; Li, X.; Wei, J.; Wu, W.; Zhang, J. Synthesis and Bioactivities Evaluation of L-Pyroglutamic Acid Analogues from Natural Product Lead. *Bioorg. Med. Chem.* **2018**, *26* (16), 4644–4649. https://doi.org/10.1016/j.bmc.2018.07.041.
(175) Buccafusco, J. J.; Terry, A. V. The Potential Role of Cotinine in the Cognitive and Neuroprotective Actions of Nicotine. *Life Sci.* **2003**, *72* (26), 2931–2942. https://doi.org/10.1016/S0024-3205(03)00226-1.
(176) Partis, A.; Mueller, A.; Chrest, J. The A-Glucosidase I Inhibitor Castanospermine Alters Endothelial Cell Glycosylation, Prevents Angiogenesis, and Inhibits Tumor Growth. **1995**.
(177) Bastola, T.; An, R.; Kim, Y.-C.; Kim, J.; Seo, J. Cearoin Induces Autophagy, ERK Activation and Apoptosis via ROS Generation in SH-SY5Y Neuroblastoma Cells. *Molecules* **2017**, *22* (2), 242. https://doi.org/10.3390/molecules22020242.
(178) Funakoshi-Tago, M.; Ohsawa, K.; Ishikawa, T.; Nakamura, F.; Ueda, F.; Narukawa, Y.; Kiuchi, F.; Tamura, H.; Tago, K.; Kasahara, T. Inhibitory Effects of Flavonoids Extracted from Nepalese Propolis on the LPS Signaling Pathway. *Int. Immunopharmacol.* **2016**, *40*, 550–560. https://doi.org/10.1016/j.intimp.2016.10.008.
(179) Marinov, T.; Kokanova-Nedialkova, Z.; Nedialkov, P. T. Naturally Occurring Simple Oxygenated Benzophenones: Structural Diversity, Distribution, and Biological Properties. *Diversity* **2023**, *15* (10), 1030. https://doi.org/10.3390/d15101030.

(180) Jin, H.-G.; Kim, A. R.; Ko, H. J.; Lee, S. K.; Woo, E.-R. Three New Lignan Glycosides with IL-6 Inhibitory Activity from *Akebia Quinata*. *Chem. Pharm. Bull. (Tokyo)* **2014**, *62* (3), 288–293. https://doi.org/10.1248/cpb.c13-00668.

(181) Jung, H. A.; Jung, Y. J.; Hyun, S. K.; Min, B.-S.; Kim, D.-W.; Jung, J. H.; Choi, J. S. Selective Cholinesterase Inhibitory Activities of a New Monoterpene Diglycoside and Other Constituents from Nelumbo Nucifera Stamens. *Biol. Pharm. Bull.* **2010**, *33* (2), 267–272. https://doi.org/10.1248/bpb.33.267.

(182) Zhao, C.; Liu, Q.; Halaweish, F.; Shao, B.; Ye, Y.; Zhao, W. Copacamphane, Picrotoxane, and Alloaromadendrane Sesquiterpene Glycosides and Phenolic Glycosides from *Dendrobium m Oniliforme*. *J. Nat. Prod.* **2003**, *66* (8), 1140–1143. https://doi.org/10.1021/np0301801.

(183) Wlodarska, M.; Luo, C.; Kolde, R.; d'Hennezel, E.; Annand, J. W.; Heim, C. E.; Krastel, P.; Schmitt, E. K.; Omar, A. S.; Creasey, E. A.; Garner, A. L.; Mohammadi, S.; O'Connell, D. J.; Abubucker, S.; Arthur, T. D.; Franzosa, E. A.; Huttenhower, C.; Murphy, L. O.; Haiser, H. J.; Vlamakis, H.; Porter, J. A.; Xavier, R. J. Indoleacrylic Acid Produced by Commensal Peptostreptococcus Species Suppresses Inflammation. *Cell Host Microbe* **2017**, *22* (1), 25-37.e6. https://doi.org/10.1016/j.chom.2017.06.007.

(184) De Andrade Gonçalves, P.; Dos Santos Junior, M. C.; Do Sacramento Sousa, C.; Góes-Neto, A.; Luz, E. D. M. N.; Damaceno, V. O.; Niella, A. R. R.; Filho, J. M. B.; De Assis, S. A. Study of Sodium 3-Hydroxycoumarin as Inhibitors in Vitro, in Vivo and in Silico of Moniliophthora Perniciosa Fungus. *Eur. J. Plant Pathol.* **2019**, *153* (1), 15–27. https://doi.org/10.1007/s10658-018-1536-2.

(185) Friedman, M. Chemistry, Antimicrobial Mechanisms, and Antibiotic Activities of Cinnamaldehyde against Pathogenic Bacteria in Animal Feeds and Human Foods. *J. Agric. Food Chem.* **2017**, *65* (48), 10406–10423. https://doi.org/10.1021/acs.jafc.7b04344.

(186) Zhu, R.; Liu, H.; Liu, C.; Wang, L.; Ma, R.; Chen, B.; Li, L.; Niu, J.; Fu, M.; Zhang, D.; Gao, S. Cinnamaldehyde in Diabetes: A Review of Pharmacology, Pharmacokinetics and Safety. *Pharmacol. Res.* **2017**, *122*, 78–89. https://doi.org/10.1016/j.phrs.2017.05.019.

(187) Filho, A. C. M. L.; Silva, I. S.; Sousa, F. B. M.; De Souza, L. K. M.; Gomes, B. D. S.; Gonçalves, R. L. G.; De Rezende, D. C.; Cunha, F. V. M.; Wong, D. V. T.; Júnior, R. C. P. L.; Medeiros, J. V.-R.; De Sousa, D. P.; Oliveira, F. D. A. Inhibition of Neutrophil Migration and Reduction of Oxidative Stress by Ethyl P-Coumarate in Acute and Chronic Inflammatory Models. *Phytomedicine* **2019**, *57*, 9–17. https://doi.org/10.1016/j.phymed.2018.09.034.

(188) Li, W.; Yuan, S.; Sun, J.; Li, Q.; Jiang, W.; Cao, J. Ethyl p -Coumarate Exerts Antifungal Activity in Vitro and in Vivo against Fruit Alternaria Alternata via Membrane-Targeted Mechanism. *Int. J. Food Microbiol.* **2018**, *278*, 26–35. https://doi.org/10.1016/j.ijfoodmicro.2018.04.024.

(189) Sanci, T. O.; Terzi, E.; Oz Bedir, B. E.; Gumustas, M.; Aydin, T.; Cakir, A. Effect of Herniarin on Cell Viability, Cell Cycle, and Erk Protein Levels in Different Stages of Bladder Cancer Cells. *Chem. Biodivers.* **2024**, *21* (3), e202301645. https://doi.org/10.1002/cbdv.202301645.

(190) Mustafa, Y. F.; Abdulaziz, N. T. ANTICANCER POTENTIAL OF HYMECROMONE-BASED COMPOUNDS : A REVIEW.
(191) Lee, J. Y.; Park, W. Anti-Inflammatory Effect of Myristicin on RAW 264.7 Macrophages Stimulated with Polyinosinic-Polycytidylic Acid. *Molecules* **2011**, *16* (8), 7132–7142. https://doi.org/10.3390/molecules16087132.
(192) Seneme, E. F.; Dos Santos, D. C.; Silva, E. M. R.; Franco, Y. E. M.; Longato, G. B. Pharmacological and Therapeutic Potential of Myristicin: A Literature Review. *Molecules* **2021**, *26* (19), 5914. https://doi.org/10.3390/molecules26195914.
(193) Zheng, G. Qiang.; Kenney, P. M.; Lam, L. K. T. Myristicin: A Potential Cancer Chemopreventive Agent from Parsley Leaf Oil. *J. Agric. Food Chem.* **1992**, *40* (1), 107–110. https://doi.org/10.1021/jf00013a020.
(194) Kim, D.-W.; Lee, K.; Kwon, J.; Lee, H. J.; Lee, D.; Mar, W. Neuroprotection against 6-OHDA-Induced Oxidative Stress and Apoptosis in SH-SY5Y Cells by 5,7-Dihydroxychromone: Activation of the Nrf2/ARE Pathway. *Life Sci.* **2015**, *130*, 25–30. https://doi.org/10.1016/j.lfs.2015.02.026.
(195) Koo, H. J.; Kwak, J. H.; Kang, S. C. Anti-Diabetic Properties of *Daphniphyllum Macropodum* Fruit and Its Active Compound. *Biosci. Biotechnol. Biochem.* **2014**, *78* (8), 1392–1401. https://doi.org/10.1080/09168451.2014.923289.
(196) Wang, B.; Wang, Q.; Yuan, R.; Yang, S.; Lu, M.; Yuan, F.; Dong, Z.; Mo, M.; Pan, Q.; Gao, H. Prenylated Chromones and Flavonoids Isolated from the Roots of Flemingia Macrophylla and Their Anti-Lung Cancer Activity. *Chin. Med.* **2023**, *18* (1), 153. https://doi.org/10.1186/s13020-023-00860-3.
(197) Hang, S.; Wu, W.; Wang, Y.; Sheng, R.; Fang, Y.; Guo, R. Daphnetin, a Coumarin in Genus *Stellera Chamaejasme* Linn: Chemistry, Bioactivity and Therapeutic Potential. *Chem. Biodivers.* **2022**, *19* (9), e202200261. https://doi.org/10.1002/cbdv.202200261.
(198) Yan, L.; Jin, Y.; Pan, J.; He, X.; Zhong, S.; Zhang, R.; Choi, L.; Su, W.; Chen, J. 7,8-Dihydroxycoumarin Alleviates Synaptic Loss by Activated PI3K-Akt-CREB-BDNF Signaling in Alzheimer's Disease Model Mice. *J. Agric. Food Chem.* **2022**, *70* (23), 7130–7138. https://doi.org/10.1021/acs.jafc.2c02140.
(199) Anderson, J. E.; Chang, C.-J.; McLaughlin, J. L. Bioactive Components of Allamanda Schottii. *J. Nat. Prod.* **1988**, *51* (2), 307–308. https://doi.org/10.1021/np50056a018.
(200) Kupchan, S. M.; Dessertine, A. L.; Blaylock, B. T.; Bryan, R. F. Isolation and Structural Elucidation of Allamandin, and Antileukemic Iridoid Lactone from Allamanda Cathartica. *J. Org. Chem.* **1974**, *39* (17), 2477–2482. https://doi.org/10.1021/jo00931a001.
(201) Cebrian-Torrejon, G. Study of the Toxicity and Antiviral Effect of Natural Compounds Extracted from Pseudospinx Tetrio and Allamanda Cathartica on Sars-Cov-2 Infection. **2024**.
(202) Zhang, L.; Ke, W.; Zhao, X.; Lu, Z. Resina Draconis Extract Exerts ANTI-HCC Effects through METTL3-M6A-SURVIVIN Axis. *Phytother. Res.* **2022**, *36* (6), 2542–2557. https://doi.org/10.1002/ptr.7467.
(203) Henley-Smith, C. J.; Botha, F. S.; Hussein, A. A.; Nkomo, M.; Meyer, D.; Lall, N. Biological Activities of Heteropyxis Natalensis Against Micro-Organisms Involved

in Oral Infections. *Front. Pharmacol.* **2018**, *9*, 291. https://doi.org/10.3389/fphar.2018.00291.

(204) Janpaijit, S.; Sillapachaiyaporn, C.; Theerasri, A.; Charoenkiatkul, S.; Sukprasansap, M.; Tencomnao, T. Cleistocalyx Nervosum Var. Paniala Berry Seed Protects against TNF-α-Stimulated Neuroinflammation by Inducing HO-1 and Suppressing NF-κB Mechanism in BV-2 Microglial Cells. *Molecules* **2023**, *28* (7), 3057. https://doi.org/10.3390/molecules28073057.

(205) Ghosh, A. K.; Lee, D. S. Enantioselective Total Synthesis of (+)-Monocerin, a Dihydroisocoumarin Derivative with Potent Antimalarial Properties. *J. Org. Chem.* **2019**, *84* (10), 6191–6198. https://doi.org/10.1021/acs.joc.9b00414.

(206) Barreca, D.; Bellocco, E.; Leuzzi, U.; Gattuso, G. First Evidence of C- and O-Glycosyl Flavone in Blood Orange (Citrus Sinensis (L.) Osbeck) Juice and Their Influence on Antioxidant Properties. *Food Chem.* **2014**, *149*, 244–252. https://doi.org/10.1016/j.foodchem.2013.10.096.

(207) Bonjardim, L. R.; Cunha, E. S.; Guimarães, A. G.; Santana, M. F.; Oliveira, M. G. B.; Serafini, M. R.; Araújo, A. A. S.; Antoniolli, Â. R.; Cavalcanti, S. C. H.; Santos, M. R. V.; Quintans-Júnior, L. J. Evaluation of the Anti-Inflammatory and Antinociceptive Properties of p-Cymene in Mice. **2014**.

(208) De Oliveira, T. M.; De Carvalho, R. B. F.; Da Costa, I. H. F.; De Oliveira, G. A. L.; De Souza, A. A.; De Lima, S. G.; De Freitas, R. M. Evaluation of *p* -Cymene, a Natural Antioxidant. *Pharm. Biol.* **2015**, *53* (3), 423–428. https://doi.org/10.3109/13880209.2014.923003.

(209) Li, J.; Liu, C.; Sato, T. Novel Antitumor Invasive Actions of *p*-Cymene by Decreasing MMP-9/TIMP-1 Expression Ratio in Human Fibrosarcoma HT-1080 Cells. *Biol. Pharm. Bull.* **2016**, *39* (8), 1247–1253. https://doi.org/10.1248/bpb.b15-00827.

(210) Marchese, A.; Arciola, C.; Barbieri, R.; Silva, A.; Nabavi, S.; Tsetegho Sokeng, A.; Izadi, M.; Jafari, N.; Suntar, I.; Daglia, M.; Nabavi, S. Update on Monoterpenes as Antimicrobial Agents: A Particular Focus on p-Cymene. *Materials* **2017**, *10* (8), 947. https://doi.org/10.3390/ma10080947.

(211) Esposito, F.; Tintori, C.; Martini, R.; Christ, F.; Debyser, Z.; Ferrarese, R.; Cabiddu, G.; Corona, A.; Ceresola, E. R.; Calcaterra, A.; Iovine, V.; Botta, B.; Clementi, M.; Canducci, F.; Botta, M.; Tramontano, E. Kuwanon-L as a New Allosteric HIV-1 Integrase Inhibitor: Molecular Modeling and Biological Evaluation. *ChemBioChem* **2015**, *16* (17), 2507–2512. https://doi.org/10.1002/cbic.201500385.

(212) Jin, S. E.; Ha, H.; Shin, H.-K.; Seo, C.-S. Anti-Allergic and Anti-Inflammatory Effects of Kuwanon G and Morusin on MC/9 Mast Cells and HaCaT Keratinocytes. *Molecules* **2019**, *24* (2), 265. https://doi.org/10.3390/molecules24020265.

(213) Wei, B.; Yang, W.; Yan, Z.-X.; Zhang, Q.-W.; Yan, R. Prenylflavonoids Sanggenon C and Kuwanon G from Mulberry (Morus Alba L.) as Potent Broad-Spectrum Bacterial β-Glucuronidase Inhibitors: Biological Evaluation and Molecular Docking Studies. *J. Funct. Foods* **2018**, *48*, 210–219. https://doi.org/10.1016/j.jff.2018.07.013.

(214) Park, H. J.; Lee, S. J.; Cho, J.; Gharbi, A.; Han, H. D.; Kang, T. H.; Kim, Y.; Lee, Y.; Park, W. S.; Jung, I. D.; Park, Y.-M. Tamarixetin Exhibits Anti-Inflammatory

Activity and Prevents Bacterial Sepsis by Increasing IL-10 Production. *J. Nat. Prod.* **2018**, *81* (6), 1435–1443. https://doi.org/10.1021/acs.jnatprod.8b00155.

(215) Song, W.; Wang, B.; Sui, L.; Shi, Y.; Ren, X.; Wang, X.; Kong, X.; Hou, J.; Wang, L.; Wei, L.; Luan, Y.; Guan, J.; Zhao, Y. Tamarixetin Attenuated the Virulence of *Staphylococcus Aureus* by Directly Targeting Caseinolytic Protease P. *J. Nat. Prod.* **2022**, *85* (8), 1936–1944. https://doi.org/10.1021/acs.jnatprod.2c00138.

(216) Xu, J.; Cai, X.; Teng, S.; Lu, J.; Zhou, Y.; Wang, X.; Meng, Z. The Pro-Apoptotic Activity of Tamarixetin on Liver Cancer Cells Via Regulation Mitochondrial Apoptotic Pathway. *Appl. Biochem. Biotechnol.* **2019**, *189* (2), 647–660. https://doi.org/10.1007/s12010-019-03033-x.

(217) El-Kersh, D. M.; Mostafa, N. M.; Fayez, S.; Al-Warhi, T.; Abourehab, M. A. S.; Eldehna, W. M.; Salem, M. A. GC-MS Metabolites Profiling of Anethole-Rich Oils by Different Extraction Techniques: Antioxidant, Cytotoxicity and *in-Silico* Enzymes Inhibitory Insights. *J. Enzyme Inhib. Med. Chem.* **2022**, *37* (1), 1974–1986. https://doi.org/10.1080/14756366.2022.2097445.

(218) Lal, M.; Begum, T.; Gogoi, R.; Sarma, N.; Munda, S.; Pandey, S. K.; Baruah, J.; Tamang, R.; Saikia, S. Anethole Rich Clausena Heptaphylla (Roxb.) Wight & Arn., Essential Oil Pharmacology and Genotoxic Efficiencies. *Sci. Rep.* **2022**, *12* (1), 9978. https://doi.org/10.1038/s41598-022-13511-8.

(219) Monteiro-Neto, V.; De Souza, C. D.; Gonzaga, L. F.; Da Silveira, B. C.; Sousa, N. C. F.; Pontes, J. P.; Santos, D. M.; Martins, W. C.; Pessoa, J. F. V.; Carvalho Júnior, A. R.; Almeida, V. S. S.; De Oliveira, N. M. T.; De Araújo, T. S.; Maria-Ferreira, D.; Mendes, S. J. F.; Ferro, T. A. F.; Fernandes, E. S. Cuminaldehyde Potentiates the Antimicrobial Actions of Ciprofloxacin against Staphylococcus Aureus and Escherichia Coli. *PLOS ONE* **2020**, *15* (5), e0232987. https://doi.org/10.1371/journal.pone.0232987.

(220) Ghiasi, F.; Eskandari, M. H.; Golmakani, M. T.; Hashemi Gahruie, H.; Zarei, R.; Naghibalhossaini, F.; Hosseini, S. M. H. A Novel Promising Delivery System for Cuminaldehyde Using Gelled Lipid Nanoparticles: Characterization and Anticancer, Antioxidant, and Antibacterial Activities. *Int. J. Pharm.* **2021**, *610*, 121274. https://doi.org/10.1016/j.ijpharm.2021.121274.

(221) Coêlho, M. L.; Islam, M. T.; Laylson Da Silva Oliveira, G.; Oliveira Barros De Alencar, M. V.; Victor De Oliveira Santos, J.; Campinho Dos Reis, A.; Oliveira Ferreira Da Mata, A. M.; Correia Jardim Paz, M. F.; Docea, A. O.; Calina, D.; Sharifi-Rad, J.; Amélia De Carvalho Melo-Cavalcante, A. Cytotoxic and Antioxidant Properties of Natural Bioactive Monoterpenes Nerol, Estragole, and 3,7-Dimethyl-1-Octanol. *Adv. Pharmacol. Pharm. Sci.* **2022**, *2022*, 1–11. https://doi.org/10.1155/2022/8002766.

VITA

Amanda Dwikarina was born in Bogor, Indonesia, on September 29th, 1992. She received her bachelor's degree in biology in 2015 from the Department of Biology, School of Science and Mathematics (FMIPA), IPB University, Indonesia. In 2017, Amanda was awarded a full scholarship from CIFOR-USAID to pursue graduate studies at the University of Missouri's School of Natural Resources, USA, where she completed her master's degree in Natural Resources, earning a graduate certificate in Agroforestry in 2019. She then worked at IPB University as a Research Specialist in the In Vitro Plant Biotechnology Laboratory, Department of Agronomy, for 3 years. In 2022, she continued her education in PhD program and completed her PhD degree in Natural Resources specialized in Metabolomics and Phytochemistry in 2025.

Amanda enjoys reading books, watching movies, and sharing good food with friends. In her leisure time, she finds relaxation both at home and through outdoor activities, which help her decompress and maintain balance outside of her academic pursuits.